A COMPARISON OF LACTO-N-FUCOPENTAOSE III (LNFPIII) AND LACTO-N-NEOTETRAOSE (LNNT) CONJUGATES AS THERAPIES TO IMPROVE IMMUNE AND METABOLIC PARAMETERS AND ALTER THE MICROBIOME IN DIET-INDUCED OBESE (DIO) MICE

By

JESSICA CHANTEL RAMADHIN

(Under the Direction of Donald Harn)

ABSTRACT

Obesity and associated metabolic syndrome (MetS) pose two of the greatest risks for development of non-communicable diseases, such as cardiovascular disease, type 2 diabetes mellitus, metabolic dysfunction-associated fatty liver disease, and even cancer. Together, obesity and MetS induce a state of chronic inflammation that results in impaired metabolic function. In order to target the inflammation caused by obesity and MetS, we investigated the therapeutic effects of two anti-inflammatory human milk oligosaccharide conjugates comprised of either lacto-N-fucopentaose III (LNFPIII) or lacto-N-neotetraose (LNnT). Herein, we demonstrate that LNFPIII, but not LNnT, conjugates reduce total weight gain, lessen adipose tissue depot size, decrease fasting blood glucose levels, improve glucose and insulin homeostasis, and ease hepatic lipid accumulation and liver damage. We report that both LNFPIII and LNnT modulate an

assortment of hematopoietic, chemoattractant, innate, and adaptive cytokines, as well as impact incretin effect hormones and adipokines. We also report that LNFPIII and LNnT conjugates alter the intestinal microbiome in unique manners, such that LNFPIII conjugates drive outgrowth of distinct species Bacteroidetes and Verrucomicrobia, while LNnT conjugates encourage growth of specific species of Actinobacteria. These studies indicate that LNFPIII conjugates, but not LNnT conjugates, are promising drugs for obesity and MetS. Furthermore, it is clear that both conjugates possess distinct mechanisms. Since there is little known about the mechanism of either LNFPIII or LNnT conjugates, we later developed monoclonal antibodies (mAbs) against the conjugates. We identified a single mAb that recognized both LNFPIII and LNnT conjugates and utilized this mAb in follow-up mechanistic studies to aid in determination of putative receptors for the compounds. Future studies will focus on continuing experiments using the generated mAb, in order to define the mechanisms of action for both conjugates.

INDEX WORDS: Human Milk Oligosaccharides (HMOs); Lacto-N-Fucopentaose III (LNFPIII); Lacto-N-Neotetraose (LNnT); Diet-Induced Obesity (DIO); Metabolic Disease; Microbiome

A COMPARISON OF LACTO-N-FUCOPENTAOSE III (LNFPIII) AND LACTO-N-NEOTETRAOSE (LNNT) CONJUGATES AS THERAPIES TO IMPROVE IMMUNE AND METABOLIC PARAMETERS AND ALTER THE MICROBIOME IN DIET-INDUCED OBESE (DIO) MICE

by

JESSICA CHANTEL RAMADHIN

BA, Cornell University, 2014

A Dissertation Submitted to the Graduate Faculty of The University of Georgia in Partial Fulfillment of the Requirements for the Degree

DOCTOR OF PHILOSOPHY

ATHENS, GEORGIA

2021

A COMPARISON OF LACTO-N-FUCOPENTAOSE III (LNFPIII) AND LACTO-N-NEOTETRAOSE (LNNT) CONJUGATES AS THERAPIES TO IMPROVE IMMUNE AND METABOLIC PARAMETERS AND ALTER THE MICROBIOME IN DIET-INDUCED OBESE (DIO) MICE

by

JESSICA CHANTEL RAMADHIN

Major Professor:	Donald Harn
Committee:	Richard Meagher
	Karen Norris
	Robert Pazdro
	Wendy Watford

Electronic Version Approved:

Ron Walcott
Vice Provost for Graduate Education and Dean of the Graduate School
The University of Georgia
May 2021

DEDICATION

To my loving parents,

Bibi and Inderdeo Ramadhin,

whose devotion and sacrifices made this educational endeavor possible.

To my only brother,

Randolph Ramadhin,

who became my greatest source of strength in 2020.

& to my dearest colleague and friend,

Vanessa Silva-Moraes,

who helped me gain confidence in science and myself.

ACKNOWLEDGEMENTS

I would like to extend my deepest gratitude to those that have made this accomplishment possible. First, I am indebted to my doctoral advisor, Dr. Donald Harn. Without his unwavering guidance and support, I would not have acquired the competence or rigor to become a successful scientist. I would also like to recognize the members of my committee, Dr. Richard Meagher, Dr. Karen Norris, Dr. Robert Pazdro, and Dr. Wendy Watford, who provided critical guidance and insight throughout the duration of this process. I would like to acknowledge past and present members of the Harn lab, who were instrumental in providing technical, professional, and emotional support. In particular, I would like to profess utmost appreciation for Dr. Vanessa Silva-Moraes. Dr. Silva-Moraes' encouragement and profound belief in my abilities served as an imperative lifeline throughout this process. I would also like to thank the Department of Infectious Diseases, our collaborators, and all support personnel.

Prior to beginning the doctoral program in Infectious Diseases at the University of Georgia, I was fortunate enough to stumble across several inspirational mentors who led me to pursue this degree. In this regard, I would like to acknowledge Dr. Tremayne Waller, Mr. Daniel Lupa, Mrs. Barbara Eaglesham, and Mrs. Catalina Cifuentes. With their guidance and supervision, I was awarded several academic scholarships that paved the route for my success.

I am thankful for my parents, Bibi and Inderdeo Ramadhin, who made substantial sacrifices to support me throughout my entire life. I am also thankful for my brother, Randolph Ramadhin, who could not be any more different from myself. I am grateful for the people who have come and gone throughout this process, but I am indebted to my best friends that have held me together each day: Janeigh Castillo-Barraza, Dr. Lishann Ingram, Dr. Jordan Davis, and Kameron Sigman-Jones.

Last, I am grateful to God for opening doors that I never thought imaginable. Thank you!

TABLE OF CONTENTS

Page

LIST OF TABLES

Page

LIST OF FIGURES

Page

CHAPTER 1

INTRODUCTION AND LITERATURE REVIEW

Obesity is a state of chronic, low-grade inflammation that originates within adipose tissue (AT) depots and spreads to surrounding tissues. In contrast to acute inflammation, excessive fat accumulation causes sustained AT inflammation that exhausts immune function and contributes to negative changes in overall metabolism. Once spread to the heart, liver, pancreas, brain, muscle, intestine, etc., the consequences of obesity-associated inflammation include type 2 diabetes mellitus (T2DM), cardiovascular disease, hepatic steatosis, and even cancer [1, 2]. We examined the potential of two human milk oligosaccharide (HMO) conjugates, composed of either lacto-N-fucopentaose III (LNFPIII) or lacto-N-neotetraose (LNnT), as therapeutics for obesity and metabolic syndrome (MetS).

Chapter 1 introduces the consequences of being obese and suffering from MetS, as well as describes the current understanding of how adipose tissue inflammation disrupts metabolic homeostasis and leads to peripheral pathologies. I continue on to describe the Hygiene Hypothesis, in which it is postulated that the absence of certain infections leads to an overactive immune response and greater incidence of chronic diseases in Western societies. I explain how helminths help regulate chronic inflammation through promotion of anti-inflammatory responses and T_H2 biasing, as well as outline the importance of Lewis^x, a structure shared between *Schistosoma mansoni*

parasites and HMOs. Next, I explain the structure and benefits of HMOs for a breastfeeding infant. Last, I introduce LNFPIII and LNnT conjugates, describe the work that has been conducted prior to this dissertation, and provide rationale for the following studies.

Chapter 2 seeks to determine how LNFPIII and LNnT conjugates alter metabolic and immune parameters in diet-induced obese (DIO) mice. We utilized a combination of *in vivo* metabolic tests and *ex vivo* analyses of serum and tissues to determine if both LNFPIII and LNnT conjugates were therapeutic for DIO. We also asked if effects were specific to each respective conjugate and if injection route mattered in terms of therapeutic strength. Additional data is presented in Appendix A. Chapter 3 investigates how LNFPIII and LNnT conjugates alter the microbiome in DIO mice. Herein, we expanded on the *in vivo* experiments presented in Chapter 2 and performed 16S RNA sequencing on fecal samples isolated from DIO mice treated with each conjugate.

We switch to more mechanistic studies in Chapter 4, wherein we generated and characterized a monoclonal antibody (mAb) that recognizes both LNFPIII and LNnT conjugates. This mAb is utilized in Chapter 5, which presents foundational studies regarding identification of putative receptors for HMO conjugates.

In Chapter 6, I return to the results presented in Chapters 2-5 to address limitations, remaining questions, and potential for future studies. Each chapter is presented in manuscript-style with all figures and figure legends located at the end of its respective chapter.

As a whole, this dissertation achieves the following project goals:

AIM 1: Determine how LNFPIII and LNnT conjugates alter metabolic and immune parameters in diet-induced obese (DIO) mice.

- Are both LNFPIII and LNnT conjugates therapeutic for DIO (Chapter 2)?
- Are effects specific to the conjugate (Appendix A)?
- Does route of injection matter (Appendix A)?

AIM 2: Determine tissue-specific effects of LNFPIII and LNnT conjugates in DIO Mice.

- White Adipose Tissue (Chapter 2)
- Liver (Chapter 2)
- Gut & Microbiome (Chapter 3)

AIM 3: Identify putative receptors for LNFPIII and LNnT conjugates.

- Generation of a monoclonal antibody (mAb) that recognizes HMO conjugates (Chapter 4)
- Immunoprecipitation of HMO conjugates and putative receptors (Chapter 5)

Literature Review

The Burden of Obesity and Metabolic Disease

Obesity is the single largest risk factor for the global burden of non-communicable diseases (NCDs), including cardiovascular disease, diabetes, stroke, and cancer. The World Health Organization (WHO) Consultation on Obesity first recognized obesity as a "global epidemic" in 1997, emphasizing its emergence in both industrialized and developing nations [3]. Of particular concern, the prevalence of this condition has doubled in over 70 countries since 1980 [4]. In the United States, the age-adjusted prevalence of obesity was estimated to be 42.4% in 2017-2018, an 11.9% increase from 1999-2000 [5]. The Behavioral Risk Factor Surveillance System (BRFSS) has released

prevalence maps for 2019, which are shown in Figure 1. It is now projected that over 2 billion adults are either overweight or obese and this number continues to increase worldwide. Furthermore, 41 million children under age 5 are considered overweight and will eventually face physical and psychological repercussions associated with their metabolic condition [6]. At this time, there appears to be little progress in terms of resolution.

Being obese not only contributes to personal health consequences, but also presents economic and societal burdens. Obese individuals often incur greater direct and indirect healthcare costs, such as those related to inpatient care, outpatient care, and prescription drug use. A model using Medical Expenditure Panel Survey (MEPS) data from 63,508 adults determined that obese adults spent an average of $5,010 per year on healthcare costs compared to normal weight adults, who spent an average of $2,504 between 2001 and 2016 [7]. In terms of societal impact, being obese contributes to decreased work output, higher insurance premiums for employers, lower quality of life, increased mental health issues, weight-related discrimination, etc. [8]. These alarming statistics suggest that obesity is an urgent health concern accompanied by a huge need for effective therapeutics.

Obesity is caused by a plethora of genetic and environmental factors and has long been defined as having a body-mass index (BMI) greater than 30kg/m^2, which is further categorized into three classes: class I (30-34.9kg/m^2), class II (35-39.9kg/m^2), and class III (≥40kg/m^2) [9]. Metabolic syndrome (MetS), in contrast, has a fluid definition that has changed over time. MetS was first described in 1988 as Syndrome X, which involved a combination of hyperglycemia, hypertension, insulin resistance, low HDL cholesterol,

and high VLDL-carrying triglycerides [10, 11]. Since then, diagnostic guidelines for MetS have been proposed by several groups. In 1998, the American Diabetes Association (ADA) and WHO Consultation agreed that MetS was defined as impaired glucose tolerance, insulin resistance, or full-blown T2DM in combination with at least two of the following factors: blood pressure ≥160/90 mmHg, triglycerides ≥150mg/dL, HDL cholesterol <35mg/dL for males and <39mg/dL for females, obesity (waist-to-hip ratio >0.90 for males and >0.85 for females or BMI >30kg/m^2), or microalbuminuria (urinary albumin excretion ≥20μg/min or an albumin to creatine ratio ≥20mg/g) [12]. In succession, the European Group for the Study of Insulin Resistance proposed hyperinsulinemia as an additional criterion, utilized different cutoff values for the aforementioned factors, and discredited the inclusion of microalbuminuria [13]. Later, the International Diabetes Foundation (IDF) adopted a worldwide definition of MetS, which included central obesity plus any two additional factors [14]. This definition is outlined in Table 1 and is considered the current standard.

In terms of treatment, obese individuals are encouraged to adopt drastic lifestyle modifications and/or are prescribed various pharmacological agents. It is now well-known that obesity is far more complex than mere caloric consumption and therefore, lifestyle modifications are rarely sufficient to combat this condition. Moreover, various "miracle" drugs (i.e. dinitrophenol, aminorex, mazindol, sibutramine, etc.) have been withdrawn from the market due to harmful side effects [15]. Currently, there are four FDA-approved drugs for weight-management (orlistat, lorcaserin, phentermine/topiramate, and naltrexone/bupropion). These drugs have had limited

success and have noticeable side effects [16]. For obese patients, surgical procedures become an expensive and risk-laden last resort.

Recent studies have demonstrated newfound interest in anti-inflammatory therapies for obesity and MetS. TNF-α inhibitors have been of particular interest, given landmark studies delineating the cytokine's clear role in contributing to insulin resistance within adipose tissue depots [17]. Nonetheless, human studies have led to sparse conclusions as anti-TNF-α therapies failed to improve insulin-related parameters in obese individuals [18, 19]. A conflicting study demonstrated that suppressing TNF-α with ethanercept reduced fasting plasma glucose concentrations and increased adiponectin over 6 months [20]. Another cytokine, IL-1β has also been implicated in mediating obesity-associated inflammation and deemed a valuable therapeutic target [21]. Antagonism of IL-1β using anakinra for 13 weeks reduced glycated hemoglobin levels, improved pancreatic beta cell function (proinsulin:insulin), and reduced markers of inflammation (IL-6 and C-reactive protein) [22]. Use of a neutralizing antibody against IL-1β also led to similar results [23].

Other drugs, such as salicylates, thiazolidinediones (TZDs), and metformin have demonstrated anti-inflammatory properties in the context of obesity and MetS. Salicylates, such as salsalate and aspirin, are some of the oldest non-steroidal anti-inflammatory drugs (NSAIDs) used to treat rheumatologic diseases [24, 25]. In several rodent and human trials, salsalate has been shown to inhibit NF-κB signaling to decrease cytokine secretion, reduce triglyceride levels, and improve insulin resistance [26-31]. TZDs are anti-diabetic drugs that bind to PPARγ to improve glycemic levels and reduce insulin resistance [32]. Similar to salsalates, TZDs have also been shown to inhibit NF-

κB signaling to decrease markers of inflammation [33]. Metformin is also an anti-diabetic drug with both metabolic and immune effects. Metformin acts on both NF-κB and JNK, thereby reducing inflammatory mediators (i.e. IL-1β, IL-6, C-reactive protein) [34-37].

Targeting inflammation in individuals diagnosed with obesity and MetS remains a promising therapeutic avenue for management of this condition and prevention of subsequent NCDs. However, it appears that these anti-inflammatory therapies must target multiple molecules to be effective. Furthermore, it is crucial that some inflammation remains for healthy cellular function [38]. The proposed mechanisms of adipose tissue inflammation and associated pathologies will be covered in the following section.

Adipose Tissue Inflammation Leads to Metabolic Dysregulation

Prior to its recognition as a complex endocrine organ, adipose tissue was well-known for its roles in lipid storage, insulation, and mechanical support. However, several landmark studies sparked a newfound interest in the role of adipose tissue in metabolic and immune homeostasis. In the 1960s, pathologists first identified immune cell infiltration in adipose tissue depots [39, 40]. However, it was not until the mid-1980s that Pekala et al. (1983) and Mahoney et al. (1985) demonstrated the first link between macrophages and adipocytes *in vitro* [41, 42]. These studies demonstrated that lipopolysaccharide (LPS) treatment of RAW 264.7 macrophages led to impaired insulin signaling in 3T3-L1 adipocytes, which provided evidence for a strong interaction between immunity and metabolism. At a similar time, Beutler et al. (1985) identified TNF-α, which was later shown to alter insulin action and cause hyperlipidemia in rodents [43-45]. Hotamisligil et al. (1993) was the first to demonstrate that TNF-α is 5 to 10-fold upregulated in adipose tissue of obese animals [17]. He also demonstrated that TNF-α is

secreted from both mature adipocytes and cells in the stromal-vascular fraction (SVF) of adipose tissue [17]. This finding was soon recapitulated in humans, when Hotamisligil et al. (1995) showed that obese individuals have a 2.5-fold increase in TNF-α in their adipose tissue [46]. This correlated with increased fasting insulin levels and BMI. Furthermore, weight loss resulted in coincident decreases in circulating insulin concentrations and adipose tissue TNF-α. Together, the studies mentioned here laid the foundation for the role of inflammation in development of metabolic disease.

Once these findings were reported, focus shifted towards a mechanistic explanation for impaired insulin resistance in the presence of inflammation. It was first reported that TNF-α reduced tyrosine phosphorylation of both the insulin receptor and insulin receptor substrate 1 (IRS-1), an adaptor protein that links the receptor to intracellular PI3K/AKT and ERK signaling [47, 48]. These findings were confirmed by Uysal et al. (1997), wherein DIO and *ob/ob* mice deficient in TNF-α exhibited improvements in insulin signaling and lowered circulating free fatty acids [49]. Since then, researchers have identified a plethora of inflammatory mediators involved in insulin function [50, 51].

Overnutrition directly impacts adipose tissue, resulting in excessive adipocyte proliferation (hyperplasia) and enlargement (hypertrophy). This leads to cellular stress, adipocyte death, and an overall adipokine imbalance that promotes immune cell influx into the tissue [52]. The identification of macrophage infiltration in obese adipose tissue was paramount to establishing the role of inflammation in metabolic disease. Macrophages are the most prominent immune cells involved in obesity-associated inflammation, accounting for up to 40% of cells in the adipose tissue of an overweight

individual [53, 54]. Upon recruitment to adipose tissue, macrophages accumulate around necrotized adipocytes to form crown-like structures and scavenge lipid droplets [55, 56]. At this point, adipose tissue macrophages (ATMs) also undergo a change in polarization to pro-inflammatory M1, which further exacerbates obesity-related inflammation [57]. M1-like macrophages are activated by LPS or T_H1 cytokines, such as IFN-γ. Activation of M1-like macrophages leads to secretion of pro-inflammatory cytokines (i.e. TNF-α, IL-6, etc.), which can promote insulin resistance within adipose tissue [58]. Two important gene expression studies were the first to determine that many genes upregulated in white adipose tissue were related to macrophages. Weisberg et al. (2003) profiled gene expression in white adipose tissue, brown adipose tissue, liver, stomach, hypothalamus, and pancreas from *ob/ob*, *db/db*, *tubby*, *agouti*, and diet-induced obese mice [53]. Of note, about 30% of the genes upregulated in white adipose tissue extracts were related to macrophage function. Confirmation experiments demonstrated that ADAM8, MIP-1α, MCP-1, MAC-1, F4/80, and CD68 were upregulated, albeit differently, in all models of obesity. This upregulation was most dramatic with onset of hyperinsulinemia. Moreover, these genes were mostly upregulated in the SVF of adipose tissue extracts. The second paper to demonstrate the importance of macrophage infiltration in obesity and insulin resistance came from Xu et al. (2003). This paper involved gene expression profiling of perigonadal adipose tissue isolated from male and female mice subjected to different diets or possessing different obesity-related mutations [54]. Results from these experiments determined that 1,304 transcripts could be correlated to body mass and that many of these transcripts were associated with macrophages. Moreover, macrophage infiltration correlated positivity with BMI and

adipocyte size. These macrophages also secreted significant amounts of TNF-α, iNOS, and IL-6. Confirmation studies in humans showed that body mass and adipocyte size were predictive of the presence of $F4/80^{+}$ macrophages in adipose tissue. Together, the two aforementioned studies established macrophages as critical cells involved in promoting adipose tissue inflammation and development of subsequent pathologies.

Now, adipose tissue has been shown to be comprised of adipocytes, fibroblasts, fibroblastic pre-adipocyte cells, endothelial cells, immune cells, and nerves [59]. Moreover, adipose tissue has been found to secrete bioactive mediators known as adipokines. These adipokines include classical cytokines and chemokines, vasoactive molecules, coagulation factors, regulators of lipoprotein metabolism, and adipocyte-specific proteins [60]. In the context of nutrient overload, these adipocyte-derived factors contribute to immune cell recruitment and subsequent inflammation within adipose tissue. This is summarized in Figure 2.

Once inflammation spreads to peripheral organs, insulin signaling is altered in insulin-sensitive tissues (i.e. pancreas, liver, skeletal muscle). The convergence of immune and insulin signaling is shown in Figure 3. One of the most notable consequences of obesity-associated inflammation is non-alcoholic fatty liver disease (NAFLD). 50% of individuals diagnosed with NAFLD are obese [61]. NAFLD is now referred to as metabolic dysfunction-associated fatty liver disease (MAFLD) and is defined by factors similar to MetS [62, 63]. Revised criteria for diagnosis of MAFLD are outlined in Table 2 [62].

During development of MAFLD, lipid accumulation in the liver impairs cellular function and triggers inflammation. Lipid accumulation occurs primarily via two

mechanisms. Breakdown of lipids in adipose tissue releases free fatty acids (FFAs), which enter circulation and become stored in the liver. Fat accumulation also occurs via *de novo lipogenesis*, in which hepatocytes produce lipids from excess carbohydrates [64]. Together, these mechanisms compromise insulin signaling and β oxidation within hepatocytes and promote immune cell infiltration [65]. Liver inflammation is perpetuated via communication with the gut, which absorbs FFAs and allows entrance of bacterial products into portal circulation [66].

Obesity and MetS are associated with changes in the gut microbiome, but it is still controversial whether these changes are causative or consequential to the condition. Obese individuals present with less diverse microbiomes, which have been correlated with increases in fat content and circulating lipids, impairments in glucose regulation, and greater degrees of inflammation [67]. In this regard, a diverse microbiome is considered healthier and several studies have reported outgrowth of heterogenous bacterial populations in response to Roux-en-Y gastric bypass (RYGB) or weight loss [68, 69]. In a comparison of lean and obese twins, being obese was correlated with reduced α-diversity, changes in biome at the phylum level, and alterations in metabolic signaling [70]. Obese twins had a greater proportion of genes from Actinobacteria and Firmicutes, whereas lean twins had a greater proportion of Bacteroidetes [70]. This is a common trend in comparisons of lean and obese humans, where the ratio of Bacteroides:Firmicutes is decreased in obese individuals and has been proposed as a biomarker for dysbiosis [71]. In *ob/ob* mice, increases in Firmicutes led to a higher proportion of genes related energy derivation from food components [72]. Gut bacterial populations contribute to obesity and MetS by exerting specialized functions and

producing metabolites that enter circulation to impact the immune response and metabolism. Identification of specific bacterial species and their respective functions are of great interest for deciphering the mechanisms of obesity and MetS, as well as developing treatments.

Obesity and MetS not only impact adipose tissue, liver, and the gut, but also other peripheral organs. These impacts are briefly illustrated in Figure 4, but reviewed in-depth elsewhere [73-76].

Helminths Help Regulate Inflammation

Despite an overall decrease in viral, microbial, and parasitic infections in industrialized countries, the coincident increase in autoimmune and inflammation-based diseases is alarming. Various epidemiological and animal studies attribute this inverse relationship to the infamous Hygiene Hypothesis, in which reduced exposure to pathogens and improved sanitation methods prompt exaggerated T_H1 immune responses against inflammatory stimuli and self-antigens [77]. It is well-known that helminth parasites induce an anti-inflammatory environment along with T_H2-biased responses that can counter-regulate exaggerated T_H1 responses, and as a result, various research efforts have been devoted to utilizing helminths and/or helminth products for amelioration of autoimmune and inflammation-based diseases.

In particular, *Schistosoma mansoni* is a digenetic trematode parasite that infects at least 200 million individuals worldwide [78]. Upon initial infection, *S. mansoni* triggers a strong T_H1 response against skin-penetrating cercariae. These cercariae transform into migrating schistosomula and egg-producing adult worms within the host, thereby continuously presenting new antigens and exacerbating T_H1 immune responses. This

causes antigen-presenting cells (APCs) to secrete IL-12, IL-18, and TNFα, which drives development of T_H1 $CD4^+$ T cells and production of IFN-γ [79, 80] . Within 2-4 weeks of initial egg deposition by adult worms, the immune response shifts from T_H1 to T_H2-biased [81]. At this point, eggs are transported through the vasculature to the intestine and various organs. Eggs that fail to reach the intestine become trapped in various organs (i.e. liver, lung, pancreas, lymph nodes, etc.), causing granuloma formation and subsequent fibrosis [82]. This leads to production of IL-4, IL-5, IL-10, and IL-13, which exert various functions to limit inflammation [83, 84].

Given that egg deposition is crucial for driving the T_H2-biased immune response during *S. mansoni* infection, numerous studies have been performed to characterize the immune mechanisms associated with this stage of disease. For instance, elimination of the T_H2 response via IL-4 ablation leads to uncontrolled damage and host death during *S. mansoni* infection [85, 86]. In terms of protection, IL-4 minimizes production of nitric oxide, reactive oxygen, and TNF-α [85, 87]. Moreover, IL-4 promotes polarization of M2-macrophages in conjunction with IL-13 [88]. IL-10 also promotes M2-macrophages and limits dendritic cell activation [88]. These actions are important in the context of inflammation because M2 macrophages secrete anti-inflammatory cytokines and dendritic cell inhibition prevents activation of T cells [88]. Overall, induction of an anti-inflammatory phenotype and T_H2-biasing of the immune response during *S. mansoni* egg deposition protects the host during chronic infection.

Okano et al. sought to determine the molecules within *S. mansoni* soluble egg antigens (SEA) that were responsible for $CD4^+$ T_H2-biasing [89]. In these experiments, SEA was treated with 10 mM sodium metaperiodate ($NaIO_4$) to alter the molecular

conformation of glycans in SEA. Mock-treated or $NaIO_4$-treated SEA was injected into mice to assess cytokine responses. Mice injected with $NaIO_4$-treated SEA did not produce IL-4 or IL-5, whereas mice injected with mock-treated SEA mounted strong T_H2-biased immune responses. These studies were corroborated by Tawill et al., who demonstrated that removal of filarial glycans eliminated T_H2-biasing [90].

Since the elucidation of *S. mansoni's* immuno-modulating properties, the parasite and its associated products have been well-studied in the context of non-communicable diseases. For instance, Zaccone et al. demonstrated that direct administration of soluble *S. mansoni* egg antigen (SEA) protects against type 1 diabetes (T1D) via expansion of T_H2 cells, polarization of M2 macrophages, and upregulation of IL-10, IL-2 and C-type lectins in antigen-presenting cells (APCs) [91, 92]. Moreover, chronic *S. mansoni* infection has been shown to decrease overall inflammation and improve insulin signaling in obese mice [93, 94]. Direct infection with *S. mansoni* has also been deemed therapeutic in murine models of collagen-induced arthritis (CIA), experimental autoimmune encephalomyelitis (EAE), asthma, etc. [95]. During collagen-induced arthritis, *S. mansoni* infection leads to decreases in IL-6, IL-17, TNF-α, and anti-collagen IgG antibodies [96]. In a similar fashion, pre-established *S. mansoni* infection leads to decreased levels of IFN-γ, IL-12, and TNF-α during EAE [97]. Last, *S. mansoni* infection has been shown to suppress allergic inflammation in the lung via production of IL-10 [98]. Overall, the examples mentioned herein emphasize the invaluable potential of helminth immunomodulation as source of anti-inflammatory therapeutics. Since helminth infection is not a viable option for clinical use, identification and isolation of helminth products is crucial for harnessing their therapeutic abilities.

Helminths and Human Milk Oligosaccharides Shared a Conserved Structure: Lewis^x

Within *S. mansoni* SEA, Lewis^x moieties have been well-studied and recognized as one of the target structures of monoclonal antibodies produced against the parasite [99-101]. Previous studies from Dr. Harn's lab demonstrated that anti-egg monoclonal antibodies were able to bind to D9-D10 fetal mouse brains, which are organs rich in various glycoproteins and useful for functional screens. Further studies demonstrated that these monoclonal antibodies bound LNFPIII, a pentasaccharide that contains Lewis^X [102]. Lewis^x has been shown to bind DC-SIGN on APCs in an interaction that is dependent on multimeric presentation of fucose residues [103]. Furthermore, co-stimulation of APCs with Lewis^x and LPS leads to enhancement of IL-10, as well as suppression of IL-6 and IL-12 [104]. The fact that *S. mansoni* co-evolved to express Lewis^x lends credence to the parasite's immune-biasing of the host as a survival advantage. Future studies have focused on the immunomodulating properties of LNFPIII, an HMO.

Human Milk Oligosaccharides (HMOs) Provide Numerous Benefits for a Breastfeeding Infant

A mother's breastmilk is often the first substance an infant consumes after birth and is known to be crucial for development of the immune system and intestinal microbiome. For these reasons, WHO recommends exclusive breastfeeding for an infant's first 6 months of life and supplemental breastfeeding for ~2 years thereafter [105]. Compared to formula-fed infants, breast-fed infants have been shown to be less susceptible to both infectious and immune-mediated diseases [106]. In this regard, the composition of human breastmilk has become an increasingly important topic of interest.

Human breastmilk provides ideal nutritional value to a breastfeeding infant, containing vitamins and minerals, as well as an abundance of bioactive compounds (i.e. immunoglobulins, cytokines, growth factors, hormones, human milk oligosaccharides, etc.). Human milk oligosaccharides (HMOs) are the third most abundant component of human breastmilk, behind the disaccharide lactose (70g/L) and lipids (40g/L) [107]. HMOs are present at concentrations from 5-15g/L and this concentration appears to be higher in colostrum (20-25g/L). Concentrations of HMOs are influenced by several factors, such as maternal health, secretor status, milk maturation, and week of delivery [107-109].

HMO biosynthesis is thought to be an expansion of lactose production, which occurs in the Golgi apparatus of cells in the mammary gland. Lactose is a disaccharide containing galactose attached to glucose via a β1,4 linkage, a reaction made possible through the work of lactose synthase. Lactose can then be bound on its non-reducing end to different combinations of glucose (Glc), galactose (Gal), N-acetylglucosamine (GlcNAc), fucose (Fuc), and sialic acid (Neu5Ac) through glycosidic linkages to form HMOs with various spatial arrangements. It is most common for lactose to be bound to lacto-N-biose via a β1,3 linkage or to N-acetyllactosamine via a β1,6 linkage. Branching is introduced via fucose or sialic acid. Fucose can be attached to terminal positions via α1,2 or α1,3/4 linkages by fucosyltransferases. Sialic acid can also be attached through α2,3 or α2,6 linkages by sialyltransferases. Over 200 HMOS have been defined to date, ranging in size from 3-22 monosaccharides [110]. Basic HMO structure is shown in Figure 5. HMOs have been divided into three categories: 1) neutral, non-fucosylated (42-55%), 2) neutral, fucosylated (35-50%), and 3) acidic, sialylated (12-14%) [111]. As

alluded to earlier, secretor status can impact HMO concentrations. Secretor mothers have active *FUT2* genes, which encode the fucosyltransferase responsible for constructing α1,2-linked structures. Women with inactive *FUT2* genes fail to produce α1,2-fucosylated HMOs, such as 2'fucosyllactose (2'FL), but possess increased concentrations of lacto-N-tetraose (LNT), lacto-N-fucopentaose I (LNFPI), lacto-N-fucopentaose III (LNFPIII), and lacto-N-difucohexaose II (LNDFHII) [112]. HMO concentrations also depend on *FUT3* genes, which encode for a fucosyltransferase responsible for constructing α1,3-linked structures. Women negative for *FUT3*, however, can still synthesize some α1,3-linked HMOs because of functional redundancies provided by *FUT4*, *5*, *6*, *7*, and *9* [113].

HMOs are indigestible and resistant to degradation in the stomach [114, 115]. HMOs are largely metabolized by bacteria in the intestinal microbiome [107]. Remaining HMOs are excreted in the urine or feces and up to 1% has been found in circulation [116-119]. Given that HMOs are present in the circulation of breastfeeding infants, it is plausible that their effects on distant organs are abundant and far-reaching. To date, HMOs are postulated to have anti-microbial, immunomodulating, cell signaling, and prebiotic functions.

HMOs act as snares for infectious pathogens via two distinct mechanisms, either binding to host epithelial cells to block invasion or forming complexes with pathogens that can be passed in the feces. In the former scenario, HMOs pass through mucosal surfaces and bind to lectin receptors on epithelial cells to block them from pathogens. This means that these receptors are no longer available for pathogen binding and thus, adhesion and colonization are prevented. In the latter scenario, HMOs mimic host

receptors to which pathogens bind. This prevents pathogens from binding to receptors on host cells because they are misled into binding to HMOs. Fucosylated HMOs provide the greatest protection against pathogens and there is some evidence that non-secretor mothers sacrifice some protective function [120]. The anti-adhesive and anti-microbial properties of HMOs have been well-documented for several pathogens, such as *Campylobacter jejuni*, *Pseudomonas aeruginosa*, and *Escherichia coli* [121-123]. HMOs also possess indirect antimicrobial functions, as fermentation processes in the gut reduce pH levels and create an unfavorable environment for harmful bacteria.

Since HMOs bind host cell receptors, such as C-type lectins, galectins, selectins, and siglectins, it is obvious that these structures can exert cellular and immune functions [124]. Some studies have shown that HMOs alter processes related to cell growth, differentiation, and apoptosis in intestinal epithelial cells [125, 126]. Transcriptional studies have also shown that HMOs alter cytokines, chemokines, and cell surface receptors in colonic epithelial cells *in vitro* [127]. In terms of immunological function, HMOs can prevent immune cell rolling and migration into tissues through binding to E- and P-selectins [128]. HMOs also bind to dendritic cells (DCs) via dendritic cell-specific intercellular adhesion molecule-3-grabbing non-integrin (DC-SIGN) and Toll-like receptor 4 (TLR4), leading to semi-maturation of DCs and promotion of T regulatory cells (Tregs) [129, 130]. These studies demonstrate that HMOs can have both local and distant effects on cellular and immune cell function.

HMOs reach the intestine intact, providing nutrients for commensal bacteria and shaping the microbiome. *Bifidobacterium* are the most well-studied commensals that can utilize HMOs as the sole carbon source [131-133]. *B. infantis*, for example, contains 24

glycosidases for sugar digestion (i.e. β-galactosidase, β-hexosaminidase, fucosidase, sialidase, etc.), while *B. breve* can only digest free monosaccharides [108, 134]. It is likely that some species of *Bifidobacterium* are able to digest and release free monosaccharides from HMOs to feed other commensals. In addition to *Bifidobacterium*, *Bacteroides a*re also known to feed on HMOs [135]. Some species, such as *Bifidobacterium longum* and *Bacteroides vulgatus* favor digestion of fucosylated HMOs [136]. Differences in the intestinal microbiome of breastfeeding infants have been reported, depending on the secretor or non-secretor status of the mother [137, 138]. 2'FL and LNnT supplementation in formula has also led to increased *Bifidobacterium* and reduced *Escherichia* and Peptostreptococcaceae in infants [139]. The postulated benefits of HMOs are shown in Figure 6.

In this work, we focus on the immunomodulating and prebiotic effects of LNFPIII and LNnT conjugates. LNFPIII is a neutral, fucosylated HMO that contains Lewis^x and is present at concentrations of 0.33g/L in human milk [140]. Due to the presence of the α1,3-linked fucose, chemical synthesis of LNFPIII has been difficult. In contrast, LNnT is a neutral, non-fucosylated HMO that is present at higher concentrations in human milk (0.74g/L) and has also been chemically synthesized by various laboratories [141-144]. Glycom A/S has registered LNnT for use in infant formula in Europe (Novel Food Application 157) and the United States (GRAS Notice 659) [145]. Furthermore, pre-clinical assessment has been conducted on a chemically synthetized version of LNnT and there were no adverse effects at doses of up to 5000mg/kg/day in rats [144]. LNnT is well-tolerated in humans at doses up to 20g/day and shifts the intestinal microbiome in favor of *Actinobacteria* and *Bacteroidetes*. Similar studies on LNFPIII are unavailable at

this time. Most studies involving LNFPIII utilize this HMO in conjugate form, which will be addressed in the following section.

HMO Conjugates Act on Different Cell Types and Differ in Mechanism

We utilize LNFPIII (mw: 853.77g/mol) and LNnT (mw: 707.6g/mol) conjugates that contain 10-12 molecules of either HMO attached to 40 kDa dextran (DEX; glucose polymer) or human serum albumin (HSA; protein carrier) via an acetylphenylenediamine (APD) linker. The total weight of a single conjugate is about 50 kDa [146]. The structure of each conjugate is shown in Figure 7. Throughout this work, we will refer to LNFPIII and LNnT dextran conjugates as P3DEX or NTDEX. We will refer to LNFPIII and LNnT HSA conjugates as P3HSA or NTHSA (Chapter 4). The combined use of a carrier molecule and this specific linker-spacer method increases the concentration of each HMO in the conjugates and allows each molecule to rotate in space. This conjugate structure is also pertinent, given that previous studies have shown that Lewis^x within LNFPIII must be presented on adjacent molecules or in multimeric form to induce an immune effect [147]. Our previous approach was to purchase purified LNFPIII (Dextra Laboratories Ltd) or LNnT (Neose Technologies, Inc.) and ship it to our collaborator, Dr. Thomas Norberg (Uppsala University, Uppsala, Sweden), for conjugation to dextran. However, the increasing costs of human breastmilk made purchasing LNFPIII and LNnT an expensive venture. Therefore, we sought collaborators capable of synthesizing LNFPIII and/or LNnT using chemical methods. We established a collaboration with Dr. Peng George Wang (Georgia State University, Atlanta, GA) for synthesis of LNnT and LNFPIII.

The earliest studies involving LNFPIII conjugates utilized P3HSA. Velupillai et al. first demonstrated that P3HSA induced B cells from infected mice to secrete large amounts of prostaglandin E_2 and IL-10 [148]. This was further elucidated in studies that determined that injection of P3HSA led to B-1 cell outgrowth in specific mouse strains [149, 150]. P3HSA-induced B-1 cell outgrowth was shown to be regulated by IL-10, IL-12, and IFNγ. IL-10 exerted an autocrine function on B-1 cells to promote expansion, while IL-12 and IFNγ acted as inhibitors [151]. P3HSA stimulation induced IL-10 production in human peripheral blood mononuclear cells (PBMCs) isolated from schistosome-infected patients [152]. Subsequent studies demonstrated that repeated P3HSA treatments induced anti-HSA-specific IgG and IgE responses in mice [153]. The anti-HSA antibodies were likely neutralizing P3HSA, thereby diminishing its therapeutic potential. Therefore, future studies switched to use of P3DEX.

P3DEX has been shown to act on APCs, such as macrophages and dendritic cells. In particular, Atochina et al. demonstrated that $F4/80^+/CD11b^+$ peritoneal macrophages isolated from mice treated with P3DEX were able to suppress proliferation of $CD4^+$ T cells [154]. Moreover, $F4/80^+$ macrophages stimulated with P3DEX also activated natural killer (NK) cells in a manner independent of IL-12 [155]. Further studies demonstrated that P3DEX upregulates several molecules and markers consistent with alternative macrophage activation. For example, P3DEX treatment promoted *arg1* and *ym1* expression in peritoneal exudate cells (PECs). PECs stimulated with P3DEX also expressed common activation markers, such as CD80 and ICAM-1. Furthermore, adoptive transfer of treated PECs into OVA-specific DO.11.10 mice induced production of IL-10 and IL-13 from T cells [156]. PDEX treatment of OVA peptide-fed dendritic

cells increased IL-4 secretion in co-cultured $CD4^+$ T cells [157]. Although P3DEX promotes TH_2-biased signaling, it still drives $CD8^+$ effector and memory responses when compared to LPS [158]. This demonstrates that P3DEX induces anti-inflammatory effects, but does not suppress the overall immune response.

In terms of mechanism, it is most probable that P3DEX binds to C-type lectin receptors to modulate TLR4 signaling. This is evidenced by the fact that P3DEX is internalized via a clathrin/dynamin-dependent, caveolin-independent endocytic pathway that requires Ca^{2+} [159]. Upon internalization, P3DEX induces a transient NF-κB response that favors accumulation of p50, but is not associated with the degradation of IkBβ [157]. Furthermore, P3DEX drives a late ERK response that occurs via an interaction with CD14 and induces a TLR4-Ras-Raf1-Syk-Tpl2-MEK signaling cascade [160]. While P3DEX influences NF-κB and ERK signaling, it does not activate JNK or p38 [160]. Overall, P3DEX induces a unique signaling cascade that is beneficial and unique in the context of inflammation.

Less studies have been performed to elucidate the mechanism of NTDEX. Terrazas et al. (2001) showed that injection with NTDEX increased $Gr1^+$ populations of $CD11b^+$ and $F4/80^+$ cells in the peritoneum. These populations secreted lower levels of IL-1β, IL-12, IL-18, and IFNγ, but higher levels of IL-10 and TGFβ. These cells also suppressed $CD4^+$ T cell proliferation, decreased IFNγ and increased IL-13 in peritoneal exudate cell and CD4+ T cell co-cultures [161]. Tundup et al. (2015) later showed that LNnT conjugates failed to activate NFκB via TLR4/CD14 in HEK293 cells, while LNFPIII conjugates did stimulate this signaling cascade [160]. This suggested that the

presence of the fucose on LNFPIII was responsible for the apparent mechanistic differences between the two conjugates.

LNFPIII Conjugates are Therapeutic for Inflammation-Based Diseases

Previous studies have shown that LNFPIII conjugates prolong cardiac allograft survival, reduce skin lesions during psoriasis, decrease brain inflammation during experimental autoimmune encephalomyelitis (EAE), prevent neurological perturbations during Gulf War Illness (GWI), ameliorate hepatic steatosis, and improve insulin signaling during obesity [162-167]. In particular, two injections of LNFPIII conjugates prolonged cardiac allograft survival in both a non-vascularized and vascularized model of neonatal ear-heart transplantation. This coincided with increased surface expression of PD-L1 on $F4/80^+$ macrophages, $CD4^+$ T cells, and $CD11b^+CD11c^+$dendritic cells. Treated mice also demonstrated an accumulation of $Foxp3^+$ regulatory T cells and increased *arg1* and *ym1* in draining lymph node cells. This response was local, as it was not observed in the spleen [162]. In the EAE murine model of multiple sclerosis, LNFPIII conjugate treatment lessened CNS infiltration of $CD4^+$ T cells, $F4/80^+$ macrophages, and $CD11c^+$ dendritic cells. This coincided with an increase in T_H2 cytokines [164]. During psoriasis, lesions were less severe and skin cells secreted less IFNγ and more IL-13 in response to LNFPIII conjugate treatment. LNFPIII conjugate treatment also normalized the ratio of CD4:CD8 T cells [163]. In two models of GWI, LNFPIII conjugate treatment prevented changes in serotonin, dopamine, and homovanillic acid in different regions of the brain that occurred in response to chemical exposure. In the spleen, LNFPIII conjugate treatment increased serotonin. Upon evaluation of immune transcripts, LNFPIII conjugates reduced increases in *fizz1*, *casp1*, *ym1*, *il1b*, and *ccl1*, but increased

il18 [166]. In the gut, LNFPIII conjugate treatment decreased lipocalin-2 and increased butyrate-producing bacteria during GWI [167].

Most relevant to this project, LNFPIII conjugates drove M2 macrophage polarization, improved insulin signaling, and alleviated hepatic steatosis in a male model of DIO mice [165] . LNFPIII conjugate treatment of bone-marrow derived macrophages (BMDMs) induced expression of *il10* and upregulated the following M2 markers: *arg1*, *ym1*, and *mgl1*. This was recapitulated *in vivo*, where LNFPIII conjugate treatment of DIO mice led to higher circulating IL-10 concentrations and improved glucose tolerance. Furthermore, LNFPIII conjugate treatment decreased macrophage infiltration and crown-like structures in WAT. This coincided with decreases in transcripts of *tnfa*, *casp1*, *nlrp3*, *il18*, and *il1β*. Overall, LNFPIII conjugate treatment decreased inflammation in WAT and improved insulin signaling via upregulation of insulin receptor β (i*nsrb*), insulin receptor substrate 2 (*irs2*), CCAAT/enhancer-binding protein α (*cebpa*), and glucose transporter 4 (*glut4*). LNFPIII conjugate treatment of DIO mice also led to improved liver function with concomitant decreases in lipogenic genes (*fas*, *acc1/2*, *scd1*, and *srebp1c*) [165].

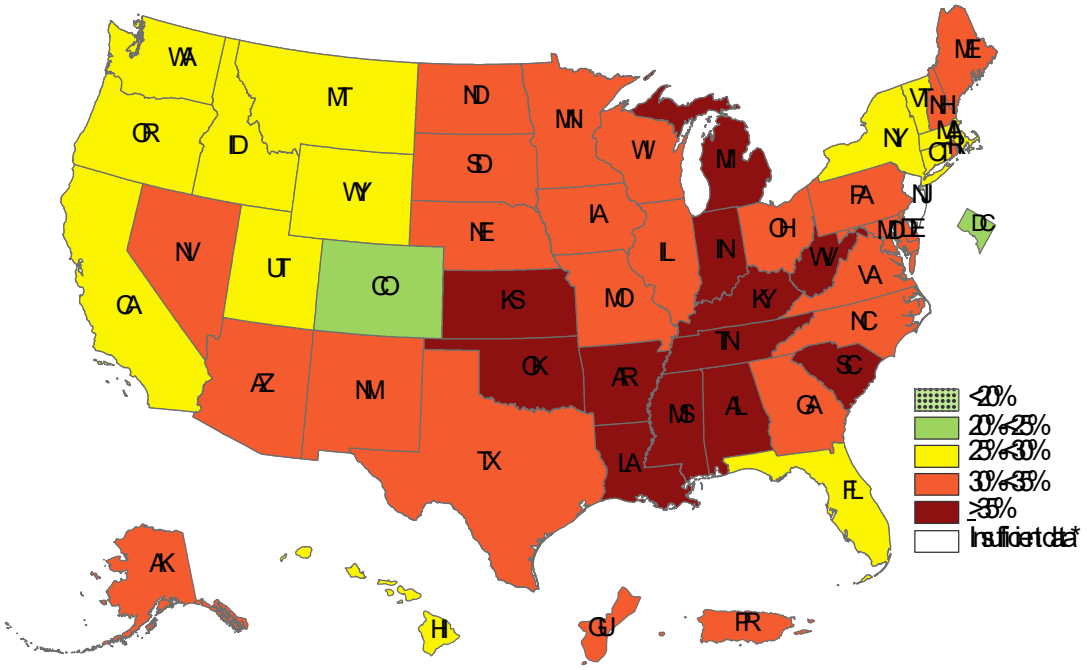

Figure 1.1: Prevalence of self-reported obesity among U.S. adults by state and territory, BRFSS, 2019. Reprinted from *CDC*, "Adult Obesity Maps." Retrieved from https://www.cdc.gov/obesity/data/prevalence-maps.html.

Table 1.1: IDF Definition of MetS

Central Obesity	BMI >30kg/m^2 or ethnicity-specific waist circumference
Increased Triglycerides	≥150mg/dL
Decreased HDL Cholesterol	≤40mg/dL for males; ≤50mg/dL for females
Increased Blood Pressure	Systolic ≥130; Diastolic ≥85
Increased Fasting Blood Glucose	≥100mg/dL

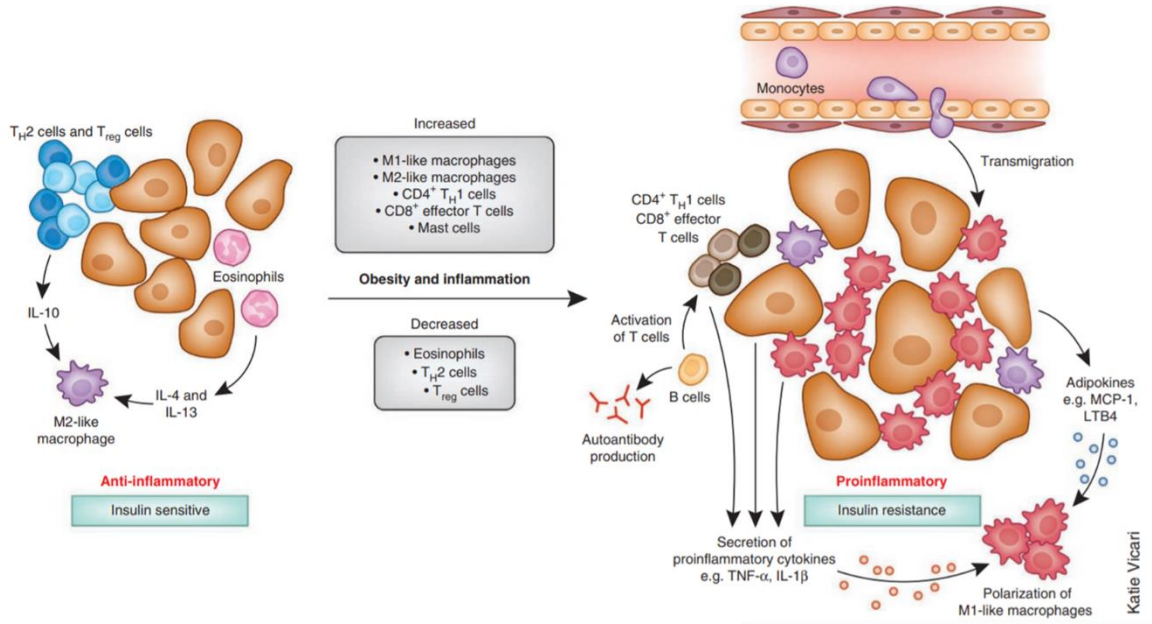

Figure 1.2: Obesity causes adipose tissue inflammation and insulin resistance. Reprinted from "The Cellular and Signaling Networks Linking the Immune System and Metabolism in Disease" by O. Osborn & J.M. Olefsky, 2012, *Nature Medicine*, 6;18(3):363-74 © 2012 *Nature Research*.

Table 1.2: Current Criteria for Diagnosis of MAFLD [62]

Overweight/Obesity or T2DM, Liver Fat Accumulation, Plus:	
Waist Circumference	≥102cm for males; ≥88cm for females
Increased Triglycerides	≥150mg/dL*
Decreased HDL Cholesterol	≤40mg/dL for males; ≥50mg/dL for females*
Increased Blood Pressure	≥130mm Hg systolic; ≥85mm Hg diastolic*
Increased Homeostasis Model Assessment of Insulin Resistance (HOMA-IR)	≥2.5
Increased High-Sensitivity C-Reactive Protein Levels	≥2mg/L

*or prescription drug treatment

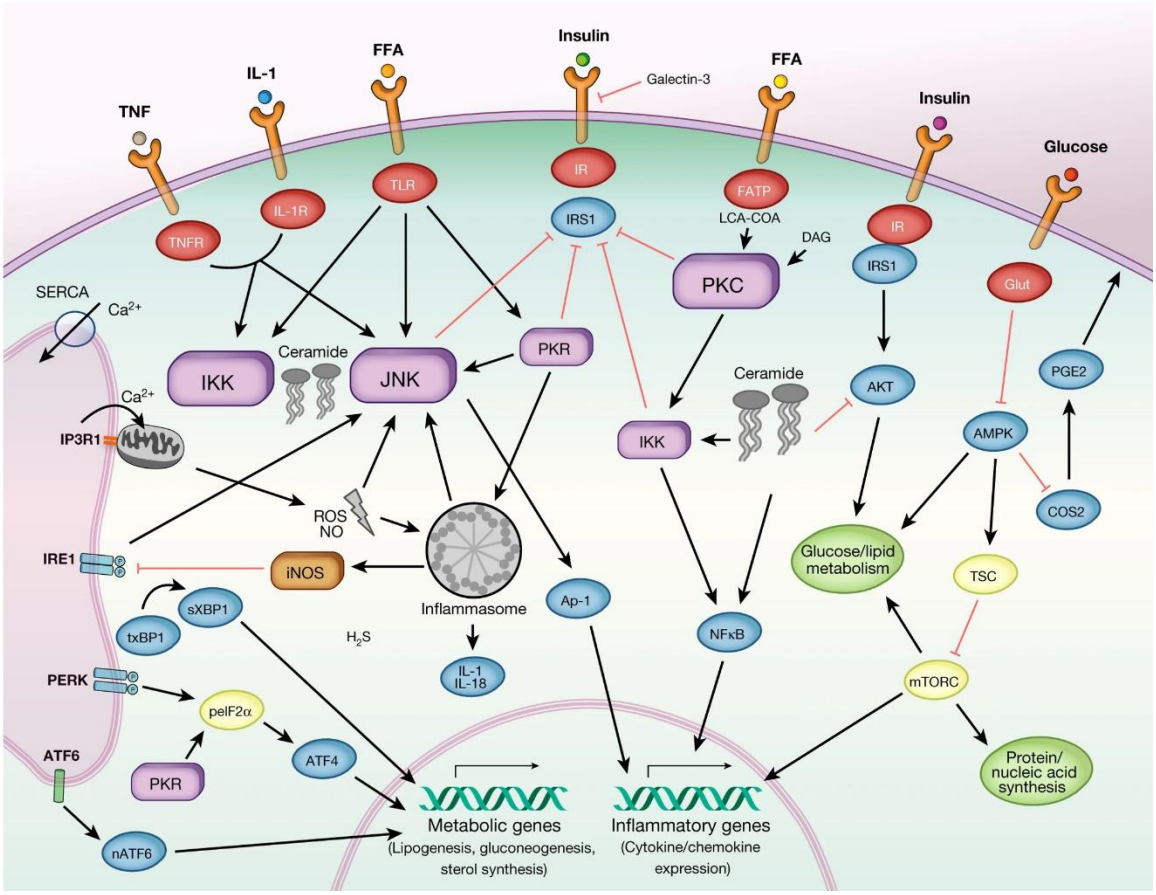

Figure 1.3: Interaction between inflammation and insulin signaling. Reprinted from "Foundations of Immunometabolism and Implications for Metabolic Health and Disease" by G.S. Hotamisligil, 2017, *Immunity 47(3):406-420 © 2017 Cell Press.*

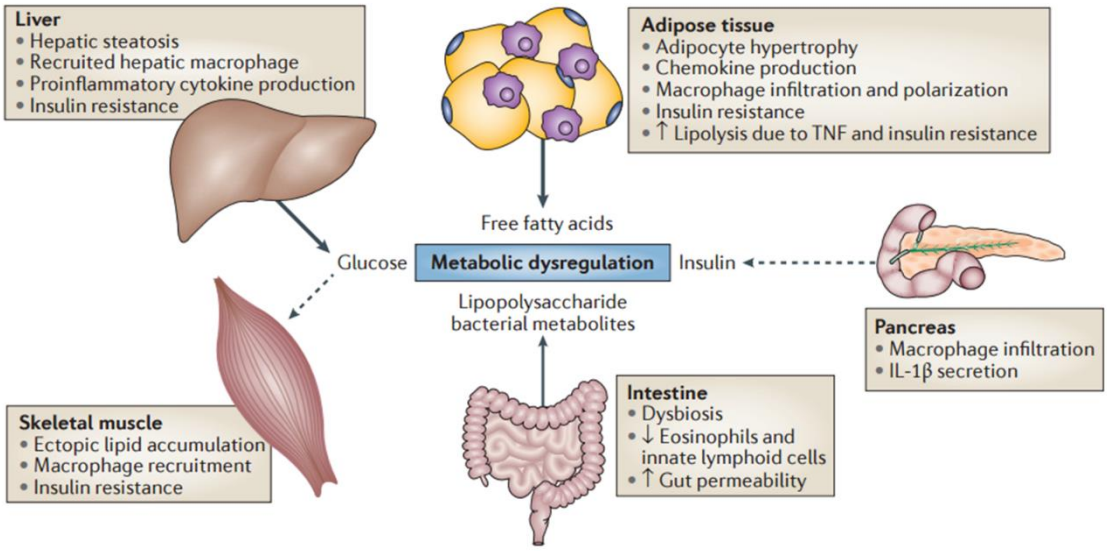

Figure 1.4: Adipose tissue inflammation spreads to peripheral organs. Reprinted from "Regulation of Metabolism by the Innate Immune System" by D.E. Lackey & J. Olefsky, 2016, *Nature Reviews Endocrinology* 12(1):15-28 © 2016 *Nature Research*.

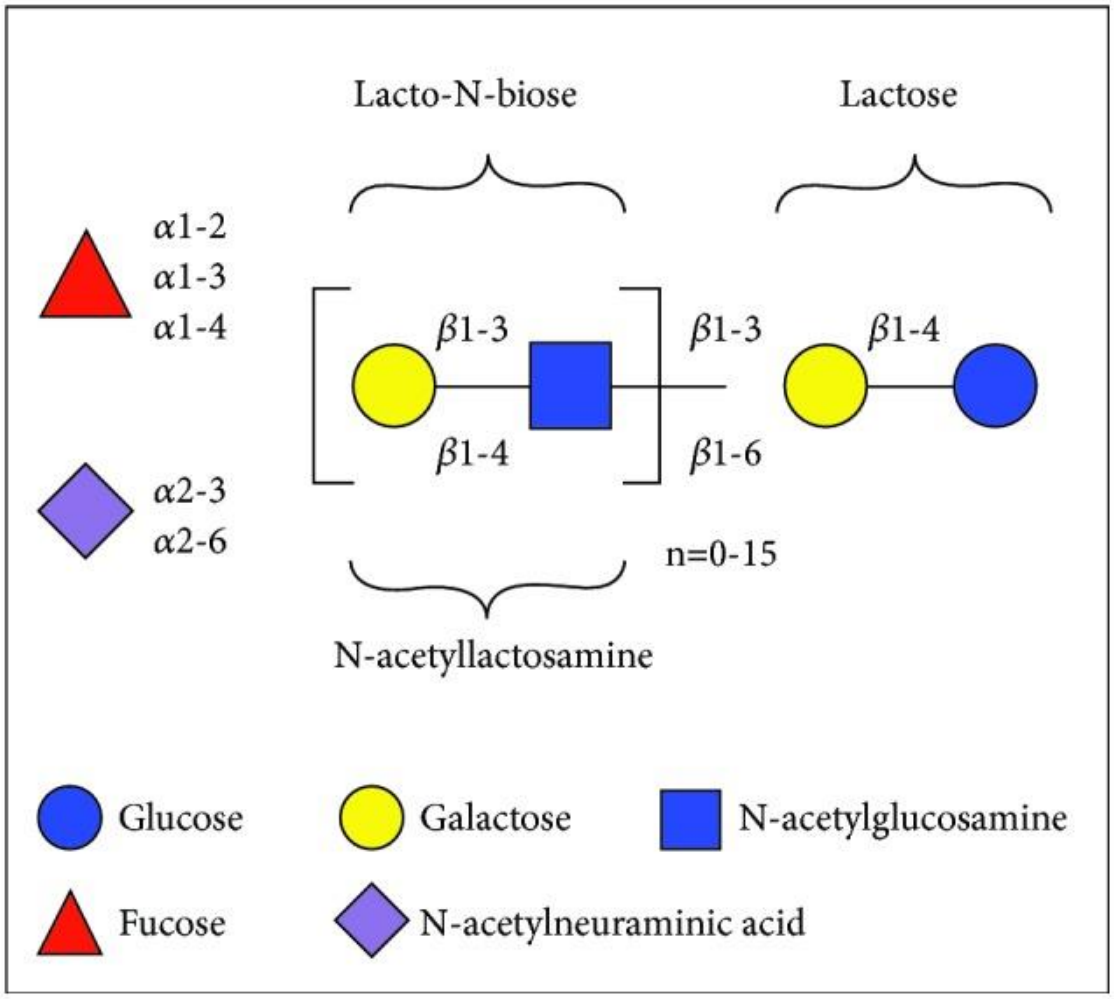

Figure 1.5: Basic HMO structure. Reprinted from "Human Milk Oligosaccharides: The Journey Ahead" by C. Ray et al., 2019, *International Journal of Pediatrics* 2390240 © 2019 *Hindawi Publishing Corporation*.

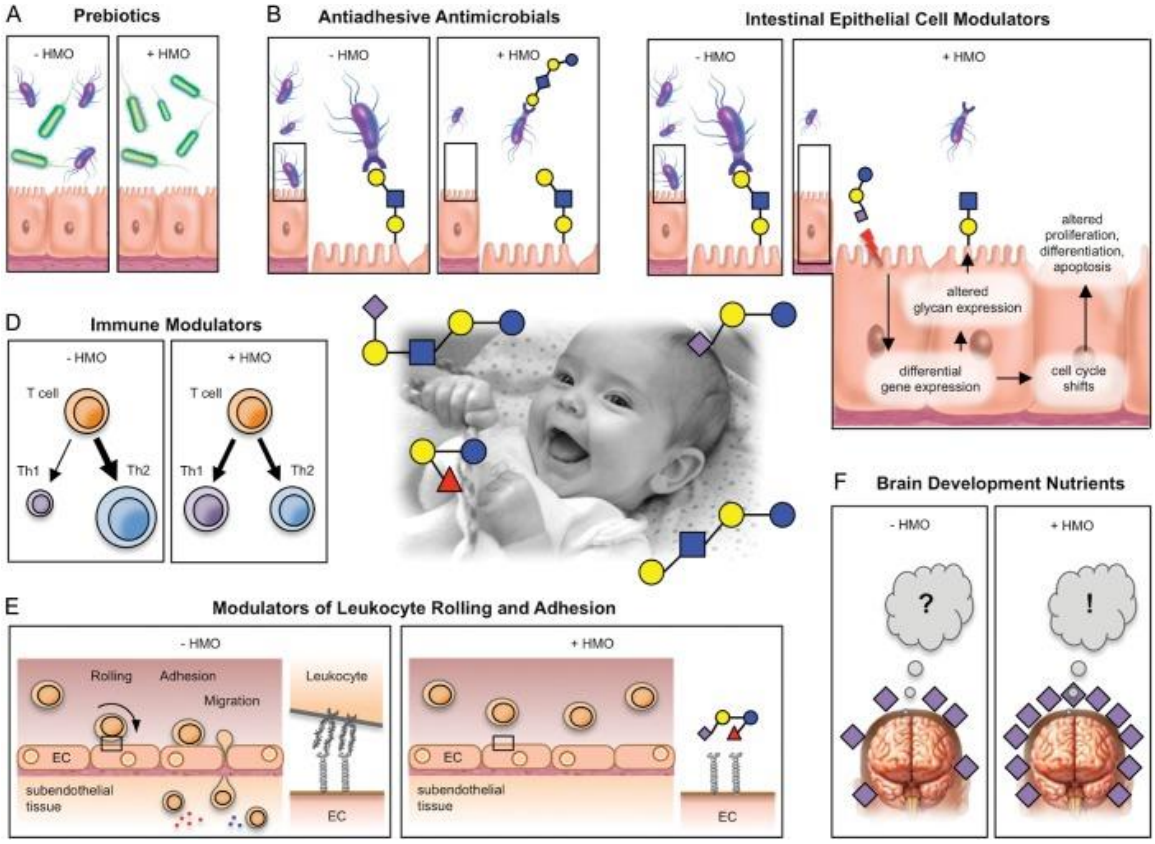

Figure 1.6: Benefits of HMOS. Reprinted from "Human Milk Oligosaccharides: Every Baby Needs a Sugar Mama" by L. Bode, 2012, *Glycobiology* 22(9): 1147–1162 © 2012 *Oxford University Press*.

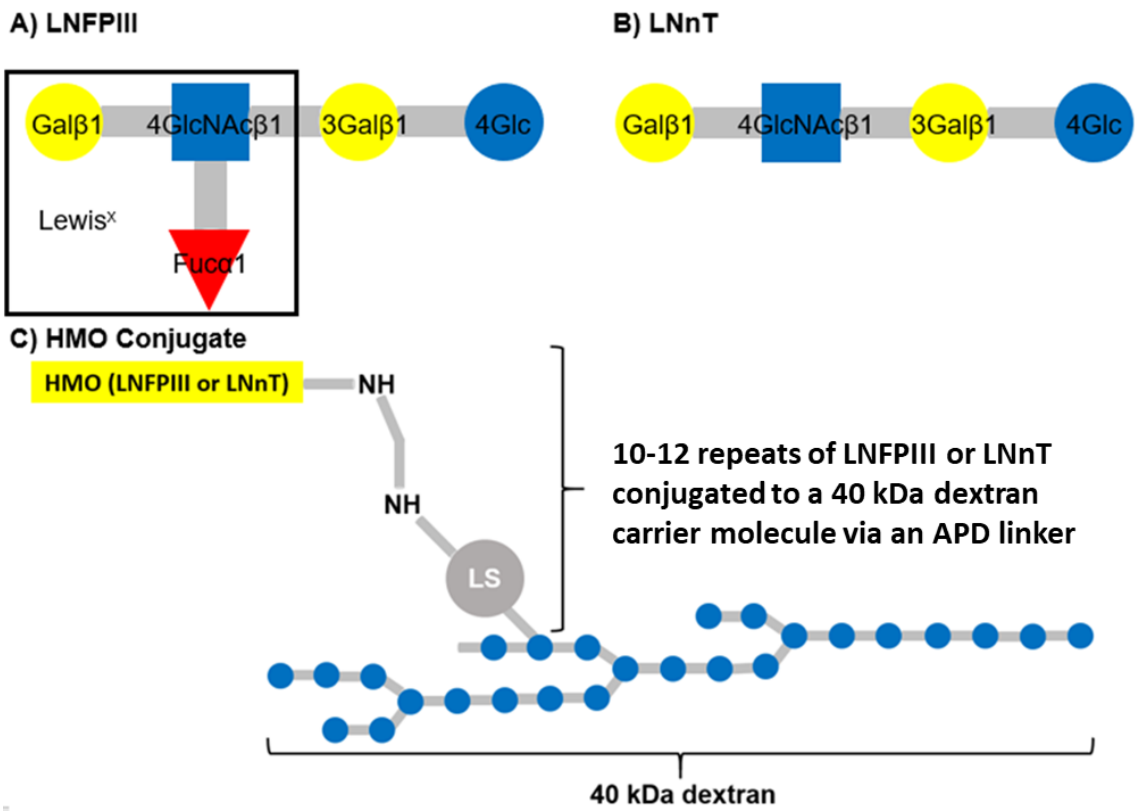

Figure 1.7: LNFPIII, LNnT, and HMO conjugate structure. Structures of **A.** LNFPIII, **B.** LNnT, and **C.** HMO conjugates.

CHAPTER 2

A COMPARISON OF TWO STRUCTURALLY RELATED HUMAN MILK OLIGOSACCHARIDE CONJUGATES IN A MODEL OF DIET-INDUCED OBESITY[1]

[1] Ramadhin et al. Submitted to *Frontiers in Immunology*, 2/15/2021. In Revision.

2.1 Abstract

Obesity is the largest risk factor for the development of chronic diseases in industrialized countries. Excessive fat accumulation triggers a state of chronic low-grade inflammation to the detriment of numerous organs. To address this problem, our lab has been examining the anti-inflammatory mechanisms of two human milk oligosaccharides (HMOs), lacto-N-fucopentaose III (LNFPIII) and lacto-N-neotetraose (LNnT). LNFPIII and LNnT are HMOs that differ in structure via presence/absence of an α1,3-linked fucose. We utilize LNFPIII and LNnT in conjugate form, where 10-12 molecules of LNFPIII or LNnT are conjugated to a 40 kDa dextran carrier (P3DEX/NTDEX). Previous studies from our lab have shown that LNFPIII conjugates are anti-inflammatory, act on multiple cell types, and are therapeutic in a wide range of murine inflammatory disease models. The α1,3-linked fucose residue on LNFPIII makes it difficult and more expensive to synthesize. Therefore, we asked if LNnT conjugates induced similar therapeutic effects to LNFPIII. Herein, we compare the therapeutic effects of P3DEX and NTDEX in a model of diet-induced obesity (DIO). Male *C57BL/6* mice were placed on a high-fat diet for six weeks and then injected twice per week for eight weeks with 25μg of 40 kDa dextran (DEX; vehicle control), P3DEX, or NTDEX. We found that treatment with P3DEX, but not NTDEX, led to reductions in body weight, adipose tissue (AT) weights, and fasting blood glucose levels. Mice treated with P3DEX also demonstrated improvements in glucose homeostasis and insulin tolerance. Treatment with P3DEX or NTDEX also induced different profiles of serum chemokines, cytokines, adipokines, and incretin hormones, with P3DEX notably reducing circulating levels of leptin and resistin. P3DEX also reduced WAT inflammation and hepatic lipid accumulation, whereas

NTDEX seemed to worsen these parameters. These results suggest that the small structural difference between P3DEX and NTDEX has significant effects on the conjugates' therapeutic abilities. Future work will focus on identifying the receptors for these conjugates and delineating the mechanisms by which P3DEX and NTDEX exert their effects.

2.2 Introduction

Obesity and related metabolic syndrome (MetS) pose major medical risks to those afflicted, often worsening outcomes to infectious diseases (i.e. COVID-19) or leading to type 2 diabetes mellitus (T2DM), cardiovascular disease, fatty liver disease, stroke, and cancer. As of 2017-2018, the age-adjusted prevalence of obesity was estimated to be 42.4%. This is an 11.9% increase from 1999-2000, suggesting that the epidemic of being obese is worsening as time progresses [5]. Obesity is defined as having a body-mass index (BMI) ≥ 30 kg/m^2, but this measure is insufficient when used as a sole indicator for classification [168]. MetS is defined as having at least three of the following criteria: waist circumference >102cm for males; >88cm for women, elevated blood glucose levels >100mg/dL, decreased HDL cholesterol <50mg/dL for males; <40mg/dL for females, elevated triglycerides >150mg/dL, or elevated blood pressure >130/85 [169]. The International Diabetes Foundation (IDF) has also suggested inclusion of additional criteria, such as elevated circulating levels of CRP, TNFα, IL-6 [11, 170]. Once an individual is diagnosed with MetS, his/her risk of serious disease is heightened.

Metabolic inflammation is a sustained, low-grade immune response that occurs as consequence of excess nutrient consumption and has been identified as the nexus between the obese state and serious complications. Within adipose tissue (AT) depots,

adipocytes (fat cells) expand in number (hyperplasia) and size (hypertrophy) to store lipids and prevent lipotoxic build-up in peripheral organs (i.e. liver, pancreas, skeletal muscle, etc.) [171-176]. This protective effect subsides, however, once adipocytes encounter mechanical stress and hypoxic conditions as a result of overexpansion [177-179]. This leads to an increase in detrimental adipokines, chemokines, and cytokines, a decrease in anti-inflammatory or insulin-sensitizing factors, immune cell infiltration, and insulin resistance (IR) [17, 46, 53, 54, 180, 181]. In this regard, targeting altered signaling or cellular composition of obese AT might have therapeutic potential for those with MetS.

We have been examining the mechanisms and biological effects of two human milk oligosaccharides (HMOs), lacto-N-fucopentaose III (LNFPIII) and lacto-N-neotetraose (LNnT). HMOs are the third most abundant component of human milk and provide numerous protective benefits to the breastfeeding infant (i.e. providing nutrients, training the immune system, preventing infection, establishing the microbiome, etc.) [182, 183]. LNFPIII and LNnT differ in structure via the presence/absence of an α1,3-linked fucose residue. Due to the α1,3-linked fucose residue, LNFPIII is difficult to produce via chemical or enzymatic methods. LNnT has been synthesized by various laboratories and is present at higher concentrations (0.74 g/L vs. 0.33 g/L) in human milk [26-29]. Glycom A/S has registered LNnT for use in infant formula in Europe (Novel Food Application 157) and the United States (GRAS Notice 659) [6]. Pre-clinical assessment has been conducted on a chemically synthesized version of LNnT and there were no adverse effects at doses of up to 5000mg/kg/day in rats [29]. Oral supplementation with LNnT has also been shown to be well-tolerated in humans [184].

LNnT is easier to synthesize and has been shown to be well-tolerated in humans, therefore we asked if the small structural difference between LNFPIII and LNnT impacts the conjugates' therapeutic effect in DIO mice. LNFPIII conjugates (P3DEX) and LNnT conjugates (NTDEX) are composed of 10-12 molecules of LNFPIII or LNnT attached to a 40 kDa dextran carrier via an acetylphenylenediamine (APD) linker. Previous studies have shown that therapeutic intervention with LNFPIII-Dex (25µg/dose) in diet-induced obese (DIO) mice twice per week for four weeks led to improved metabolic homeostasis and increased concentrations of circulating IL-10. Of note, P3DEX treatment improved glucose and insulin tolerance, as well as enhanced insulin signaling in WAT. This was shown via increased expression of insulin receptor β (*insrb*), insulin receptor substrate 2 (*irs2*), CCAAT/enhancer-binding protein α (*cebpa*), and glucose transporter 4 (*glut4*). P3DEX treatment also decreased macrophage infiltration and crown-like structures in WAT. This coincided with decreased expression of tumor-necrosis factor α (*tnfa*), caspase-1 (*casp1*), NLR family pyrin domain containing 3 (nlrp3), interleukin-18 (il18), and interleukin-1β (*il1b*). In addition to restoring metabolic homeostasis and ameliorating insulin resistance, LNFPIII-Dex treatment also decreased lipogenic genes (*fas*, *acc1/2*, *scd1*, and *srebp1c*) and fat accumulation in the liver [165].

We report here that treatment with P3DEX, but not NTDEX, decreases total weight gain, reduces AT, improves glucose tolerance, and ameliorates insulin resistance. P3DEX and NTDEX exert wide-ranging effects on circulating chemokines, cytokines, adipokines, and incretin hormones when compared to DIO control mice treated with the 40 kDa dextran (DEX) carrier. Most striking, P3DEX, but not NTDEX, reduces WAT inflammation and hepatic lipid accumulation. This suggests that the slight structural

difference between P3DEX and NTDEX alters the conjugates therapeutic abilities and exemplifies the differential roles that individual HMOs might execute *in vivo.*

2.3 Materials and Methods

2.3.1 Preparation of HMO Conjugates

LNFPIII was synthesized by Dr. Peng George Wang (Georgia State University, Atlanta, GA) [143, 185]. LNnT was synthesized by Neose Technologies, Inc. LNFPIII (MW: 853.877 g/mol) and LNnT (MW: 707.60 g/mol) were sent to Dr. Thomas Norberg (Uppsala University, Uppsala, Sweden) for conjugation to 40 kDa dextran from *Leuconostoc mesenteroides* (DEX; Sigma Aldrich, Cat. No. D1662) using APD linker-spacers. On average, conjugates had 10-12 LNFPIII or LNnT monomers per 40 kDa dextran carrier. LNFPIII accounts for ~17-20% of the molecular weight of the P3DEX conjugate. LNnT accounts for ~15-17% of the molecular weight of the NTDEX conjugate.

2.3.2 Animal Experiments

6 to 8-week old male *C57BL/6* mice were purchased from The Jackson Laboratory and maintained on a 12h light/dark cycle in the University of Georgia's AALAC-accredited College of Veterinary Medicine Animal Resources Facility with food and water available *ad libitum.* After one week of acclimation, mice were housed n=3/cage and placed on a high-fat diet (HFD: Bio-Serv Cat. No. F3282) as described in Bhargava et al. [165]. Given that the HFD is subject to spoilage, food was replenished 3 times per week. After 6 weeks of HFD, mice were divided into 3 cohorts and injected twice per week for 8 weeks via the intraperitoneal route with 25µg of 40 kDa dextran (DEX), LNFPIII conjugated to 40 kDa dextran (P3DEX), or LNnT conjugated to 40 kDa

dextran (NTDEX). An experimental timeline is shown in Figure 1. DEX, P3DEX, and NTDEX were dissolved in 0.9% NaCl prior to injection in a volume of 200µL. Experiments were performed in two independent mouse cohorts (n=6-8/group). Metabolic studies (GTT/ITT) were performed after 4 weeks of treatment with a 2-week rest period between *in vivo* assays. We performed a glucose tolerance test (GTT) at W10 of the experiment and an insulin tolerance test (ITT) at W12 (described below). Body weights were measured once/week and fasting blood glucose levels were measured prior to start of HFD (W0), pre-treatment (W6), and post-treatment (W14). Mice were euthanized at the end of W14 via CO_2 asphyxiation followed by cervical dislocation after a 6h fast. Organs and serum samples were collected and stored at -80°C until use.

2.2.3 Measurement of Body and Organ Weights

Mice were placed in a clean plastic container on a tared compact scale (Ohaus, Cat. No. CS200) to acquire body weight measurements (in grams). Body weights were recorded each week on Monday afternoon to minimize daily fluctuations. Body weights were recorded to the nearest hundredth. At sacrifice, organs (i.e. heart, spleen, liver, kidney, AT) were placed on clean Fisherbrand™ Polystyrene Antistatic Weighing Dishes (Fisher Scientific, Cat. No. 08-732-112) on a tared analytical scale (Sartorius, Cat. No. TE313S) for measurement. Organ weights were recorded to the nearest thousandth.

2.2.4 Glucose Tolerance Test (GTT)

A glucose tolerance test (GTT) were performed after 4 weeks of treatment (W10), according to Beguinot & Nigro with some modifications [186]. Mice were fasted for 6h to obtain baseline blood measurements. Various fasting periods have been utilized in published studies involving GTTs and ITTs, but 6h fasts appear to be more physiological

than longer 14-16h fasts. Previous studies have shown that prolonged fasting in mice results in increased insulin sensitivity, whereas fasting in humans leads to inhibition of insulin-stimulated glucose uptake [187, 188] . Moreover, prolonged fasting in mice may lead to a state of starvation [189]. To ensure translatable results, we utilized a 6h fasting period in our experiments. During GTTs, blood was acquired via tail snip and measured using a Bayer Contour® Next blood glucose monitoring system (Bayer, Parsippany, NJ). Basal glucose measurements were taken before mice were administered 2g glucose/kg (Sigma, Cat. No. G8270) in 10µL/g body weight via oral gavage. Thereafter, blood glucose measurements were taken at 15, 30, 60, 90, 120, 150, and 180-minute timepoints.

2.2.5 Insulin Tolerance Test (ITT)

An insulin tolerance test (ITT) was performed after 6 weeks of treatment (W12) to allow for a 2-week rest period between metabolic tests. The ITT was also performed according to Beguinot & Nigro with the aforementioned fasting modification [186]. During the ITT, mice were fasted for 6h prior to baseline blood glucose measurements and intraperitoneal injection of 0.5IU/kg insulin (Humulin® R U-100, Lilly, Cat. No. HI-210) diluted in 0.9% NaCl in an injection volume of 3.6µL/g body weight. Thereafter, blood glucose measurements were taken at 15, 30, 60, and 90-minute timepoints. If blood glucose levels dropped below 36mg/dL, mice were rescued via injection of 20% aqueous glucose solution (Sigma, Cat. No. G8270).

2.2.6 Serum Evaluation of Adipokines, Chemokines, and Cytokines

The Bio-Plex Pro Mouse Cytokine 23-Plex Assay (Bio-Rad, Cat. No. M60009RDPD) and the Bio-Plex Pro Mouse Diabetes 8-Plex Assay (Bio-Rad, Cat. No. 171F7001M) were performed in multi-plex, according to Bio-Rad's Technical Note

5975. These two panels can be performed via multiplex without altering assay sensitivity, specificity, and accuracy. Serum samples collected at sacrifice after a 6h fast and frozen at -80°C were prepared according to manufacturer's instructions. Adipokines, chemokines, and cytokines were detected and quantified using the Bio-Rad Bio-Plex® 200 System, available at UGA's Cytometry Shared Resource Laboratory.

2.2.7 Histopathology

WAT and liver samples were preserved in 10% formalin and processed, sectioned, and stained with hematoxylin & eosin (H&E) by the Comparative Pathology Lab in the College of Veterinary Medicine at the University of Georgia. Dr. Tamas Nagy, a board-certified pathologist, then assessed inflammation with WAT sections and lipid accumulation in the liver.

2.2.8 Measurement of ALT and AST

Liver function was assessed via measurement of alanine aminotransferase (AST) and aspartate aminotransferase (ALT). ALT was measured in serum using the Alanine Aminotransferase (ALT or SGPT) Activity Colorimetric/Fluorometric Assay Kit (Biovision, Cat. No. K752), according to manufacturer's instructions. AST was measured in serum using the Aspartate Aminotransferase (AST or SGOT) Activity Colorimetric Assay Kit (Biovision, Cat. No K753), according to manufacturer's instructions. Absorbance was measured using the SPECTROstar Nano Microplate Reader (BMG Labtech).

2.2.9 Statistical Analysis

Statistics were performed using One-Way or Two-Way ANOVA with Dunnett's Multiple Comparisons Tests in GraphPad Prism 8. * or ** was used to indicate

significance (*p<0.05 or **p<0.01). ^ was used to indicate a trend (^p<0.10). Values are presented as mean ± SEM. Experiments were repeated twice for a total n=12-14 per treatment group.

2.4 Results

2.4.1 LNFPIII conjugates reduce total body and organ weights

Male *C57BL/6* mice were placed on HFD for 6 weeks (W0-6) prior to beginning treatment twice per week with 25ug DEX, P3DEX, or NTDEX (W7-14) via the intraperitoneal route. Body weight was monitored weekly throughout the duration of the experiment (W0-W14). An experimental timeline is shown in Figure 1a. Mice treated with P3DEX weighed less overall than mice treated with the DEX carrier control or NTDEX (Figure 1b). Compared to DEX, P3DEX treatment reduced total body weight. This reduction trended towards significance (Two-Way ANOVA with Dunnett's Multiple Comparisons Test; ^<0.10) at W9, 12, and 13. Treatment with NTDEX did not cause a significant reduction in total body weight at any point of measurement. Furthermore, there was no significant difference in total body weight between the 3 groups prior to treatment. When normalizing the body weights and examining total weight gain over time, it is clear that P3DEX treatment led to a reduction in total weight gain when compared to DEX-treated animals (Figure 1b). This trended toward significance at W8, 9, 10, 11, and 12 (Two-Way ANOVA with Dunnett's Multiple Comparisons Test; *<0.05, ^p<0.10), and became significant at W13 (Two-Way ANOVA with Dunnett's Multiple Comparisons Test; *p<0.05, ^p<0.10). Again, treatment with NTDEX did not cause a significant reduction in total weight gain at any point of measurement and nearly mirrors the DEX control.

At sacrifice (W14), we collected and weighed subcutaneous (scWAT), visceral (VAT), and brown (BAT) adipose tissue, as well as livers, hearts, spleens, and kidneys. Figure 1c demonstrates that we saw a trend towards reduction of scWAT in P3DEX-treated mice compared to those treated with DEX (One-Way ANOVA with Dunnett's Multiple Comparisons Test; *$p<0.05$, ^$p<0.10$). We saw no effect of NTDEX on scWAT compared to DEX. In terms of vWAT, we noted a significant reduction in P3DEX-treated mice compared to those treated with DEX (Figure 1d. One-Way ANOVA with Dunnett's Multiple Comparisons Test; *$p<0.05$). We observed no differences in BAT between groups, but this is a smaller AT depot (Figure 1e). We did not observe a significant difference in liver, heart, spleen, or kidney weights (Figure 1f-i).

2.4.2 LNFPIII conjugates improve glucose tolerance and reduce insulin resistance

We measured 6h-fasting blood glucose levels prior to HFD (W0), prior to treatment (W6), and prior to sacrifice (W14). Prior to HFD (W0), the average fasting blood glucose for all male mice was within normal range (88.5-154.9 mg/dL) [190]. This was elevated prior to treatment (W6), demonstrating that the HFD induced metabolic dysfunction. Prior to sacrifice and post-treatment, mice treated with P3DEX had significantly lower fasting blood glucose levels (Figure 2a. One-Way ANOVA with Dunnett's Multiple Comparisons Test; *$p<0.05$) than those treated with DEX. NTDEX treatment did not result in reductions in fasting blood glucose levels compared to those treated with DEX. When administered an oral gavage of 2g glucose/kg body weight during a GTT, mice treated with P3DEX exhibited a less dramatic increase in blood glucose levels at the 15-minute timepoint compared to those treated with DEX or NTDEX. P3DEX-treated animals were able to return to basal blood glucose levels more

quickly than DEX- or NTDEX-treated mice. Mice treated with P3DEX had significantly lower blood glucose levels throughout the duration of the GTT and this was significant at 30, 60, 90, 120, 150, and 180 minutes (Figure 2b. Two-Way ANOVA with Dunnett's Multiple Comparisons Test; *$p<0.05$, **$p<0.01$). When given an intraperitoneal injection of 0.5IU/kg body weight insulin, mice treated with P3DEX exhibited a greater decrease in blood glucose levels overall compared to those treated with DEX or NTDEX. Mice treated with P3DEX had significantly lower blood glucose levels throughout the duration of the ITT and this trended towards significance at 15 minutes (Figure 1c. Two-Way ANOVA with Dunnett's Multiple Comparisons Test; ^$p<0.10$). Blood glucose levels of P3DEX-treated mice was significantly lower than DEX-treated mice at the 30-minute timepoint (Figure 1c. Two-Way ANOVA with Dunnett's Multiple Comparisons Test; *$p<0.05$). Thereafter, blood glucose levels between groups appeared to stabilize. This shows that DIO mice treated with DEX or NTDEX were less responsive than mice treated with P3DEX when injected with a bolus of insulin, suggesting the presence of IR in the DEX and NTDEX groups.

2.4.3 LNFPIII and LNnT conjugates alter hematopoietic signals

Individuals diagnosed with MetS are at higher risk of infection and illness, suggesting that the constant presence of low-grade inflammation exhausts and dampens the immune response to other pathogens or insults [191, 192]. In order to maintain function, progenitor cells depend on nutrients and hematopoietic signals to proliferate and differentiate into diverse white blood cells (WBC) populations [193, 194]. IL-3, for example, promotes proliferation of hematopoietic cells [193, 195]. G-CSF and GM-CSF are then responsible for differentiation of cells into specific lineages (i.e. granulocytes

and monocytes) and subsequent activation [193, 196]. High levels of IL-3, G-CSF, or GM-CSF can lead to increased populations of WBCs, which can exacerbate inflammation and damage normal tissues. High WBC counts have been associated with parameters related to inflammation and well-documented in obese subjects [197-202].

We measured IL-3, G-CSF, and GM-CSF in serum samples collected from fasting DIO mice treated with DEX, P3DEX, or NTDEX. Serum from DIO mice treated with P3DEX or NTDEX trended towards decreased IL-3 levels compared to the DEX control (Figure 3a. One-Way ANOVA with Dunnett's Multiple Comparisons Test; ^$p<0.10$). G-CSF and GM-CSF were also slightly reduced, with the reduction in G-CSF becoming significant following NTDEX treatment (Figure 3b-c. One-Way ANOVA with Dunnett's Multiple Comparisons Test; <0.05). These results suggest that both P3DEX and NTDEX have potential to dampen the excessive immune response associated with the obese state.

2.3.4 LNFPIII and LNnT conjugates alter chemoattractant signals

WBCs depend on chemoattractant signals for migration to injured sites. In the obese state, expansion of WAT enhances chemokine release and attracts WBCs to AT depots [203]. This worsens metabolic inflammation and associated comorbidities.

We measured eotaxin/CCL11, KC/CXCL1, MCP-1/CCL2, MIP-1α/CCL3, MIP-1β/CCL4, and RANTES in serum samples collected from fasting DIO mice treated with DEX, P3DEX, or NTDEX. We saw no differences in circulating levels of eotaxin/CCL11, a chemokine known to attract eosinophils (Figure 4a. One-Way ANOVA with Dunnett's Multiple Comparisons Test). While circulating eotaxin/CCL11 is known to increase in the obese state, neither P3DEX, nor NTDEX altered these levels [204, 205]. This makes sense as we have no evidence that either conjugate alters eosinophil

function. KC/CXCL1 is a neutrophil chemoattractant that increases in patients with T2DM, as well as in diabetic-prone *db/db* mice with evidence of impact on pancreatic islet function [206-208]. P3DEX treatment resulted in a significant decrease in serum KC/CXCL1 compared to the DEX control (Figure 4b. One-Way ANOVA with Dunnett's Multiple Comparisons Test, *$p<0.05$). NTDEX treatment did not reduce serum KC/CXCL1, suggesting mechanistic differences between NTDEX and P3DEX conjugates. It is well-reported in the literature that P3DEX and NTDEX act on macrophages [154, 156, 159-161]. MCP-1/CCL2 is instrumental for macrophage recruitment to AT depots and circulating concentrations are increased in the obese state [209]. Furthermore, mice deficient in MCP-1 signaling exhibit lessened macrophage infiltration and inflammation in AT depots [210, 211]. P3DEX treatment resulted in a significant decrease in serum MCP-1/CCL2 compared to the DEX control (Figure 4c. One-Way ANOVA with Dunnett's Multiple Comparisons Test, *$p<0.05$). Although NTDEX also appeared to decrease circulating MCP-1/CCL2 levels, this decrease was not significant (Figure 4c. One-Way ANOVA with Dunnett's Multiple Comparisons Test). Neither P3DEX, nor NTDEX had an effect on MIP-1α/CCL3 or MIP-1β/CCL4 (Figure 4d-e. One-Way ANOVA with Dunnett's Multiple Comparisons Test). MIP-1α and MIP-1β are also elevated in genetic (*ob/ob*, *db/db*) and DIO mice, as well as obese humans [54, 212, 213]. While MIP-1α and MIP-1β both increase in the obese state, there is evidence that they do not alter macrophage infiltration in AT. RANTES is responsible for T cell recruitment and is also increased in the obese state [58, 59]. We noted a significant reduction in serum RANTES following P3DEX treatment (Figure 4f. One-Way ANOVA with Dunnett's Multiple Comparisons Test, *$p<0.05$). NTDEX also appeared to reduce

serum concentration of RANTES, but this was not significant (Figure 4f. One-Way ANOVA with Dunnett's Multiple Comparisons Test). Overall, these results demonstrate that P3DEX is more effective at decreasing circulating chemoattractant signals than NTDEX.

2.4.5 LNFPIII and LNnT alter cytokines involved in innate and adaptive immunity

Given their pleiotropic nature, cytokines are difficult to characterize in the context of DIO. We measured numerous innate and adaptive cytokines in serum samples collected from fasting DIO mice treated with DEX, P3DEX, or NTDEX. Once macrophages are recruited to AT depots, IFNγ secretion helps these cells maintain classical (M1) activation [214]. Neither P3DEX, nor NTDEX, had a significant effect on circulating concentrations of IFNγ (Figure 5a. One-Way ANOVA with Dunnett's Multiple Comparisons Test). P3DEX treatment led to a slight, nonsignificant, reduction in IL-1α (Figure 5b. One-Way ANOVA with Dunnett's Multiple Comparisons Test). IL-1β was unaffected by P3DEX or NTDEX treatment (Figure 5c. One-Way ANOVA with Dunnett's Multiple Comparisons Test). Both IL-1α and IL-1β are elevated in obese individuals with reductions documented following weight loss [215-217]. IL-2, involved in T cell proliferation and activation, was lowered, but nonsignificant, in response to P3DEX and NTDEX (Figure 5d. One-Way ANOVA with Dunnett's Multiple Comparisons Test). IL-4 trended towards reduction in P3DEX-treated mice and was significant for those treated with NTDEX (Figure 5e. One-Way ANOVA with Dunnett's Multiple Comparisons Test, ^$p<0.10$). This reduction was unanticipated, given that both P3DEX and NTDEX promote T_H2 responses and alternative activation (M2) of macrophages [156, 159-161]. P3DEX and NTDEX treatment also led to slight reductions

in IL-5, another T_H2 cytokine, which tends to help maintain homeostasis in WAT depots (Figure 5f. One-Way ANOVA with Dunnett's Multiple Comparisons Test) [218]. P3DEX did not impact circulating IL-6 levels, but NTDEX eliminated IL-6 compared to the DEX control (Figure 5g. One-Way ANOVA with Dunnett's Multiple Comparisons Test, *$p<0.05$). IL-9, a T_H2 cytokine, trended toward decreased circulating levels in DIO mice treated with NTDEX (Figure 5h. One-Way ANOVA with Dunnett's Multiple Comparisons Test, ^$p<0.10$) [219]. Neither P3DEX, nor NTDEX treatment, had a significant effect on circulating IL-10 levels (Figure 5i. One-Way ANOVA with Dunnett's Multiple Comparisons Test). While P3DEX and NTDEX did not impact levels of IL-12(p40), P3DEX treatment led to a significant reduction in IL-12(p70) (Figure 5j-k. One-Way ANOVA with Dunnett's Multiple Comparisons Test, *$p<0.05$). This reduction in the bioactive form of IL-12 suggests quelling of the T_H1 immune response, which might contribute to P3DEX's therapeutic effects [220]. We observed no differences in serum IL-13, another T_H2 cytokine that aids in overcoming insulin resistance (Figure 5l. One-Way ANOVA with Dunnett's Multiple Comparisons Test) [221]. IL-17a increased in response to P3DEX and NTDEX treatment, but this increase was not significant (figure 5m. One-Way ANOVA with Dunnett's Multiple Comparisons Test). Last, we observed a slight, but nonsignificant, reduction in TNFα in response to P3DEX and NTDEX treatment (Figure 5n. One-Way ANOVA with Dunnett's Multiple Comparisons Test). Similar to other markers, circulating TNFα is elevated in obese individuals [180]. Moreover, neutralization of TNFα led to improved insulin responses [17]. Overall, P3DEX treatment seems to decrease circulating cytokine levels, both inflammatory and TH_2-associated. While these cytokine responses are ambiguous when considered on their

own, they are indispensable for delineating how P3DEX treatment reduces body weight and improves glucose homeostasis *in vivo*.

2.4.6 LNFPIII conjugates modulate adipokine secretion

Measurement of AT-specific markers (adipokines), rather than pleiotropic cytokines, might provide more insight on the therapeutic or non-therapeutic effects of P3DEX and NTDEX in the context of DIO. Ghrelin, for instance, is an orexigenic adipokine that stimulates food intake [222]. Circulating levels of ghrelin are lower in the obese state and higher in those that are lean [223-225]. Ghrelin also quells secretion of markers related to inflammation and inhibits NF-κB signaling [226, 227]. In our studies, P3DEX treatment led to a slight, but nonsignificant, increase in ghrelin (Figure 6a. One-Way ANOVA with Dunnett's Multiple Comparisons Test). P3DEX treatment also led to a significant decrease in leptin, a hormone generated in AT in proportion to fat content (Figure 6b. One-Way ANOVA with Dunnett's Multiple Comparisons Test, $p<0.05$) [228]. Circulating leptin concentrations coincide with reductions in AT [229, 230]. Decreases in leptin also coincide with increases in orexigenic peptides (i.e. ghrelin), which might explain the slight increase shown in Figure 6a [231, 232]. NTDEX treatment led to a trending reduction in circulating levels of resistin, while P3DEX treatment led to a significant decrease (Figure 6c. One-Way ANOVA with Dunnett's Multiple Comparisons Test, $*p<0.05$, $\wedge p<0.10$). P3DEX treatment seems to have beneficial effects on specific adipokines (i.e. leptin and resistin), which corresponds with its effects on adipose tissue and glucose homeostasis.

2.4.7 LNnT conjugates alter the incretin effect

During the incretin effect, glucose-dependent insulinotropic polypeptide (GIP) and glucagon-like peptide 1 (GLP-1) are released from the gut to stimulate insulin secretion in response to food intake [233]. P3DEX and NTDEX reduced circulating levels of GIP, with the reduction induced via NTDEX being significant (Figure 7a. One-Way ANOVA with Dunnett's Multiple Comparisons Test, **$p<0.01$). In pancreatic islets, decreases in GIP correspond with decreases in insulin and glucagon secretion [234]. Both P3DEX and NTDEX did not have an effect on GLP-1, another incretin hormone (Figure 7b. One-Way ANOVA with Dunnett's Multiple Comparisons Test). P3DEX treatment led to a slight reduction in glucagon and NTDEX treatment led to a significant reduction (Figure 7c. One-Way ANOVA with Dunnett's Multiple Comparisons Test, *$p<0.05$). NTDEX treatment led to a significant reduction in GIP, which aligns with the corresponding decrease in glucagon. We observed a trending increase in the ratio of insulin to glucagon in response to NTDEX treatment, an indicator of excess nutrient load (Figure 7d. One-Way ANOVA with Dunnett's Multiple Comparisons Test, ^$p<0.10$) [235]. We conclude here that P3DEX treatment has beneficial effects on specific adipokines (i.e. ghrelin, leptin, and resistin), while NTDEX might impact incretin hormones and postprandial insulin release. These findings further support that these two HMO conjugates differ in terms of mechanism and therapeutic potential.

2.4.8 LNFPIII conjugates reduce WAT inflammation and hepatic lipid accumulation

We report various *in vivo* changes in response to both P3DEX and NTDEX. Upon examination of vWAT tissue, we observed what appeared to be decreased immune cell infiltrate and crown-like structures in DIO mice treated with P3DEX compared to DEX

and NTDEX (Figure 8a-c). DIO mice treated with NTDEX exhibited greater inflammation within vWAT even when compared to the DEX control (Figure 8c). In the liver, we observed significant lipid accumulation in DIO mice treated with the DEX control (Figure 9a). In contrast, we observed reduced lipid accumulation in the livers of DIO mice treated with P3DEX (Figure 9b). DIO mice treated with NTDEX showed greater lipid accumulation than the DEX control, suggesting a worsening of MetS (Figure 9c). This was corroborated by the increased ratio of aspartate aminotransferase (AST) to alanine aminotransferase (ALT) detected in the serum of DIO mice treated with NTDEX (Figure 9d. One-Way ANOVA with Dunnett's Multiple Comparisons Test, *$p<0.05$). At the tissue level, it is clear that NTDEX does not induce the same therapeutic benefit as P3DEX.

2.5 Discussion

Although LNFPIII and LNnT differ only by the presence or absence of an α1,3-linked fucose in their structures, their therapeutic effects in a DIO model differ significantly *in vivo*. In general, HMOs present in human breastmilk are known to block infection, modulate the immune response, shape the intestinal microbiome, and serve as nutrients for brain development [183, 236]. However, the effects of specific groups of HMOs (nonfucosylated neutral HMOs, fucosylated HMOs, and sialylated HMOs) or individual HMOs themselves have not been thoroughly studied. 2'-fucosyllactose (2'FL; fucosylated) and LNnT (neutral) are the two most abundant and well-studied HMOs to date [237]. 2'FL has been reported at ~2.74g/L in secretor mothers, while LNnT has been reported at ~0.74g/L [182]. Both HMOs have been purified from human breastmilk and/or synthesized at industrial levels for supplementation in infant formula [238, 239].

LNFPIII, in contrast, is less abundant (~0.33g/L) and expensive to acquire from purified human breastmilk [140]. It has also not been synthesized via chemical or enzymatic methods at an industrial level. To determine if LNnT would function *in vivo* like LNFPIII, we initiated studies to compare the therapeutic effects of LNFPIII conjugates to LNnT conjugates in a murine model of DIO.

Previous studies demonstrate both LNFPIII and LNnT conjugates promote M2 macrophage polarization, an immune process that has been deemed important for regulating and ameliorating adipose tissue inflammation and treating T2DM [156, 157, 161, 240]. Several anti-diabetic drugs on the market, such as metformin and several thiazolidinediones target insulin resistance in part via altering M1/M2 macrophage polarization and reducing inflammation within WAT [241, 242]. Bhargava et al. (2012) demonstrated that LNFPIII conjugates improve glucose tolerance and insulin resistance, as well as reduce WAT inflammation and ameliorate non-alcoholic hepatic steatosis in a similar model of DIO [165]. We expand on these studies herein, demonstrating that DIO mice treated with LNFPIII conjugates (P3DEX) exhibit reductions in total weight gain and subcutaneous/visceral AT (Figures 1b-e). Reductions in total weight gain and subcutaneous/visceral AT depots were not reported in Bhargava et al. (2012), but it is important to note the difference in treatment duration between the two studies. In Bhargava et al. (2012), DIO mice treated with LNFPIII conjugates twice per week for four weeks. The experimental timeline here differs, during which treatment was performed twice per week for eight weeks. It is possible that the longer duration of treatment used in this experiment allowed for differences in weight gain and subcutaneous/visceral AT depots to become apparent. Similar to Bhargava et al. (2012),

we observed significant reductions in fasting blood glucose levels post-treatment (Figure 2a), as well as improved glucose and insulin tolerance (Figure 2b-c). It is striking that the LNnT conjugates (NTDEX) did not induce these effects. We have shown in previous studies that P3DEX acts on B cells, macrophages, dendritic cells, adipocytes, and hepatocytes [89, 146, 150, 154-160, 165]. NTDEX activates macrophages, but not dendritic cells, suggesting differences in cellular mechanisms between the two glycans [161]. We also have evidence that P3DEX and NTDEX act on adipocytes *in vitro* (unpublished). Thus, it is likely that M2 macrophage polarization is not the sole mechanism via which P3DEX exerts its therapeutic effect. Furthermore, additional studies must be performed in parallel to delineate the mechanistic differences present between the two HMO conjugates.

This is the first *in vivo* report comparing the therapeutic effects of P3DEX and NTDEX in a DIO model. Compared to P3DEX, NTDEX did not reduce weight gain or improve glucose homeostasis. Both P3DEX and NTDEX had differential effects on circulating chemokines, cytokines, adipokines, and incretin hormones (Figures 3-7). Only P3DEX reduced weight gain and improved glucose homeostasis, yet both P3DEX and NTDEX altered cytokines involved in haematopoiesis and may each have roles in reducing inflammation (Figure 3). The effects of P3DEX appear to be more pronounced as treatment of DIO mice led to reductions in several chemotactic cytokines (i.e. KC, MCP-1, RANTES) (Figure 4). This could be due to reductions in AT mass and subsequent decreases in pro-inflammatory signals from AT depots. P3DEX and NTDEX also altered numerous innate and adaptive cytokines, but given the pleiotropic nature of these markers, it is difficult to make conclusions about the role that they might have in

ameliorating MetS (Figure 5). Furthermore, an increase/decrease in one marker can lead to a compensating increase/decrease in another. We saw a trending decrease in IL-4 for animals treated with P3DEX and a significant decrease for those treated with NTDEX. P3DEX and NTDEX both promote T_H2 responses and alternative activation (M2) of macrophages, so this result was unexpected. [156, 159-161]. The role of IL-6 in DIO is controversial, as some studies suggest that IL-6 exacerbates insulin resistance and others note beneficial effects [243-245]. Given that we do not observe improvements in glucose or insulin tolerance in DIO mice treated with NTDEX, it is likely that elimination of IL-6 does not have a significant therapeutic impact in our studies. Furthermore, deletion of IL-6 in *in vivo* studies have not been successful in delineating its role in DIO and T2DM [245]. P3DEX has been shown to increase circulating IL-10 levels in DIO mice, but the studies presented herein are different in terms of experimental conditions and design (i.e. animal housing facilities, longer treatment period, etc.) [165]. IL-17a is a prominent marker of inflammation and is elevated in obese individuals, but there is also evidence of an anti-adipogenic role for this cytokine [246]. The fasting serum samples analyzed here offer a snapshot in time following 8 weeks of DEX, P3DEX, or NTDEX treatment. It is well-known that these markers fluctuate over time and/or depend on disease progression. Another method to determine the specific roles and importance of the documented adipokines, chemokines, or cytokines would be to eliminate these molecules in DIO mice on DEX, P3DEX, and NTDEX treatment regimens and evaluate whether the conjugates' therapeutic capabilities are altered.

While the chemokine and cytokine results do not allow us to focus on a distinct mechanism, it is clear that P3DEX and NTDEX altered adipokines and incretin hormones

in a more straight-forward manner (Figures 6-7). Adipokines, such as ghrelin, leptin, and resistin, are directly secreted from AT depots and indispensable for metabolic regulation. We observed a slight, but non-significant increase in ghrelin in response to P3DEX treatment (Figure 6a). Ghrelin is known to decrease in the obese state and inversely correlates with BMI, so the observed increase in response to P3DEX treatment aligns with the decreased weight gain that we report here [247-249]. In the obese state, individuals often present with low ghrelin levels and high leptin levels to which they become resistant [250]. P3DEX slightly increased circulating ghrelin, as well as significantly decreased circulating leptin, an adipokine generated in proportion to fat content (Figure 6b) [251]. P3DEX also significantly decreased resistin, an adipokine known to increase with inflammation and insulin resistance (Figure 6c) [252]. Resistin also perpetuates states of inflammation via induction of pro-inflammatory cytokines (i.e. IL-1, IL-6, IL-12, TNFα, etc.) and molecules related to chemoattraction (i.e. VCAM-1, ICAM-1, MCP-1, etc.) [253, 254]. Whether these changes occur because of overall decreases in AT or if P3DEX acts directly on adipocytes to modulate ghrelin, leptin, and resistin secretion is yet to be investigated. In contrast to P3DEX, NTDEX induced significant changes in incretin hormones. NTDEX treatment led to a significant decrease in GIP, a hormone that stimulates insulin secretion and synthesis, as well as glucagon secretion (Figure 7a) [234]. In this regard, the observed decrease in response to NTDEX treatment could be damaging in the context of DIO. This decrease also corresponded with a significant decrease in glucagon secretion (Figure 7c) and a trending increase in the ratio of insulin:glucagon (Figure 7d).

Similar to Bhargava et al. (2012), P3DEX decreased WAT inflammation and lipid accumulation in the liver (Figures 8-9). However, NTDEX treatment seemed to worsen WAT inflammation and increase hepatic lipid accumulation even compared to DEX treatment (Figures 8-9). This was exemplified by the significant increase in the ratio of AST:ALT in DIO mice treated with NTDEX (Figure 9d). We expected NTDEX to ameliorate WAT inflammation and hepatic lipid accumulation similar to P3DEX, however, NTDEX appeared to have a damaging effect at the tissue level. Future studies will further investigate P3DEX and NTDEX at the tissue level in this DIO model. We have generated monoclonal antibodies (mAbs) that will serve as useful probes for mechanistic studies (i.e. co-immunoprecipitation), in order to determine the receptors that P3DEX and NTDEX bind to in various cells, elucidate their mechanisms, and determine if P3DEX might be a useful treatment for humans with MetS.

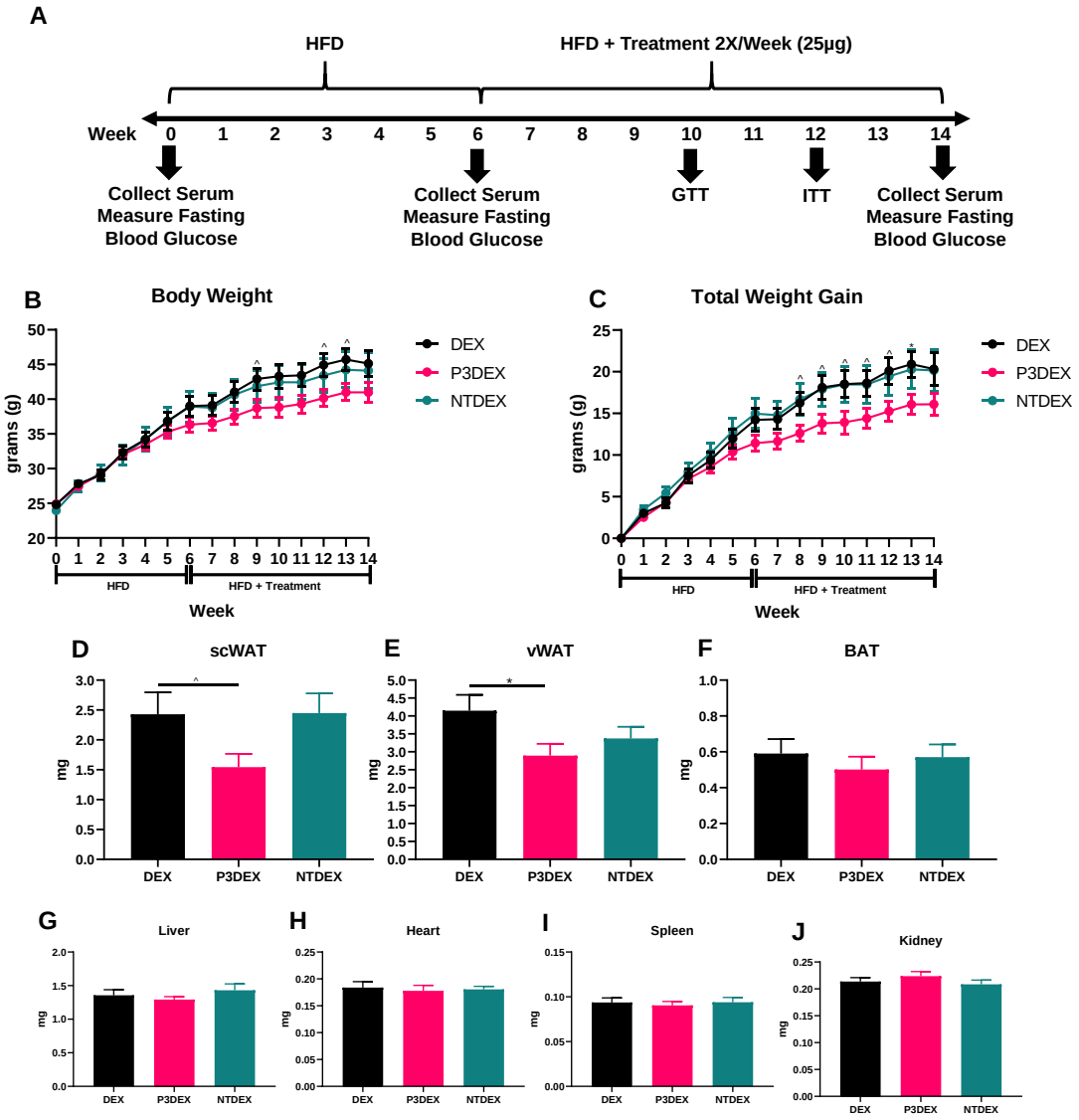

Figure 2.1: LNFPIII conjugates reduce total body and organ weights. A. Experimental design. Male *C57BL/6* mice were placed on HFD for 6 weeks prior to intervention twice per week with 25µg DEX, P3DEX, or NTDEX. **B-C.** P3DEX reduces total body weight and weight gain. Two-way ANOVA with Dunnett's Multiple Comparisons Test. **D-F.** P3DEX reduces scWAT and WAT, but not BAT. **G-J**. P3DEX and NTDEX have no effect on liver, heart, spleen, and kidney weights. One-way ANOVA with Dunnett's Multiple Comparisons Test. *indicates a significant difference between DEX and P3DEX ($p \leq 0.05$). ^indicates a trend between DEX and P3DEX ($p \leq 0.10$).

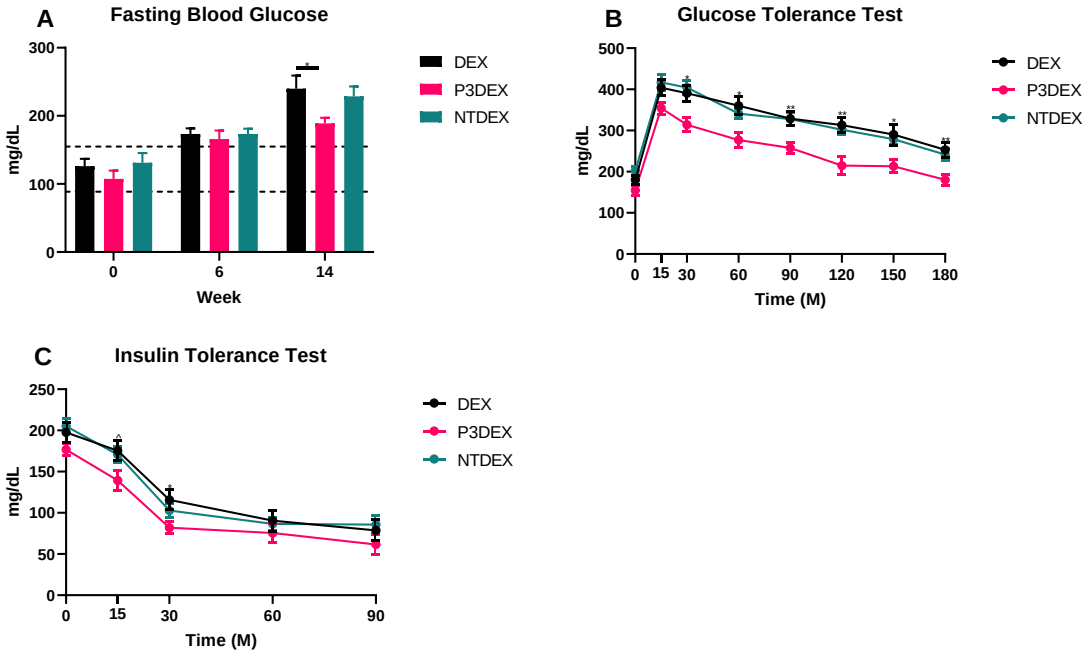

Figure 2.2: LNFPIII conjugates improve glucose homeostasis and reduce insulin resistance. **A.** P3DEX reduces fasting blood glucose levels. **B.** P3DEX improves glucose tolerance. **C.** P3DEX improves insulin sensitivity. Two-way ANOVA with Dunnett's Multiple Comparisons Test. *indicates a significant difference between DEX and P3DEX ($p \leq 0.05$). ^indicates a trend between DEX and P3DEX ($p \leq 0.10$).

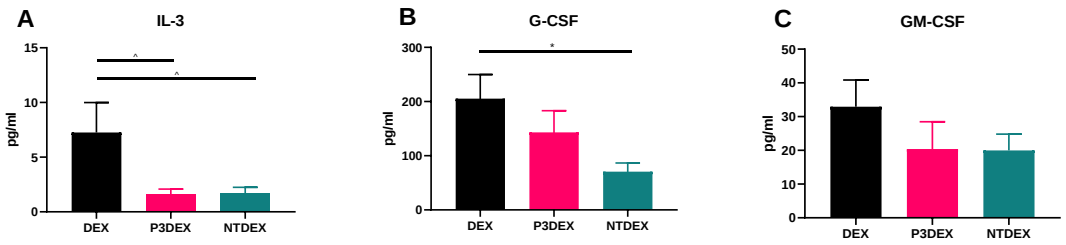

Figure 2.3: LNFPIII and LNnT conjugates alter cytokines involved in hematopoiesis. A. IL-3. **B.** G-CSF. **C.** GM-CSF. One-way ANOVA with Dunnett's Multiple Comparisons Test. *indicates a significant difference ($p \leq 0.05$). ^indicates a trend ($p \leq 0.10$).

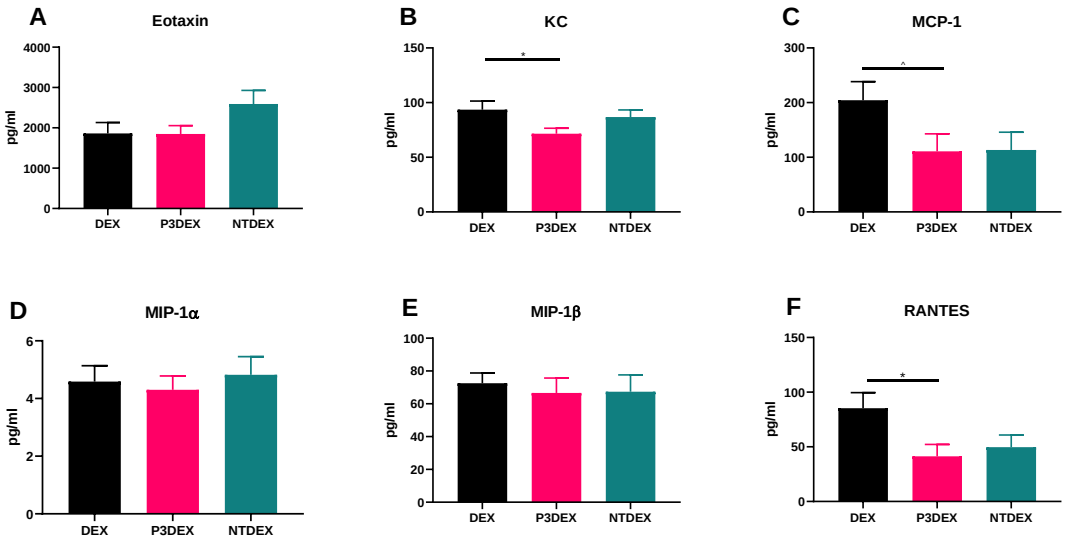

Figure 2.4: LNFPIII and LNnT conjugates alter chemotactic cytokines. A. Eotaxin. **B.** KC. **C.** MCP. **D.** MIP-1α. **E.** MIP-1β **F.** RANTES. One-way ANOVA with Dunnett's Multiple Comparisons Test. *indicates a significant difference ($p \leq 0.05$). ^indicates a trend ($p \leq 0.10$).

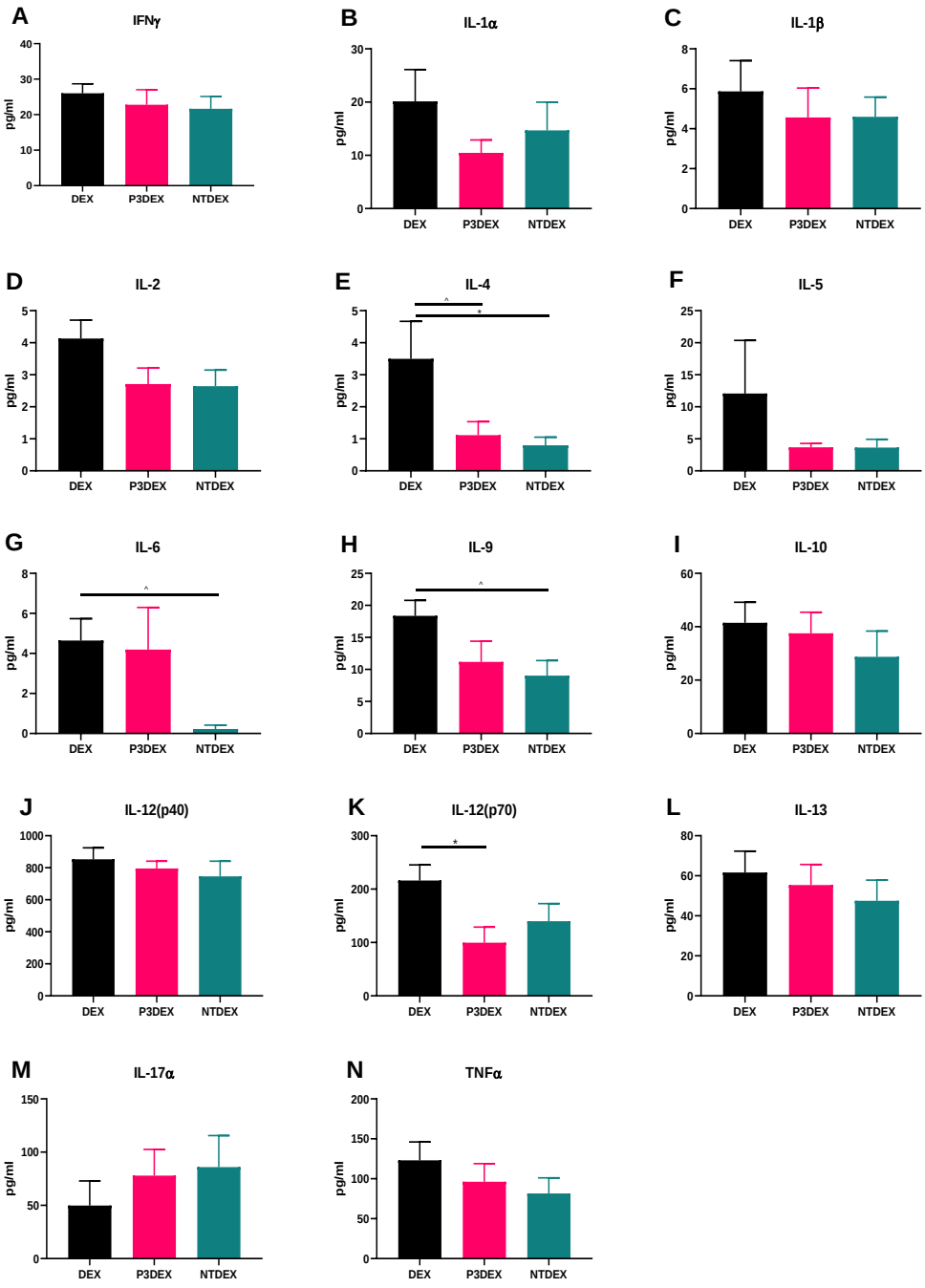

Figure 2.5: LNFPIII and LNnT conjugates alter cytokines involved in innate and adaptive immunity. A. IFNγ. **B.** IL-1α **C.** IL-1β. **D.** IL-2 **E.** IL-4 **F.** IL-5 **G.** IL-6. **H.** IL-9. **I.** IL-10. **J.** IL-12(p40). **K.** IL-12(p70). **L.** IL-13 **M.** IL-17α. **N.** TNFα. One-way ANOVA with Dunnett's Multiple Comparisons Test. *indicates a significant difference ($p \leq 0.05$). ^indicates a trend ($p \leq 0.10$).

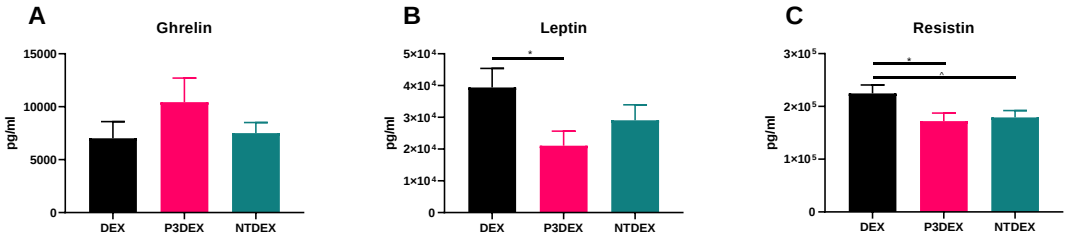

Figure 2.6: LNFPIII conjugates modulate adipokine secretion. **A.** Ghrelin. **B.** Leptin. **C.** Resistin. One-Way ANOVA with Dunnett's Multiple Comparisons Test. *indicates a significant difference ($p \leq 0.05$). ^indicates a trend ($p \leq 0.10$).

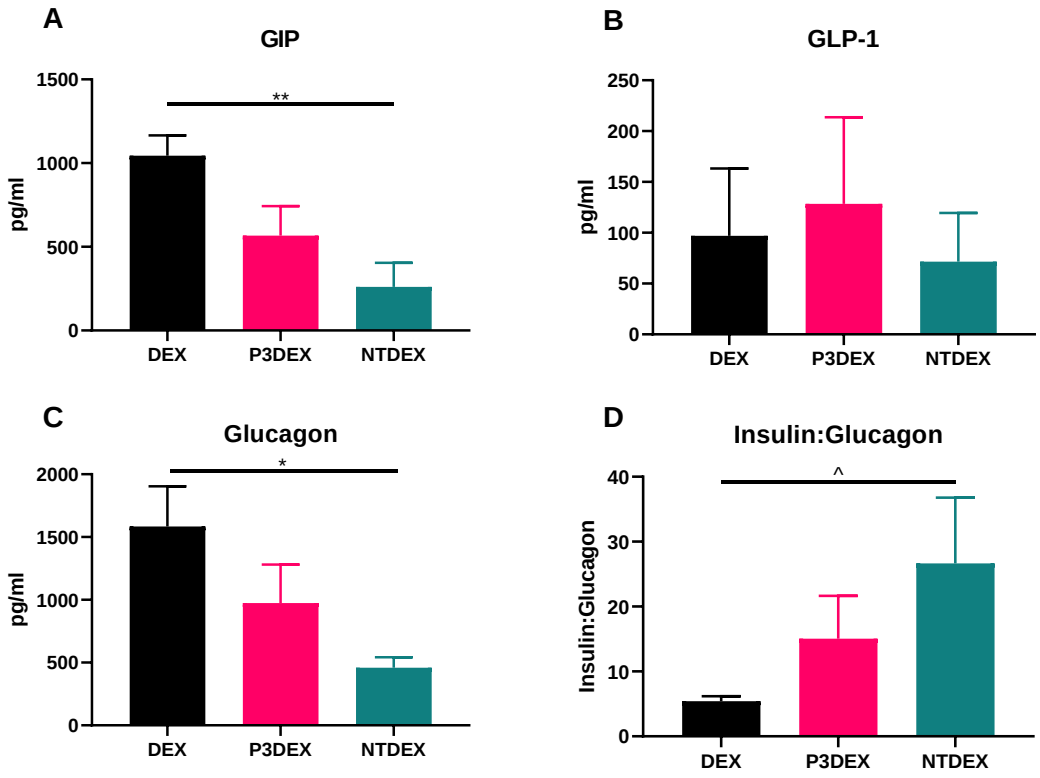

Figure 2.7: LNnT conjugates alter the incretin effect. A. GIP. **B.** GLP-1. **C.** Glucagon. **D.** Insulin:Glucagon Ratio. One-way ANOVA with Dunnett's Multiple Comparisons Test. *indicates a significant difference ($p \leq 0.05$). ^indicates a trend ($p \leq 0.10$).

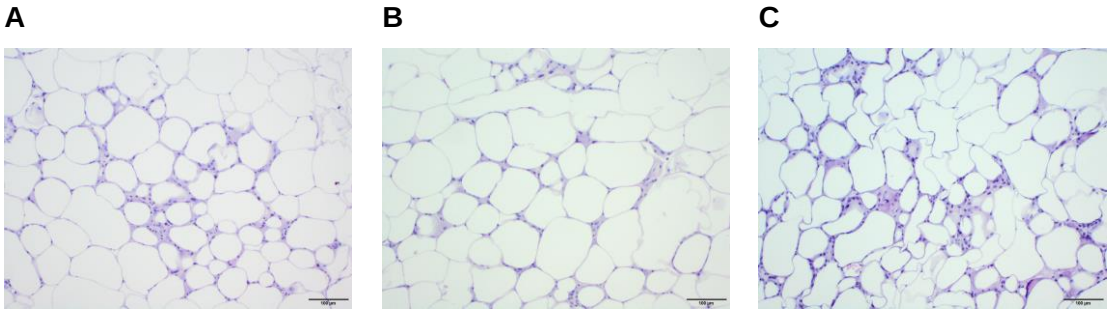

Figure 2.8: LNFPIII conjugates reduce WAT inflammation. vWAT sections from DIO mice treated with: **A.** DEX. **B.** P3DEX. **C.** NTDEX.

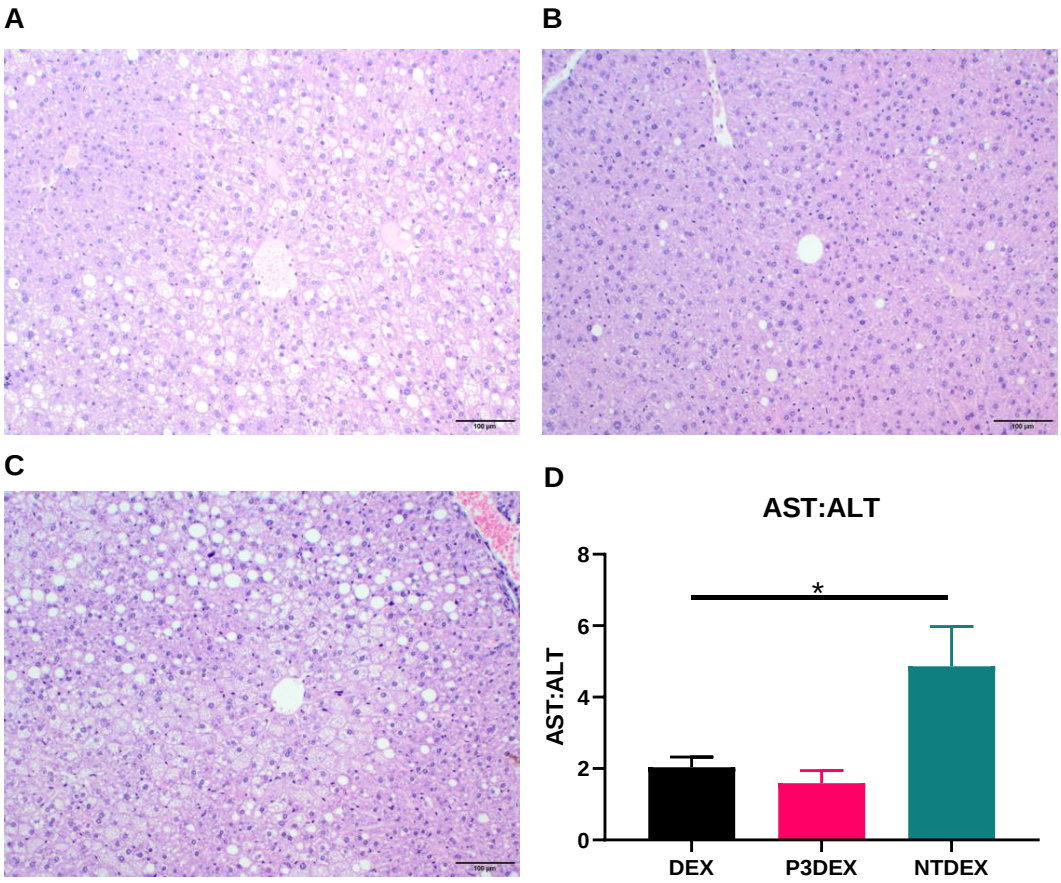

Figure 2.9: LNFPIII conjugates reduce hepatic lipid accumulation and liver damage. Liver sections from DIO mice treated with: **A.** DEX. **B.** P3DEX. **C.** NTDEX. **D.** Ratio of circulating AST:ALT. One-way ANOVA with Dunnett's Multiple Comparisons Test. *indicates a significant difference ($p \leq 0.05$).

CHAPTER 3

LACTO-N-FUCOPENTAOSE III (LNFPIII) AND LACTO-N-NEOTETRAOSE (LNNT) CONJUGATES INDUCE DIFFERENTIAL CHANGES IN THE MICROBIOME OF DIET-INDUCED OBESE (DIO) MICE[1]

[1] Ramadhin et al. (2021). Submitted to *Gut Microbes*, 4/3/2021.

3.1 Abstract

Gut dysbiosis is a hallmark of obesity and metabolic syndrome (MetS). As a result, numerous studies have focused on altering the microbiome to improve metabolic parameters. Human milk oligosaccharides (HMOs) are present in human colostrum and mature milk and are well-regarded as powerful prebiotics for a breastfeeding infant. In the described studies, we treated diet-induced obese (DIO) mice with HMO conjugates containing 10-12 molecules of lacto-N-fucopentaose III (LNFPIII) or lacto-N-neotetraose (LNnT). We collected fecal samples and performed 16S sequencing to identify microbial alterations as a result of treatment. Herein, we report that HMO conjugates decrease absolute abundance and increase species richness. We also report differential changes in response to LNFPIII or LNnT conjugate treatment. LNFPIII conjugates promoted outgrowth of Bacteroides, Proteobacteria, and Verrucomicrobia. LNFPIII conjugates also increased the ratio of Bacteroidetes to Firmicutes compared to the dextran control. LefSe analysis revealed significant enrichment of *Akkermansia muciniphila* and *Bacteroides thetaiotamicron* in response to LNFPIII conjugate treatment. LNnT conjugate treatment enriched *Bifidobacterium pseudolongum*, which is one of the core bacterial species found in the gut of breastfeeding infants. These results suggest that microbial effects are unique to specific HMOs and harbor different therapeutic implications in the context of obesity and MetS.

3.2 Introduction

Obesity and metabolic syndrome (MetS) are complex conditions thought to arise from an imbalance between energy intake and expenditure. Despite this, weight-loss interventions that target energy balance are usually unsuccessful. In 2017-2018, obesity

and MetS afflicted at least 42.4% of the U.S. population and it is estimated that 48.9% of U.S. adults will be considered obese by 2030 [255, 256]. Compared to normal weight individuals, obese individuals face economic ramifications and expend between 68.4% and 233.6% more in healthcare costs related to inpatient, outpatient, and prescription drug services [7].

Obesity is defined as exceeding a body-mass index (BMI) of 30 kg/m^2, while MetS is defined as having a combination of the following factors: waist circumference >102cm for males; >88cm for women, elevated blood glucose levels >100mg/dL, decreased HDL cholesterol <50mg/dL for males; <40mg/dL for females, elevated triglycerides >150mg/dL, or elevated blood pressure >130/85 [169]. Obesity and MetS are predisposing factors for numerous non-communicable diseases (NCDs), including type 2 diabetes mellitus (T2DM), non-alcoholic steatohepatitis (NASH), cardiovascular disease (CVD), stroke, and even cancer. In this regard, identifying underlying causes and developing effective treatment strategies for obesity and MetS are of utmost importance in terms of tackling this growing epidemic.

Recent studies have implicated disturbances in the gut microbiome as both causative of weight gain and consequential of consuming a high-fat diet (HFD). Turnbaugh et al. (2006) was the first to demonstrate that transplanting feces, and hence the microbiome, from an obese mouse to a germ-free (GF) mouse established a microbiome tailored for weight gain [257]. This was exemplified when GF mice receiving fecal transplants from pairs of lean and obese twins gained more weight after receiving microbiota from obese donors than from lean donors [258]. In a randomized clinical trial, transferring microbiota from lean males to those with MetS improved

insulin resistance [259]. In the inverse scenario, it is undeniable that dietary habits modulate the intestinal microbiome as food passes directly through the digestive tract and microbes are specialized to extract and metabolize specific nutrients, such as indigestible carbohydrates. Diet-induced changes in the microbiome are rapid, but modest, and mostly sustained by long-term habits [260]. High-fat, high-sugar diets have led to consistent and reproducible changes in 5 inbred mouse strains, over 200 outbred mice, and 4 transgenic lines [261]. In gnotobiotic mice transplanted with microbial communities from human feces, switching from a plant-based diet to a high-fat, high-sugar diet shifted the microbiome within 24h and this shift stabilized within 7 days [262]. High-fat diets and consequential shifts in microbial communities have also been associated with exacerbations in adiposity, insulin resistance, and inflammation [263]. Moreover, mice injected with lipopolysaccharide (LPS; from gram-negative bacteria) had higher body weights, greater fasting blood glucose, insulin, and triglyceride levels, and marked inflammation [264]. Overweight men fed three different diets in succession also exhibited rapid microbiome changes in response to each different dietary regimen [265]. Furthermore, human consumption of a plant-based or animal-based diet altered the microbiome in a manner that favors appropriate metabolism (i.e. digestion of plant polysaccharides vs. animal protein) [266, 267]. Overall, changes in the gut microbiome, whether causative or consequential, are variable and able to modulate metabolic, immune, and remote organ responses.

While there is no definite consensus, obesity and MetS are generally associated with reduced α-diversity (species richness and evenness) and changes in specific microbes in the gut [67]. Reduced microbial gene richness has been associated with

greater levels of insulin resistance, serum triglycerides, LDL cholesterol, and inflammation [67, 268]. In a comparison of lean and obese twins, Turnbaugh et al. (2008) demonstrated that obese individuals had less diverse bacterial populations, changes in bacterial genes, and altered metabolism compared to their lean counterparts [70]. For example, 75% of genes enriched in the obese phenotype were derived from Actinobacteria, while 25% were derived from Firmicutes. In contrast, 42% of genes enriched in the lean phenotype were derived from Bacteroidetes [70]. At the phylum level, Bacteroidetes and Firmicutes represent ~90% of the microbiome [269]. An increase in the ratio of Firmicutes/Bacteroidetes has often been reported during obesity and has been proposed as a biomarker for dysbiosis [71, 72, 270]. While this change is purported by numerous studies, it is still controversial. Other bacterial changes have also been reported in the obese state, but these changes vary significantly based on experimental design. In this regard, more research must be done to move beyond associations between obesity and microbial populations and towards causation and mechanism.

There have been numerous natural and therapeutic approaches to re-establishing a "healthy" biome to prevent or ameliorate disease. Establishing the microbiome begins at birth, depending on whether a child was born vaginally or via cesarean section and whether that child was breast-fed or formula-fed. Human milk oligosaccharides (HMOs) are the third most abundant component of human breastmilk and are critical for establishing the microbiome [183]. HMOs are diverse in structure and composed of different monosaccharide chains (i.e. glucose, galactose, *N*-acetylglucosamine, fucose, or *N*-acetylneuraminic acid) that can be modified via fucosylation or sialylation [183]. In a study of 3-month old infants, the relative abundance of *Bacteroides* and *Bifidobacterium*

spp. correlated with consumed HMOs [271]. Breast-fed infants also had higher abundances of Bacteroidetes and lower abundances of Firmicutes compared to formula-fed infants [271]. These data align with *in vitro* studies that show that *Bacteroides* and *Bifidobacterium* spp. can grow in minimal media with HMOs as the sole carbon source [135, 272]. In recent years, the importance of HMOs has been increasingly recognized and specific HMOs, such as 2'fucosyllactose and lacto-N-neotetraose, have been approved for supplementation in infant formula [237].

We asked if conjugates of two HMOs, lacto-N-fucopentaose III (LNFPIII) and lacto-N-neotetraose (LNnT) can ameliorate dysbiosis in diet-induced obese (DIO) mice. LNFPIII (β-D-Gal-(1→4)-[α-L-Fuc-(1→3)]-β-D-GlcNAc-(1→3)-β-D-Gal-(1→4)-D-Glc) and LNnT (β-D-Gal-(1→4)-β-D-GlcNAc-(1→3)-β-D-Gal-(1→4)-D-Glc) share identical backbone structures, while LNFPIII contains an α1,3-linked fucose residue. Conjugates of LNFPIII and LNnT are composed of 10-12 molecules of either HMO attached to a 40 kDa dextran carrier (P3DEX/NTDEX) and have been studied extensively [146, 150, 155-160, 165]. Most relevant to this work, P3DEX, but not NTDEX, has been shown to improve insulin resistance and reduce non-alcoholic fatty liver disease (NAFLD) in DIO mice [165]. P3DEX has also been shown to increase butyrate-producing bacteria in a murine model of Gulf War Illness [273]. To our knowledge, this is the first investigation of microbial changes induced by LNFPIII and LNnT conjugates in DIO mice. We present here that DIO mice treated with HMO conjugates have increased species richness, but microbial profiles specific to each conjugate.

3.3 Materials and Methods

3.3.1 Preparation of HMO Conjugates

Lacto-N-fucopentaose III (LNFPIII) pentasaccharides were synthesized by Dr. Peng George Wang (Georgia State University, Atlanta, GA) using chemical methods [143, 185]. Lacto-N-neotetraose (LNnT) tetrasaccharides were acquired from Neose Technologies, Inc. Both LNFPIII and LNnT were conjugated to a dextran carrier (MW: 40,000 g/mol) from *Leuconostoc mesenteroides* (DEX; Sigma Aldrich, Cat. No. D1662). On average, 10-12 monomers of LNFPIII (MW: 853.877 g/mol) or LNnT (MW: 707.60 g/mol) to) were coupled per dextran. Therefore, ~17-20% of the molecular weight of the P3DEX conjugate is composed of LNFPIII, while ~15-17% of the molecular weight of the NTDEX contains LNnT.

3.3.2 Animal Experiments

We purchased 6 to 8-week old male C57BL/6 mice from The Jackson Laboratory and allowed them to acclimate for 1 week prior to handling. Mice were housed 3 per cage and maintained on a 12h light/dark cycle at the University of Georgia's AALAC-accredited College of Veterinary Medicine Animal Resources Facility. Food and water were available *ad libitum*. Mice were placed on a high-fat diet (HFD: Bio-Serv Cat. No. F3282) for 6 weeks, identical to Bhargava et al. [165]. Throughout the experiment, food was refreshed three times per week to avoid spoilage. After 6 weeks, mice were divided into 3 experimental cohorts and injected intraperitoneally twice per week for 8 weeks with 25µg of dextran (DEX), LNFPIII conjugated to dextran (P3DEX), or LNnT conjugated to dextran (NTDEX) diluted in 200µl of 0.9% NaCl. Experiments were conducted in two independent mouse cohorts (n=6-8/group). At week 14, mice were euthanized using CO_2 asphyxiation and a guillotine.

3.3.3 Collection of Fecal Samples

During week 14, fecal samples were collected by placing a single mouse in a sterile plastic container. Mice were given time to defecate and then returned to their cages. Fecal pellets were collected using sterile tweezers and placed into a 1.5mL Eppendorf tube. Tubes were stored at -80°C until sent to Zymo Research Inc. for 16S RNA sequencing.

3.3.4 DNA Extraction

DNA extraction was performed by the ZymoBIOMICS® Service (Zymo Research, Irvine, CA) using the ZymoBIOMICS®-96 MagBead DNA Kit (Zymo Research, Irvine, CA) on an automated platform. Each DNA extraction included the ZymoBIOMICS® Microbial Community Standard (Zymo Research, Irvine, CA) as a positive control. Blank extraction controls were used as negative controls.

3.3.5 Targeted Library Preparation

DNA was prepared for targeted library sequencing by the ZymoBIOMICS ® Service (Zymo Research, Irvine, CA) using The *Quick*-16S™ NGS Library Prep Kit (Zymo Research, Irvine, CA). Each targeted library preparation used the ZymoBIOMICS® Microbial Community DNA Standard (Zymo Research, Irvine, CA) as a positive control. Blank library preparations were used as negative controls. The *Quick*-16S™ Primer Set V3-V4 (Zymo Research, Irvine, CA) was used to provide the best coverage of the 16S gene. The final library was cleaned up using the Select-a-Size DNA Clean & Concentrator™ (Zymo Research, Irvine, CA). DNA Quantification was performed using the TapeStation® (Agilent Technologies, Santa Clara, CA) and Qubit® (Thermo Fisher Scientific, Waltham, WA).

3.3.6 Sequencing

An Illumina® MiSeq™ with a v3 reagent kit (600 cycles) was used to sequence the final library preparation. Sequencing was performed using a 10% PhiX spike-in to calculate absolute abundances. For absolute abundances, quantitative real-time PCR (qRT-PCR) reactions were set-up using a 10-fold serial dilution of plasmid DNA containing a single copy of the 16S gene. The resultant equation from the standard curve was used to calculate the number of gene copies in each reaction. Next, the sample input volume (2μL) was utilized to calculate the number of gene copies/μL in each DNA sample.

3.3.7 Bioinformatics Analysis

The DADA2 pipeline was used for inference of unique amplicon sequence variants (ASVs) from raw reads and removal of potential sequencing errors and chimeric sequences [274]. Assignment of taxonomies were done using Uclust from Qiime v.1.9.1 with the Zymo Research Database. Alpha-diversity and beta-diversity analyses were conducted using Qiime v.1.9.1 [275]. Significant biomarkers were identified via LEfSe using standard settings [276]. Once acquired from Zymo Research Inc., raw data was visualized using GraphPad Prism 9. Kruskall Wallis with Dunn's Multiple Comparisons Tests were performed to determine significant differences in absolute abundance, species richness/evenness, and bacterial species at all taxonomic levels.

3.3.8 Accession Number(s) of DNA Sequences

DNA sequences are available in the NCBI Sequence Read Archive under BioProject Accession No. PRJNA716417.

3.4 Results

3.4.1. HMO Conjugates Reduce Absolute Abundance of Bacterial Species in DIO Mice

Absolute abundance can provide important information about microbial communities and overcome limitations associated with determining relative abundance alone. In these studies, a standard curve was constructed using 10-fold serial dilutions of plasmid DNA comprised of a single copy of the 16S gene and ran via qRT-PCR using the *Quick*-16S™ Primer Set V3-V4 (Zymo Research, Irvine, CA). The resulting equation and the 2µl DNA input volume were then used to determine the absolute number of gene copies per microliter in each sample. DIO mice treated with LNFPIII or LNnT conjugates both exhibited reductions in absolute abundance of bacterial species. However, this reduction was only significant in fecal samples from DIO mice treated with LNnT conjugates (Figure 1. Kruskall Wallis with Dunn's Multiple Comparisons Test, *$p<0.05$).

3.4.2 LNnT Conjugates Significantly Increase Species Richness

Alpha diversity indices are used to measure species richness (how many bacterial species are present?) and evenness (are these species present in equal or unequal abundance?). There are several common richness indices, such as chao1, fisher alpha, observed species, and phylogenetic diversity (PD) [277]. The chao1 method is useful for identifying species of low abundance [278]. We observed a significant increase in chao1 in gut microbial communities from DIO mice treated with LNnT conjugates (Figure 2a. Kruskall Wallis with Dunn's Multiple Comparisons Test, *$p<0.05$). We saw a similar, but nonsignificant, increase in chao1 in gut microbial communities from DIO mice treated with LNFPIII conjugates. We also saw a significant increase in fisher alpha in gut microbiota analyzed from DIO mice treated with LNnT conjugates, further emphasizing an observed increase in species richness (Figure 2b. Kruskall Wallis with Dunn's Multiple Comparisons Test, *$p<0.05$). Mice treated with LNFPIII or LNnT conjugates

also had a greater number of observed species present in fecal samples overall, compared to the DEX control and significant only for those treated with NTDEX (Figure 2c. Kruskall Wallis with Dunn's Multiple Comparisons Test, *p<0.05). These observed species were also more phylogenetically diverse in DIO mice treated with LNFPIII or LNnT conjugates, again compared to the DEX control and significant only for those treated with NTDEX (Figure 2d. Kruskall Wallis with Dunn's Multiple Comparisons Test, *p<0.05). We saw no significant differences in indices that measured both species richness and evenness (i.e. Shannon or Simpson) (Figure 2e-f. Kruskall Wallis with Dunn's Multiple Comparisons Test, *p<0.05).

3.4.3 Beta Diversity

To determine microbial diversity differences between samples, we calculated Bray-Curtis dissimilarity using ASVs. The matrix of paired-wise distance between samples was used to construct a three-dimensional principle coordinate analysis (PCoA) plot, in which each point represents the 16S rRNA gene sequences from a single mouse. As shown in Figure 3, DIO mice treated with DEX and NTDEX clearly cluster together. There is some variation between samples in DIO mice treated with P3DEX. Of note, our PCoA analysis was able to explain 79.7% of the variance between the three axes. In general, the variance explained should be greater than 60% for the data to be considered useful [279].

3.4.4 LNFPIII Conjugates Increase Bacteria of the Phyla Bacteroides, Proteobacteria, and Verrucomicrobia

At the phylum level, we identified six prominent groups: Actinobacteria, Bacteroidetes, Firmicutes, Proteobacteria, Tenericutes, and Verrucomicrobia. We saw a

slight, but nonsignificant decrease in Actinobacteria in response to P3DEX treatment compared to the DEX and NTDEX groups (Figure 4a. Kruskall Wallis with Dunn's Multiple Comparisons Test, *p<0.05). We saw a significant increase in Bacteroidetes in response to P3DEX treatment (Figure 4b. Kruskall Wallis with Dunn's Multiple Comparisons Test). However, we did not see a corresponding decrease in Firmicutes (Figure 4c. Kruskall Wallis with Dunn's Multiple Comparisons Test). We observed a significant increase in Proteobacteria in response to P3DEX (Figure 4d. Kruskall Wallis with Dunn's Multiple Comparisons Test, *p<0.05). We did not observe a significant difference in Tenericutes, but this phylum was only detected in 1/5 of the P3DEX samples (Figure 4e. Kruskall Wallis with Dunn's Multiple Comparisons Test). P3DEX significantly increased bacteria of the phylum Verrucomicrobia (Figure 4f. Kruskall Wallis with Dunn's Multiple Comparisons Test, *p<0.05). About 15-20% of the gut microbial communities for each group were unidentified (Figure 4g. Kruskall Wallis with Dunn's Multiple Comparisons Test, *p<0.05). Last, P3DEX treatment significantly increased the ratio of Bacteroidetes/Firmicutes, suggesting a major shift in the microbial population (Figure 4h. Kruskall Wallis with Dunn's Multiple Comparisons Test, **p<0.01). A complete composition bar plot of all phyla present is depicted in Supplementary Figure 1.

3.4.5 LNFPIII Conjugates Increase Bacteria of the Bacteroidia, Erysipelotrichia, Betaproteobacteria, and Verrucomicrobiae Classes, While Both LNFPIII and LNnT Conjugates Decrease Bacilli

At the class level, we identified 10 prominent groups. Within Actinobacteria, we observed bacteria of the Actinobacteria and Coriobacteriia classes. We saw the class

Bacteroidia within the phylum Bacteroidetes. Within Firmicutes, we detected the Bacilli, Clostridia, and Erysipelotrichia classes. We observed Alphaproteobacteria and Betaproteobacteria within the phylum Proteobacteria. Within Tenericutes, we saw bacteria of the Mollicutes class. Last, we detected Verrucomicrobiae within the phylum Verrucomicrobia. Again, 15-20% of the gut microbial communities for each group were unidentified. A complete composition bar plot of all classes present is depicted in Supplementary Figure 1. Figure 4 demonstrates significant alterations at the class level in response to either P3DEX or NTDEX treatment. P3DEX treatment significantly increased the class Bacteroidia (Figure 5a. Kruskall Wallis with Dunn's Multiple Comparisons Test, *$p<0.05$). Within the Firmicutes, both P3DEX and NTDEX significantly decreased the class Bacilli (Figure 5b. Kruskall Wallis with Dunn's Multiple Comparisons Test, *$p<0.05$). P3DEX alone, however, increased the class Erysipelotrichia (Figure 5c. Kruskall Wallis with Dunn's Multiple Comparisons Test, *$p<0.05$). We also observed a significant increase in Betaproteobacteria (p__Proteobacteria) and Verrucomicrobiae (p__Verrucomicrobia) (Figure 5d-e. Kruskall Wallis with Dunn's Multiple Comparisons Test, *$p<0.05$).

3.4.6 LNFPIII Conjugates Increase Bacteria of the Orders Bacteroidales, Burkholderiales, and Verrucomicrobiales

At the order level, we identified 12 different taxa present in our samples. A complete composition bar plot of all orders present is depicted in Supplementary Figure 2. P3DEX treatment significantly increased bacteria of the orders Bacteroidales (p__Bacteroidetes; c__Bacteroidia), Burkholderiales (p__Proteobacteria; c__Betaproteobacteria), and Verrucomicrobiales (p__Verrucomicrobia;

c__Verrucomicrobiae) (Figures 6a-c. Kruskall Wallis with Dunn's Multiple Comparisons Test, *p<0.05). This increases align with the increases in Bacteroidia, Betaproteobacteria, and Verrucomicrobiae we observed at the class level.

3.4.7 LNFPIII Conjugate-Induced Trends Continue at the Family Level, While LNnT Conjugates Cause Specific Outgrowths from the Order Clostridiales

We identified 22 bacterial families. A complete composition bar plot of all families is depicted in Supplementary Figure 3. LNnT conjugates significantly increased an undefined family of p__Bacteroidetes; c__Bacteroidia; o__Bacteroidales (Figure 7a. Kruskall Wallis with Dunn's Multiple Comparisons Test, *p<0.05). Both LNFPIII and LNnT conjugates significantly decreased *Lactobacillaceae*, which corresponds to the significant decreases we observed at the class and order levels (p__Firmicutes; c__Bacilli;o__Lactobacillales) (Figure 7b. Kruskall Wallis with Dunn's Multiple Comparisons Test, *p<0.05). While we did not observe significant increases in c__Clostridia or o__Clostridiales, NTDEX treatment enriched for two families from this class and order. NTDEX encouraged outgrowth of a population of *Defluviitaleaceae*, which we did not detect in neither the DEX, nor P3DEX group (Figure 7c. Kruskall Wallis with Dunn's Multiple Comparisons Test, *p<0.05). NTDEX also increased *Family XIII* (Figure 7d. Kruskall Wallis with Dunn's Multiple Comparison's Test, *p<0.05). P3DEX significantly increased an unknown family of p__Tenericutes; c__Mollicutes (Figure 7e. Kruskall Wallis with Dunn's Multiple Comparison's Test, *p<0.05). Last, P3DEX treatment increased *Verrucomicrobiaceae*, consistent with findings at higher taxonomic levels (Figure 7f. Kruskall Wallis with Dunn's Multiple Comparisons Test, *p<0.05).

3.4.8 LNFPIII and LNnT Conjugates Significantly Altera Genera from Each Phylum

We identified 39 genera present in our fecal samples and observed specific, significant differences in each phylum (Supplementary Figure 4). Within Actinobacteria, we observed a trending increase in *Adlercreutzia-Assacharobacter* (Figure 8a. Kruskall Wallis with Dunn's Multiple Comparisons Test, p=0.0969). Although not significant, we also saw the absence of *Bifidobacterium* in DIO mice treated with P3DEX (Figure 8b. Kruskall Wallis with Dunn's Multiple Comparisons Test, p=0.1530). This is noted here, given that it is well-regarded that *Bifidobacterium* feed on HMOs [280-282]. NTDEX also increased populations of p__Actinobacteria; c__Coriobacteriia; o__Coriobacteriales; f__Coriobacteriaceae, notably *Enterorhabdus* and *Parvibacter* (Figures 8c-d. Kruskall Wallis with Dunn's Multiple Comparisons Test, *p<0.05, ***p<0.001). Within Bacteroidetes, P3DEX significantly increased *Bacteroides* (Figure 9a. Kruskall Wallis with Dunn's Multiple Comparisons Test, *p<0.05). NTDEX significantly increased an unknown genus of Bacteroidetes, which also seemed to be increased by P3DEX (non-significantly) compared to DEX (Figure 9b. Kruskall Wallis with Dunn's Multiple Comparisons Test,*p<0.05). We observed the most diverse responses within the phylum Firmicutes. Within the order Clostridiales, we noted a trending decrease in *Clostridium* in P3DEX-treated animals (Figure 10a. Kruskall Wallis with Dunn's Multiple Comparisons Test, p=0.0571). We observed a significant increase in an unknown genus of the *Christenellaceae* family in these DIO mice as well (Figure 10b. Kruskall Wallis with Dunn's Multiple Comparisons Test, p<0.05). NTDEX increased unknown genera of f__Defluviitaleaceae and f_Family XIII (Figures 10c-d. Kruskall Wallis with Dunn's Multiple Comparisons Test, p<0.05). Both P3DEX and NTDEX treatment induced

trending increases in *Marvinbryantia* from the family *Lachnospiraceae* (Figure 10e. Kruskall Wallis with Dunn's Multiple Comparisons Test, p=0.1272 for P3DEX; p=0.1005 for NTDEX). In the family *Erysipelotrichaceae,* we observed a significant increase in an unknown genus in NTDEX-treated animals (Figure 10f. Kruskall Wallis with Dunn's Multiple Comparisons Test, **p<0.01). Both P3DEX and NTDEX decreased *Lactobacillus* compared to the DEX control (Figure 10g. Kruskall Wallis with Dunn's Multiple Comparisons Test, *p<0.05). P3DEX also increased *Oscillibacter* and *Ruminoclostridium* from the family *Ruminococcaceae* (Figure 10h-i. Kruskall Wallis with Dunn's Multiple Comparisons Test,*p<0.05). In terms of *Proteobacteria,* P3DEX treatment increased the *Parasutterella* genus (Figure 11. Kruskall Wallis with Dunn's Multiple Comparisons Test, *p<0.05). Last, P3DEX-treated animals had higher levels of *Akkermansia* from the phylum Verrucomicrobia (Figure 12. Kruskall Wallis with Dunn's Multiple Comparisons Test, *p<0.05).

3.4.9 LEfSe Analysis Reveals Significant Biomarkers for DEX, P3DEX, and NTDEX

LEfSe analysis is used to determine changes in bacterial species with biological relevance [276]. In this experiment, LEfSe identified different bacterial signatures for each treatment group. Figure 13 shows biomarkers with LDA scores > 2. Figure 14 summarizes this information in a cladogram plot. DIO mice treated with DEX exhibited outgrowths of Lactobaccillus, a controversial characteristic of consuming a high-fat diet [283]. We specifically identified *L. johnsonni* in these animals. DEX treatment did not appear to have a significant effect on the microbiome between pre-treatment and post-treatment timepoints (Supplementary Figure 6). For DIO animals treated with P3DEX, we noted the significant presence of *Akkermansia muciniphila, Bacteroides*

thetaiotaomicron, and several species from the families *Ruminococcaceae, Lachnospiraceae,* and *Christensenellaceae* (phylum: Firmicutes). For NTDEX-treated animals, we saw significant appearances in *Bifidobacterium pseudolongum, Clostridium celatum, Enterorhabdus caecimuris, Parvibacter caeciola, Enterorhabdus mucosicola,* as well as several other species of the classes Coriobacteriia (p__Actinobacteria), Clostridia (p__Firmicutes), and Erysipelotrichia (p__Firmicutes). In this regard, it is clear that each treatment caused unique and specific effects.

3.5 Discussion

Numerous studies have shown that obesity and MetS contribute to maladaptation of the microbiome, and for this reason, researchers have sought to pinpoint prebiotic and/or probiotic factors that can re-establish microbial balance to aid in amelioration of disease. Herein, we describe the microbial alterations induced by systemic administration of conjugates of two known prebiotic HMOs: LNFPIII and LNnT. Previous studies have shown that systemic administration of LNFPIII conjugates are successful therapeutics in DIO mice, in part via improving glucose homeostasis, increasing insulin signaling, decreasing crown-like structures and inflammation in white adipose tissue, and reducing lipogenesis and fat accumulation in the liver [165]. In a direct comparison of LNFPIII and LNnT conjugates in DIO mice, we demonstrated that LNnT did not harbor the same therapeutic effects (in review). It is even plausible that LNnT conjugates led to worse metabolic outcomes.

While LNFPIII and LNnT differ in structure via the presence of a single α1,3-linked fucose on LNFPII, the difference between their cellular mechanisms in conjugate form have long been recognized. LNFPIII conjugates, for example, induce M2 and DC2

polarization in both macrophages and dendritic cells [146, 156, 157, 159, 160]. In contrast, LNnT conjugates activate M2 macrophages, but do not act on dendritic cells [161]. LNFPIII conjugates also act on B cells, adipocytes, and hepatocytes, as well as have indirect effects on NK cells, CD4+ T cells, and CD8+ T cells via interactions with antigen-presenting cells (APCs) [148, 155, 158, 165]. Since we injected both conjugates through the intraperitoneal route in this experiment, it is uncertain whether these cellular effects drove the microbial changes we depict here. As with most microbiome studies that evaluate therapeutic intervention, it is possible that bidirectional communication between microbial populations and the immune system led to the overall changes reported.

We report a decrease in absolute bacterial abundance and an increase in species richness (chao1, fisher alpha, observed species, PD_whole tree) in response to HMO conjugate treatment. These changes were significant for the LNnT conjugate-treated group, as shown in Figures 1 & 2. What could be the explanation for these reciprocal changes? It is possible that diverse bacterial populations competed for the same resources within the gastrointestinal tract of DIO mice, and therefore, reduced overall growth or abundance [284]. It is also possible that HMO treatment expanded the metabolic capabilities of the intestinal microbiome, therefore reducing the ecological need for such a large abundance. There are numerous factors (pH, O_2 levels, nutrients, etc.) that can alter both the number and assortment of bacteria present in the gut [285]. Regardless of these postulated reasons, an increase in species richness is considered beneficial to the host. In humans, decreased α-diversity has been associated with increased fat accumulation, insulin resistance, and inflammation [67, 268]. While the importance of

diverse bacterial populations is well-recognized, the exact mechanisms are still undetermined.

Upon initial investigation of microbial composition changes in DIO mice treated with DEX, P3DEX, or NTDEX, we first observed significant alterations at the phylum level (Figure 3a-h). In general, the microbiome is resistant to acute perturbations. At this level, however, we observed significant increases in *Bacteroidetes*, *Proteobacteria*, and *Verrucomicrobia* in response to treatment with LNFPIII conjugates (Figure 3b, 3d, & 3f). This resulted in a highly significant increase in the ratio of *Firmicutes* to *Bacteroidetes* (Figure 3h). The ratio of *Firmicutes* to *Bacteroidetes* has been proposed as a potential biomarker for gut dysbiosis, given that these two phyla are the most abundant in the intestinal microbiome and have been shown to be altered in obese mice and humans [286]. While other trends have been reported, it is well-accepted that *Bacteroidetes* decrease and *Firmicutes* increase in obese individuals [287]. Studies concerning *Firmicutes* have shown that this increase might be attributed to the notion that these bacteria are more efficient at harvesting energy and absorbing calories [70, 288]. The ratio of *Firmicutes* to *Bacteroidetes* is often normalized in response to diet and weight loss [287].

While we observed differences at each taxonomic level, the most important changes were identified at the species level via LefSe analysis (Figure 12a-c). In the DEX-treated group, the most unique population was *Lactobacillus johnsonii* (Figure 12a). Several species of *Lactobacilli* have long been used as probiotics and *Lactobacillus johnsonii* is considered part of the “acidophilus complex” [289, 290]. Nonetheless, *Lactobacilli* are increased in obese patients and have been implicated in weight gain [287,

291-293]. In this regard, is unsurprising that this was the most unique population in our DIO mice treated with the DEX control.

In our P3DEX-treated DIO mice, we observed specific enrichment of *Akkermansia muciniphila* and *Bacteroides thetaiotaomicron*, as well as several undefined species of the following families (p__Firmicutes; c__Clostridia; o__Clostridiales): *Ruminoccocaceae, Lachnospiraceae*, and *Christensenellaceae. A. muciniphila* has been associated with a healthy biome, inversely related to obesity and MetS, and used as a successful intervention in DIO mice and humans [294-300]. In particular, the presence of *A. muciniphila* was correlated with decreased fasting glucose, lessened waist-to-hip ratio, reduced adipocyte size, and improved insulin parameters [294]. This is exciting because *A. muciniphila* has also been shown to feed on HMOs *in vitro* [301]. This species is also able to metabolize fucose [302]. In this regard, the fact that we observe outgrowth of *A. muciniphila* and improvement in metabolic function in response to LNFPIII conjugate treatment aligns well with previous studies.

We saw an increase in Bacteroidetes in response to LNFPIII conjugate treatment and a specific increase in *B. thetaiotaomicron* (Figure 12b). Correlative studies have shown decreased levels of *B. thetaiotamicron* in obese rodents and humans, which have been restored via dietary interventions or bariatric procedures [303, 304]. *B. thetaiotaomicron* has been shown to grow on both fucose- and sialic acid-bearing HMOS (2'FL, 3'FL, 3'-SL, 6'-SL), but has not been tested on LNFPII *in vitro* [305]. Its wide range of metabolic capabilities is unsurprising, given that 20% of its genome contains enzymes and transporters for polysaccharide utilization [306-309]. This includes at least 226 different glycosidase hydrolases and 15 polysaccharide lyases [310]. *B.*

thetaiotamicron has also been shown to increase host fucosylation in the gastrointestinal tract when fucose is available as a nutrient source [311, 312]. This suggests that LNFPII conjugates might provide a nutritional source for *B. thetaiotamicron* and encourage upregulation of fucose-utilization genes in *B. thetaiotamicron*, thereby leading to enhanced host cell fucosylation and increased production of soluble factors beneficial for maintaining gut homeostasis. The caveat here, however, is that we administered LNFPIII conjugates via the intraperitoneal route and there is no evidence that the conjugates directly enter the lumen of the gut to alter the microbiome. It is likely that these effects are exerted via an indirect mechanism.

Last, we observed increases in *Ruminoccocaceae, Lachnospiraceae*, and *Christensenellaceae* (p__Firmicutes; c__Clostridia; o__Clostridiales) in response to P3DEX treatment (Figure 12b). Oral Administration of 2'FL has been shown to enrich *Ruminoccocaceae* in mice, but there are no studies on LNFPIII [313]. Both *Ruminoccocaceae* and *Lachnospiraceae* have been reported to be increased in the obese state, but also increased in the context of therapeutic intervention with various compounds. At this time, investigations concerning these two families seem to be based on correlation alone. *Christensenellaceae* is slightly more well-studied during obesity and MetS. The presence of *Christensenellaceae* is higher in individuals with normal versus obese BMIs and enriched after weight loss [314, 315]. *Christensenellaceae* has also been associated with lower triglyceride and low-density lipoprotein (LDL) levels, as well as increased levels of high-density lipoprotein (HDL) cholesterol [316, 317]. Overall, it can be concluded that LNFPIII conjugates induce beneficial changes in the gut microbiome. However, the exact mechanisms that lead to these changes have yet to be defined.

LNnT conjugate treatment in DIO mice led to diverse set of changes. The most notable change was enrichment of *Bifidobacterium pseudolongum* (Figure 12c). Little is known about *Bifidobacterium* during obesity and MetS, but the presence of this genus declines significantly after weaning and throughout adulthood [318]. However, *Bifidobacterium* was the first genus known to feed on HMOs. Some species, such as *B. infantis*, have over 20 glycosidases to cleave sugars. In contrast, other species (i.e. *B. breve*) can only metabolize free monosaccharides [108, 133, 319]. Infants fed formula supplemented with 2'FL and LNnT have greater quantities of *Bifidobacterium spp*. in their gut [237]. In this regard, treatment of DIO mice with LNnT conjugates might have introduced a selective advantage for *Bifidobacterium* in the gut. Again, it cannot be concluded whether this effect is direct or indirect.

Similar to LNFPIII conjugate treatment, we also observed an increase in species from the *Ruminoccocaceae* and *Lachnospiraceae* families (p__Firmicutes; c__Clostridia; o__Clostridiales) in response to LNnT conjugate treatment (Figure 12c). At this time, there is no well-supported explanation for this. We also observed increases in *Family XIII* and *Defluvitaleaceae* (p__Firmicutes; c__Clostridia; o__Clostridiales), as well as *Erysipelotrichaceae* (p__Firmicutes; c__Erysipelotrichia; o__Erysipelotrichales) (Figure 12c). At the species level, we identified *Clostridium celatum*, *Enterorhabdus caecimuris*, *Parvibacter caecicola*, and *Enterorhabdus mucosicola* (Figure 12c). Little is known about these bacteria, but *C. celatum* has been shown to be pathogenic to humans and *E. mucosicola* was first isolated from the inflamed mucosa of rodents [320, 321]. It is possible that treatment with LNFPIII induced protective functions because it contains fucose, but these protective functions are lost with LNnT treatment and allows

colonization with pathogenic bacteria. This is similar to what is observed in the breastmilk of secretor vs. non-secretor mothers, wherein non-secretor mothers lack many fucosylated HMOs and lose some anti-bacterial functions in their breastmilk [108].

The 16S sequencing presented here adds to the growing literature of the effects of HMOs on the microbiome. We also identify specific bacteria (i.e. *A. muciniphila* and *B. thetaiotamicron*) that might complement the therapeutic abilities of LNFPIII conjugates, especially in obese patients. There are several limitations to this work. First, we are lacking 16S sequencing data on the microbial composition of these DIO mice prior to therapeutic intervention. Second, published studies on microbiome composition are variable. Differences in experimental design, starting microbiomes, and analysis techniques make interpretation difficult. Furthermore, the field is still novel and studies are often correlational, not mechanistic, in nature. Third, studies involving the effects of obesity and HMO supplementation on the microbiome often have conflicting results. For each report on one bacterial genus, an opposite or opposing trend has been found. This emphasizes the vast importance of investigating species-dependent effects. To our knowledge, this is the first comparison of the effects of two different HMOs on the microbiome of diet-induced obese (DIO) mice. We hope that this report sheds light on the microbial changes induced both in the obese state and in response to HMO supplementation, which can open novel therapeutic avenues for this condition.

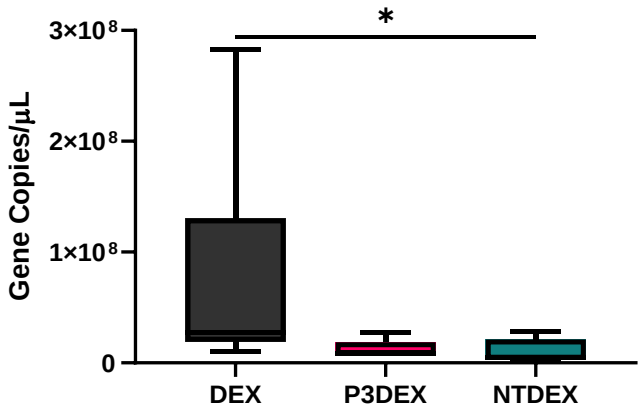

Figure 3.1: Absolute abundance of bacterial species determined by the diversity of 16S rDNA sequences measured in fecal samples of DIO mice treated with DEX, P3DEX, or NTDEX. Kruskall Wallis with Dunn's Multiple Comparisons Test, *p<0.05.

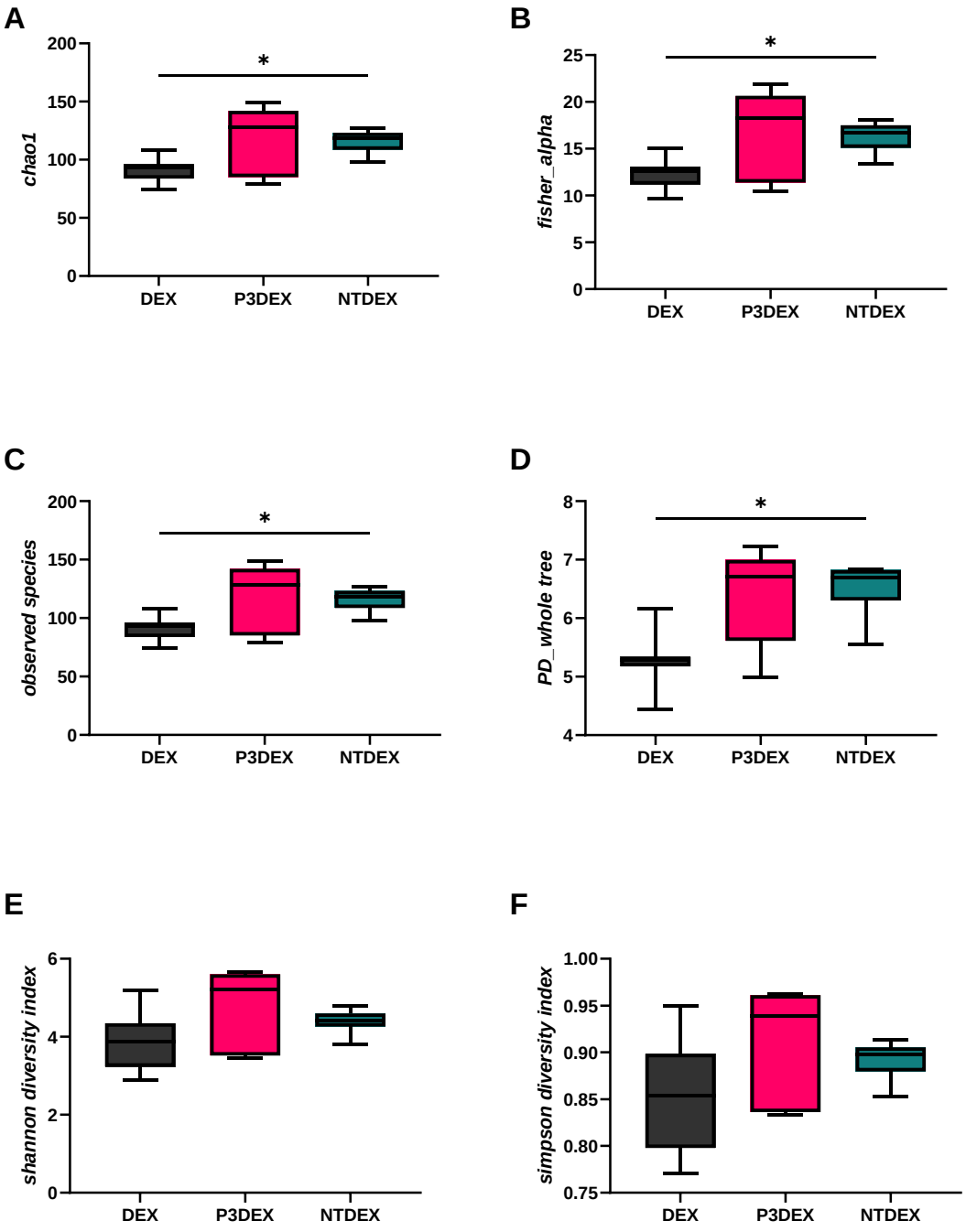

Figure 3.2: α-diversity (species richness and evenness). Alpha-diversity indices measured as **A.** chao1, **B.** fisher_alpha, **C.** observed species, **D.** PD_whole tree, **E.** Shannon diversity, and **F.** Simpson diversity. Kruskall-Wallis with Dunn's Multiple Comparisons Test, *p<0.05.

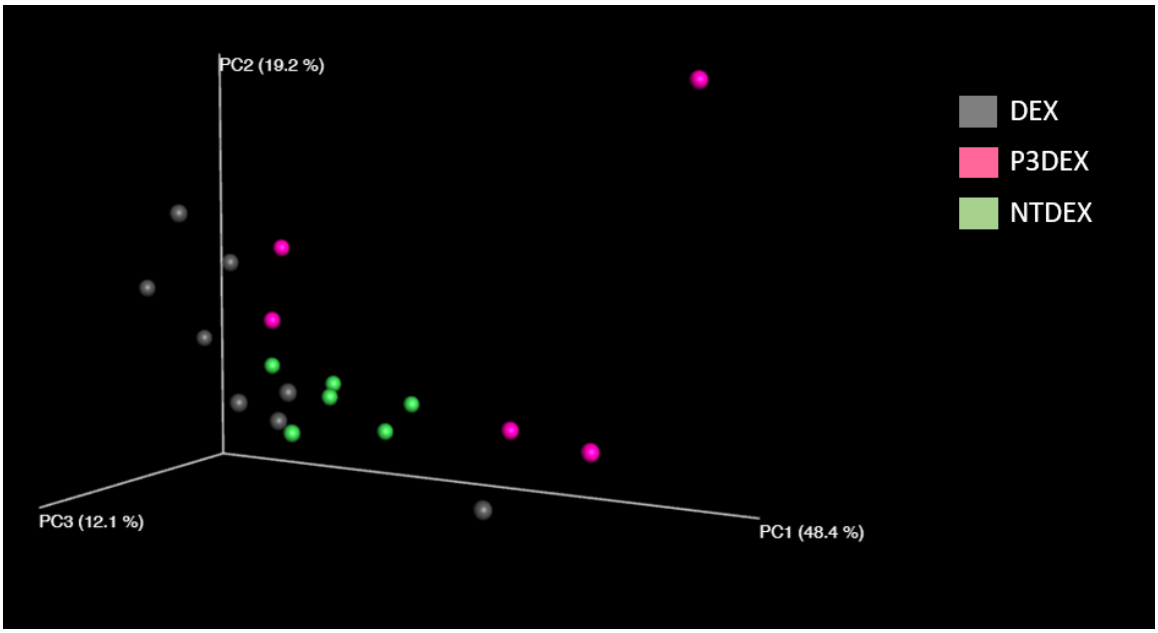

Figure 3.3: β-diversity. Bray-Curtis dissimilarity using ASVs. Matrix of paired-wise distance between samples was used to construct a 3D PCoA plot (shown here). Each point represents the 16S rRNA gene sequences from a single mouse.

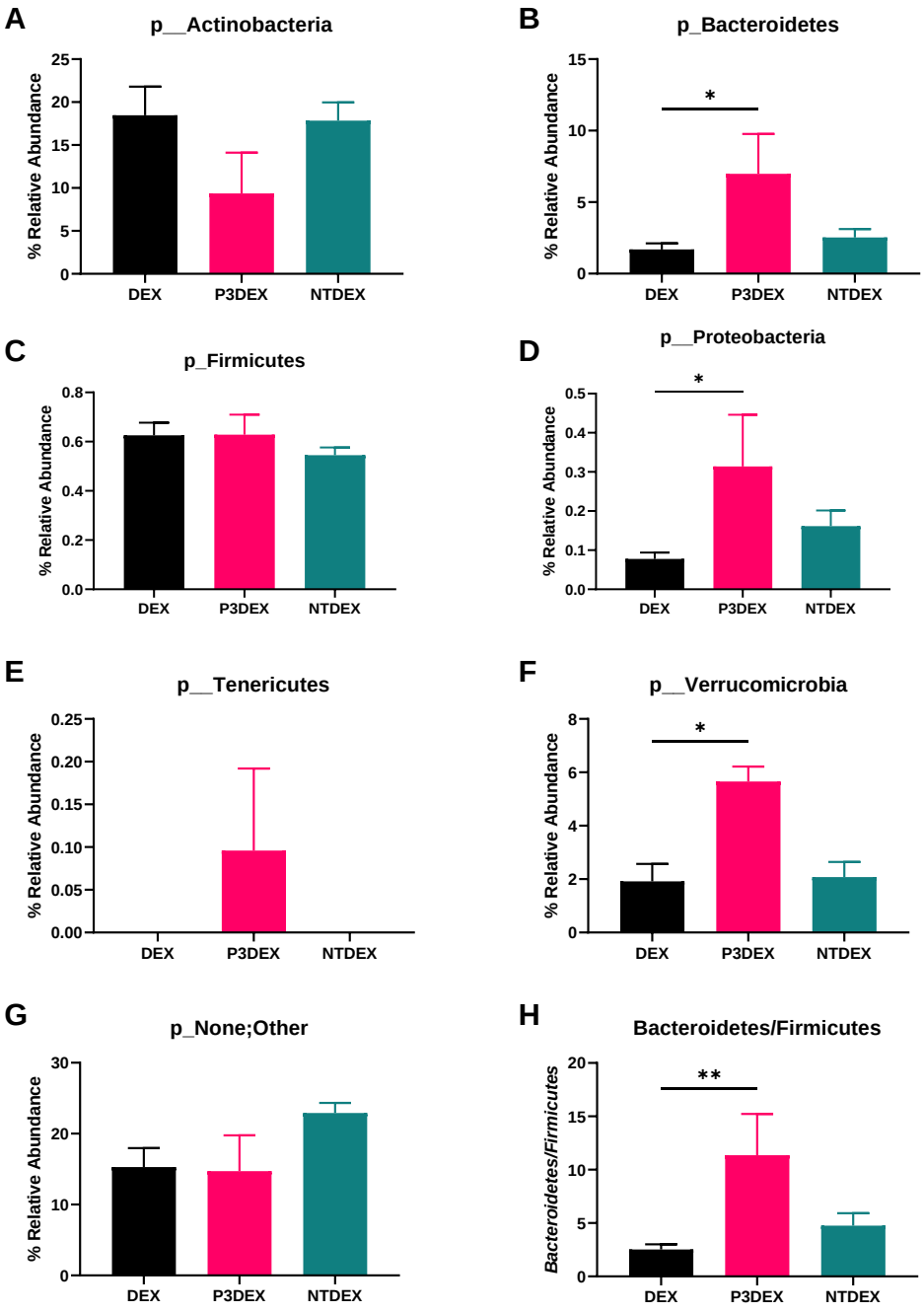

Figure 3.4: Relative abundance of all present phyla. Relative abundances for **A.** Actinobacteria, **B.** Bacteroidetes, **C.** Firmicutes, **D.** Proteobacteria, **E.** Tenericutes, **F.** Verrucomicrobia, and **G.** None;Other. **H.** Ratio of Bacteroidetes/Firmicutes. Kruskall-Wallis with Dunn's Multiple Comparisons Test. *p<0.05, **p<0.01. Mean ± SEM shown here.

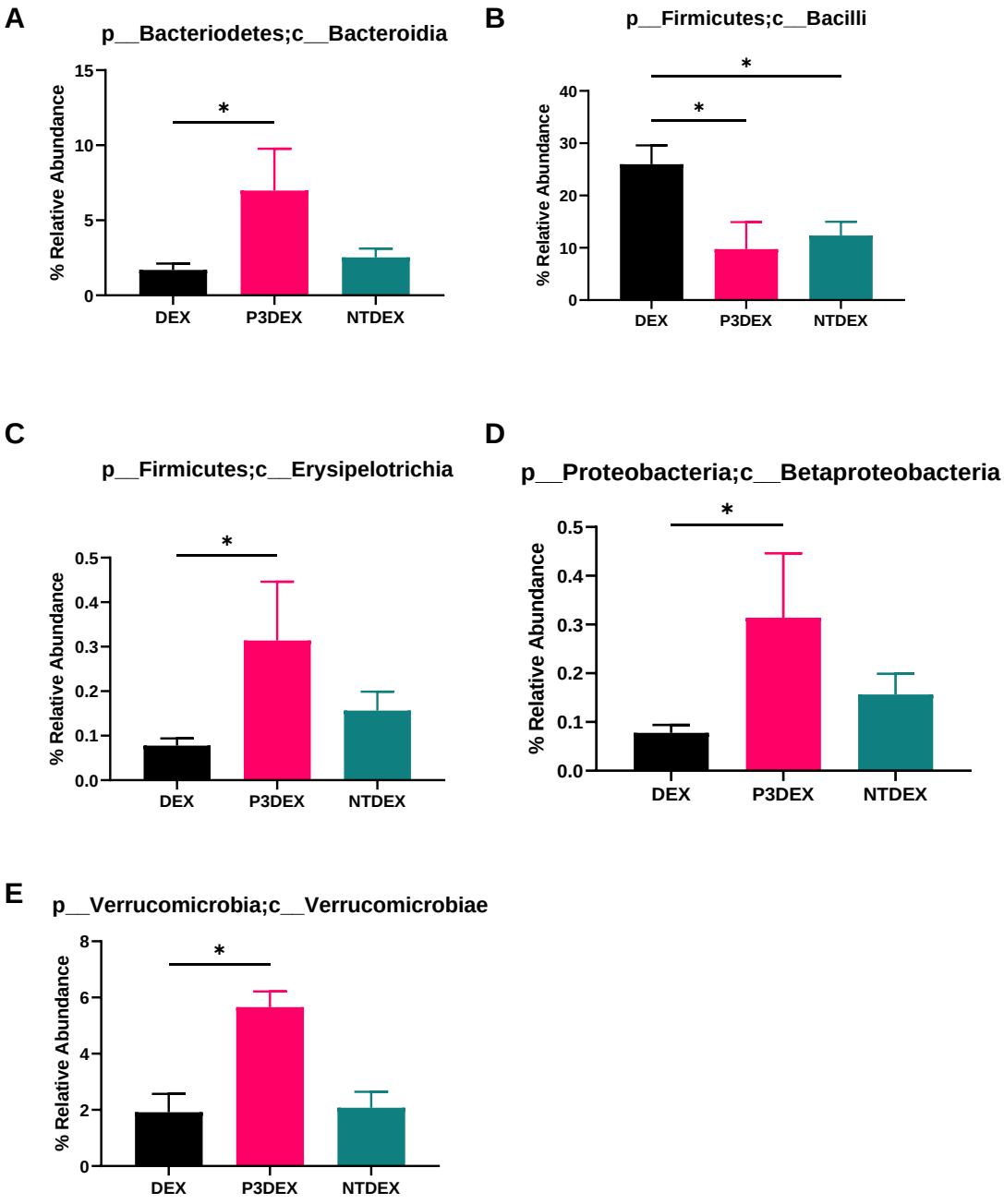

Figure 3.5: Relative abundance at the class level. Significant differences were observed in the following classes: **A.** Bacteroidia, **B.** Bacilli, **C.** Erysipelotrichia, **D.** Betaproteobacteria, and **E.** Verrucomicrobiae. Kruskal-Wallis with Dunn's Multiple Comparisons Test. *$p<0.05$. Mean ± SEM shown here.

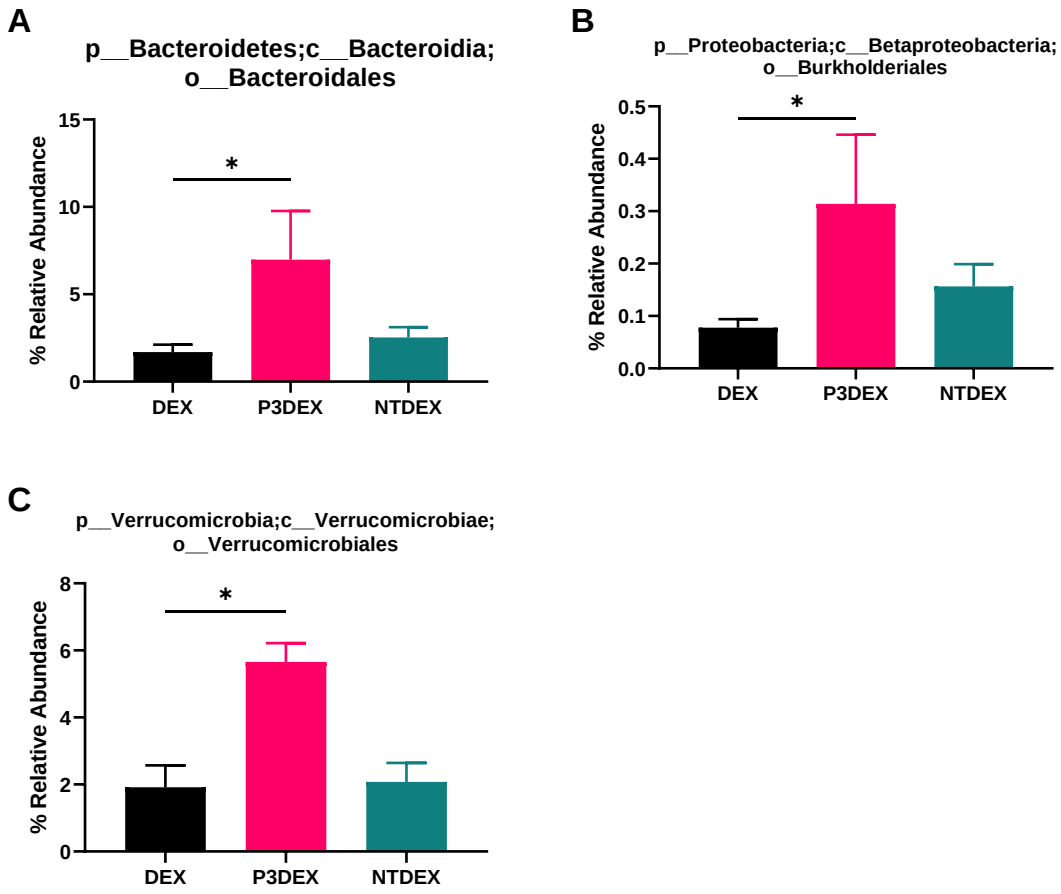

Figure 3.6: Relative abundance at the order level. Significant alterations were observed in the following orders: **A.** Bacteroidales, **B.** Burkholderiales, and **C.** Verrucomicrobiales. Kruskal-Wallis Test with Dunn's Multiple Comparisons Test. *p<0.05.

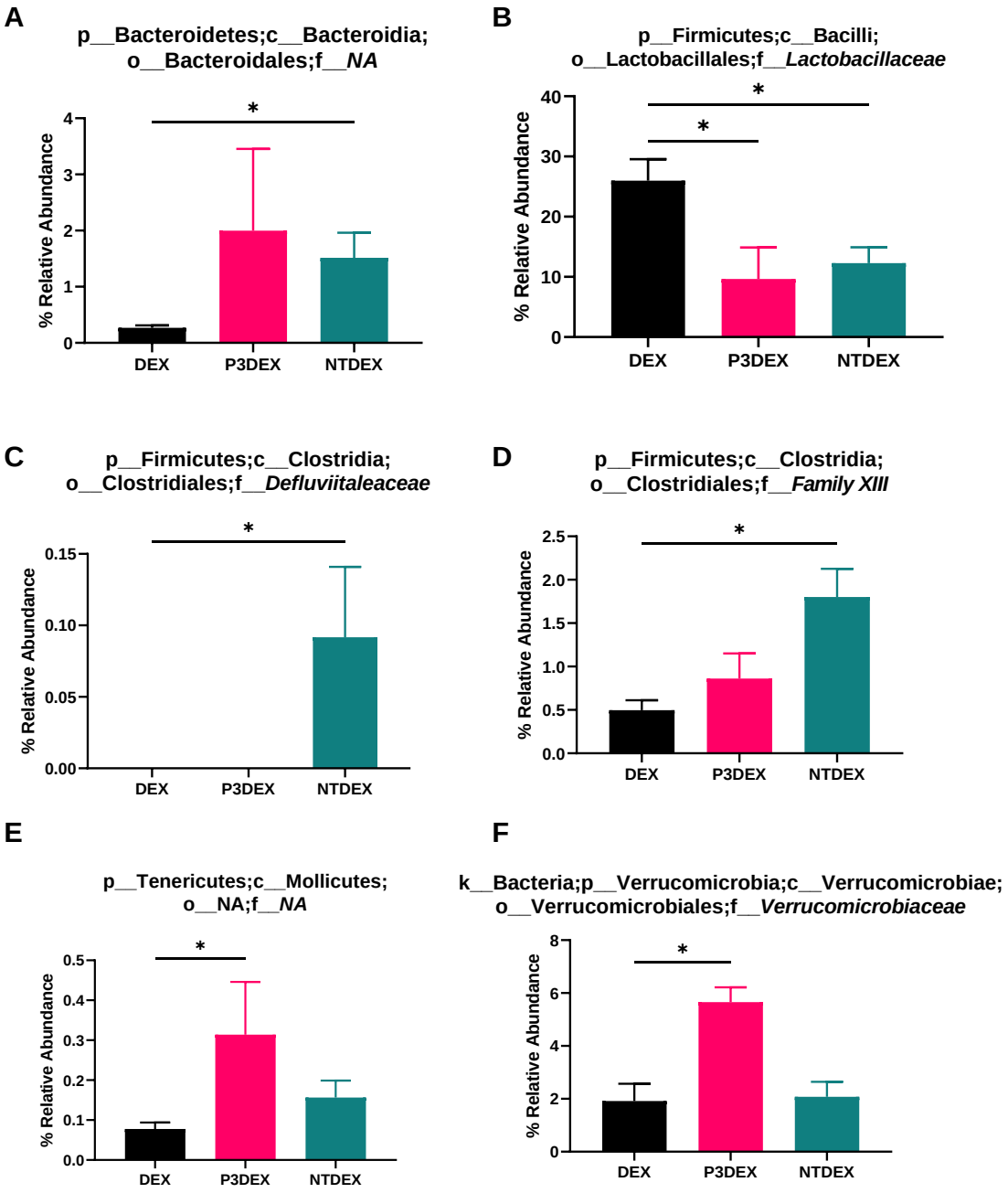

Figure 3.7: Relative abundance at the family level. Significant differences were observed in the following families: **A.** o__Bacteroidales (unknown family), **B.** *Lactobacillaceae*, **C.** *Defluviitaleaceae*, **D.** *Family XIII*, **E.** c__Mollicutes (unknown family), and **F.** *Verrucomicrobiaceae*. Kruskal-Wallis with Dunn's Multiple Comparisons Test. *p<0.05. Mean ± SEM shown here.

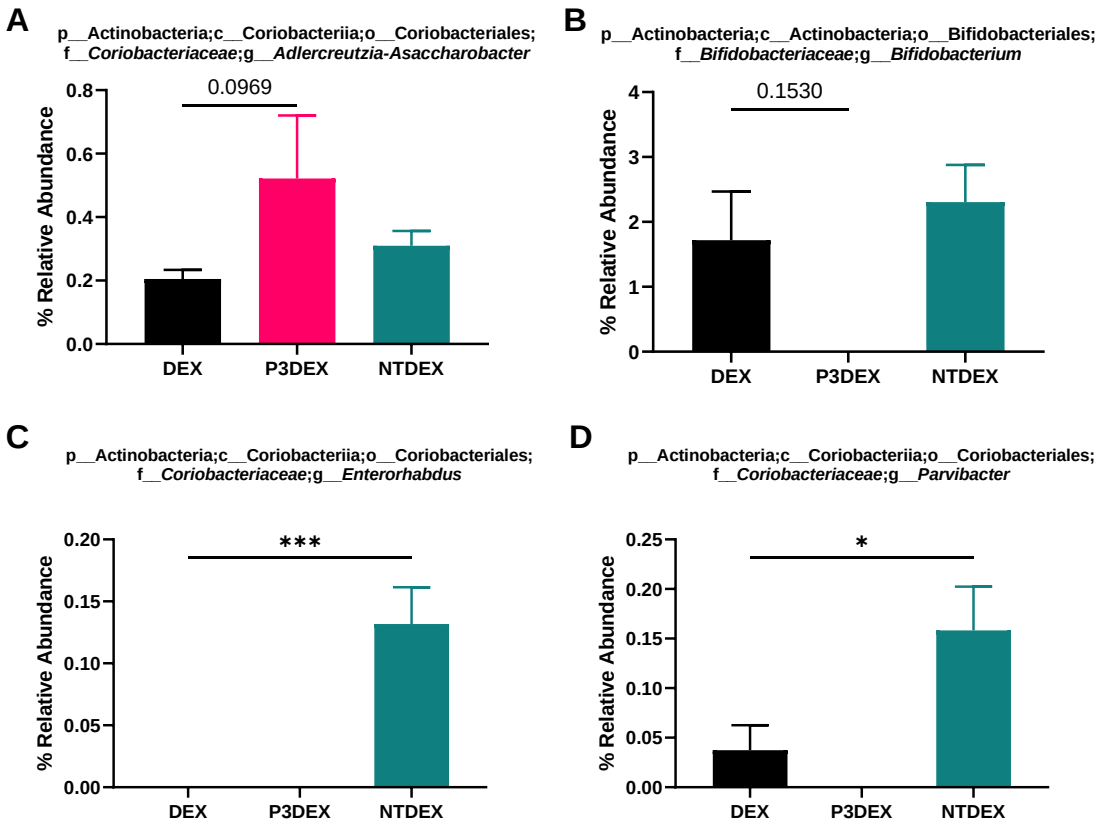

Figure 3.8: Relative abundance of select genera within phylum Actinobacteria. Significant or trending differences were observed in the following genera: A. *Adlercreutzia-Assacharobacter*, B. *Bifidobacterium*, C. *Enterorhabdus*, and D. *Parvibacter*. Kruskal-Wallis Test with Dunn's Multiple Comparisons Test. *p<0.05, ***p<0.001. Mean ± SEM shown here.

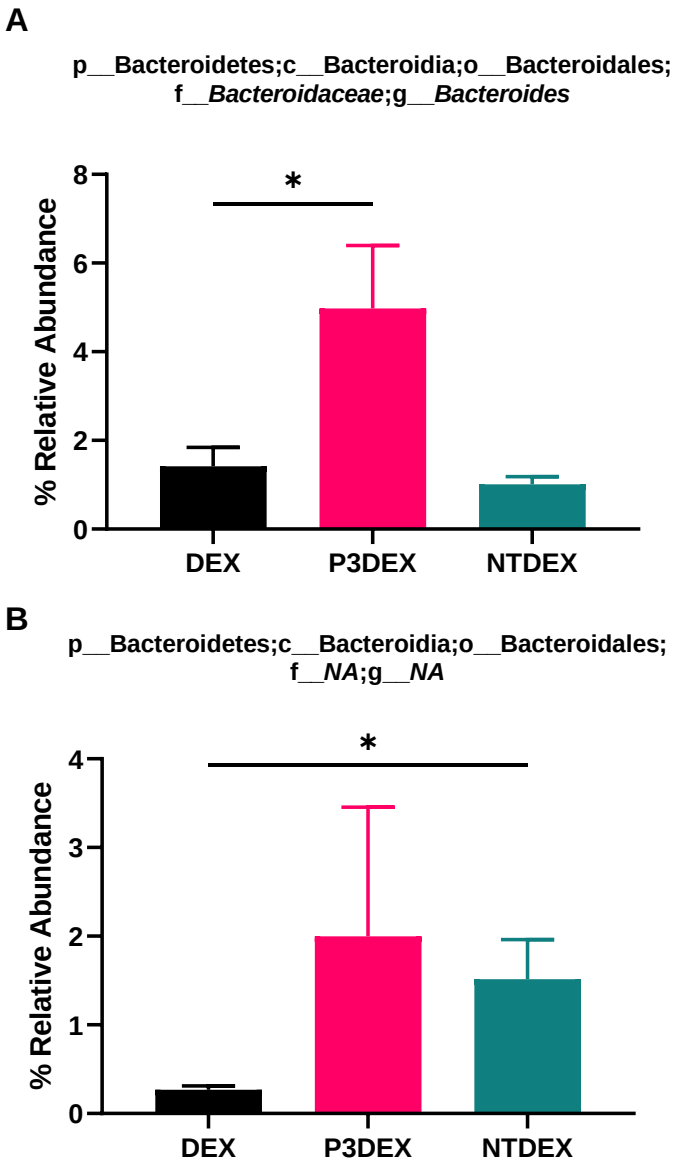

Figure 3.9: Relative abundance of select genera within phylum Bacteroidetes. Significant differences were observed in the following genera: **A.** *Bacteroides*, and **B.** o__Bacteroidales (genus unknown). Kruskal-Wallis Test with Dunn's Multiple Comparisons Test. *p<0.05. Mean ± SEM shown here.

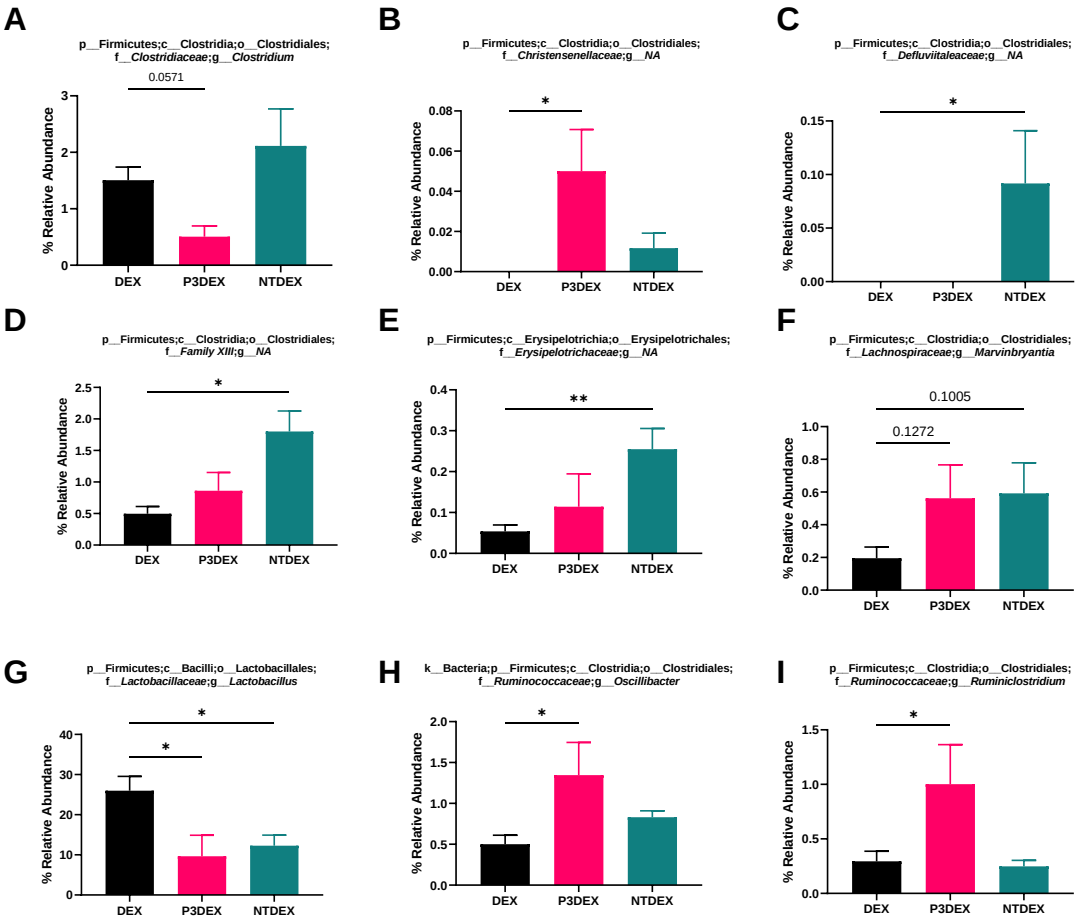

Figure 3.10: Relative abundance of select genera within phylum Firmicutes. Significant or trending differences were observed in the following genera: **A.** *Clostridium*, **B.** f__*Christensenellaceae* (genus unknown) **C.** f__*Defluviitaleaceae* (genus unknown), **D.** f__*Family XIII* (genus unknown), **E.** f__*Erysipelotrichaceae* (genus unknown), **F.** *Marvinbryantia*, **G.** *Lactobacillus*, **H.** *Oscillobacter*, and **I.** *Ruminoclostridium*. Kruskal-Wallis Test with Dunn's Multiple Comparisons Test. *p<0.05, **p<0.01. Mean ± SEM shown here.

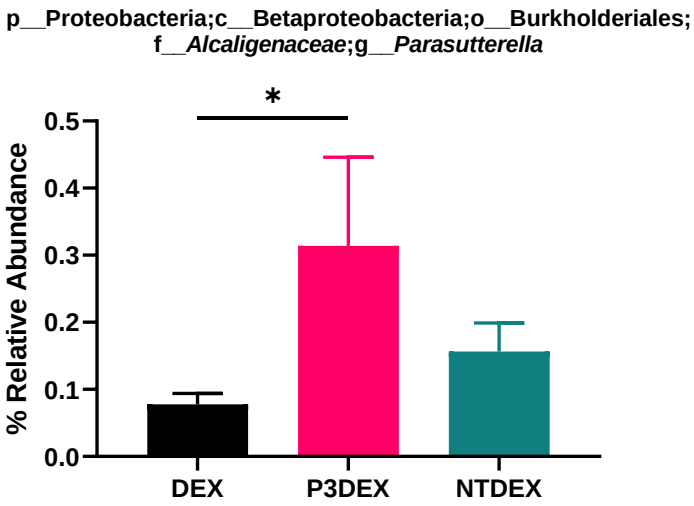

Figure 3.11: Relative abundance of select genera within phylum Proteobacteria. Significant differences were observed in the *Parasutterella* genus. Kruskal-Wallis Test with Dunn's Multiple Comparisons Test. *p<0.05. Mean ± SEM shown here.

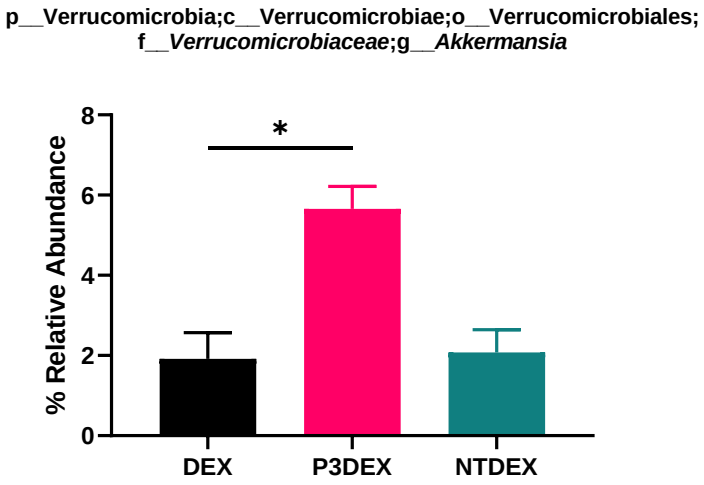

Figure 3.12: Relative abundance of select genera within phylum Verrucomicrobia. Significant differences were observed in the *Akkermansia* genus. Kruskal-Wallis Test with Dunn's Multiple Comparisons Test. *p<0.05. Mean ± SEM shown here.

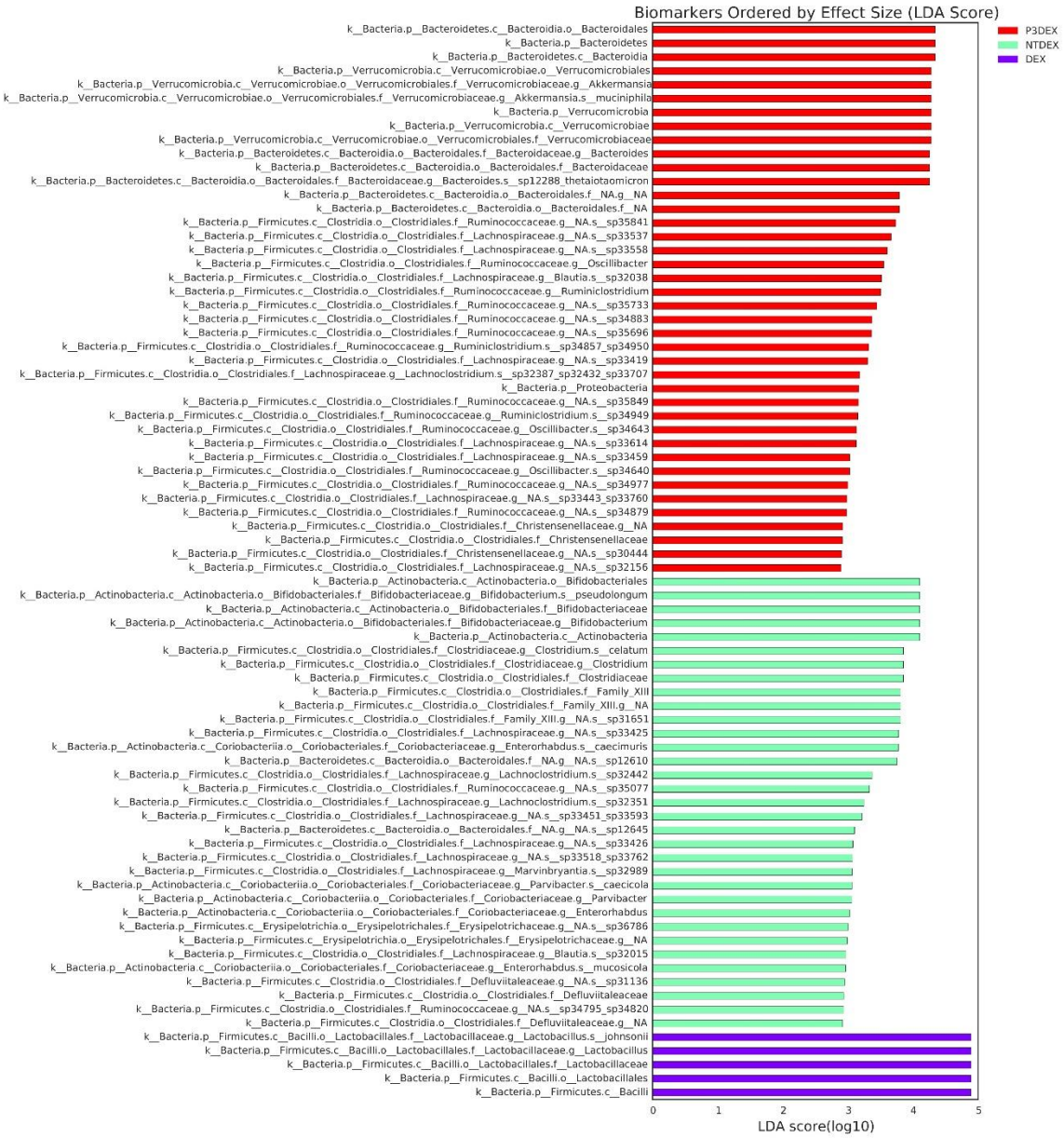

Figure 3.13: LEfSe analysis of microbiome changes following DEX, P3DEX, or NTDEX treatment. Significantly different biomarkers were identified via LEfSE analysis with a threshold score of 2.5 and $p \leq 0.05$.

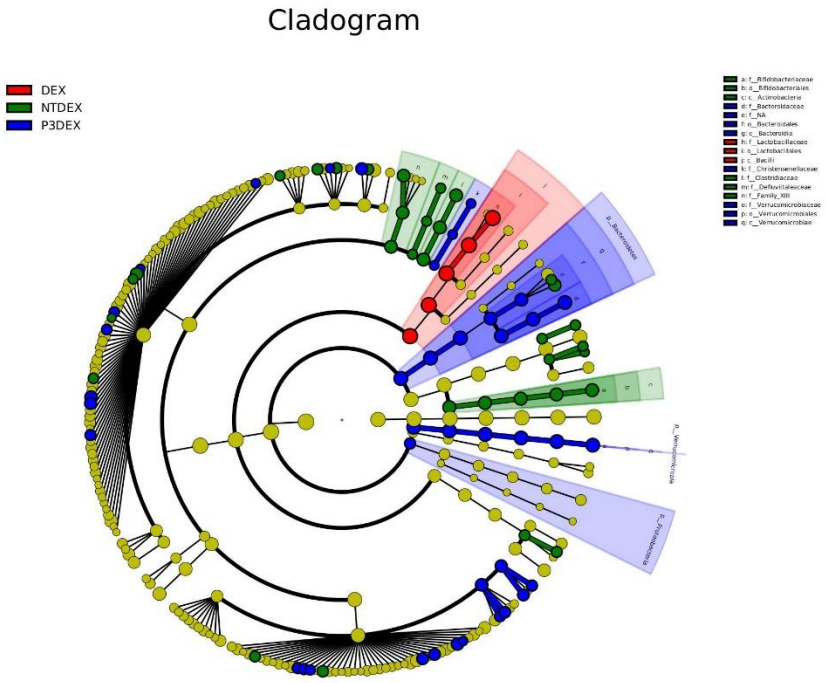

Figure 3.14: Cladogram of LEfSe analysis. Significantly different biomarkers were identified via LEfSE analysis with a threshold score of 2.5 and $p \leq 0.05$.

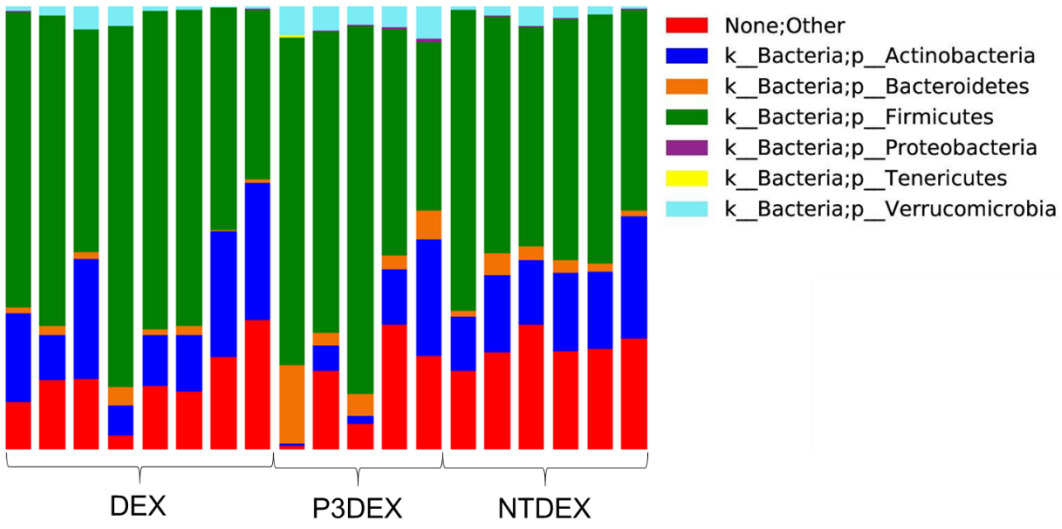

Figure 3.S1: Composition bar plots of all phyla present. Color-coded bar plot shows the distribution of bacterial phyla in the gut of DIO mice treated with DEX, P3DEX, or NTDEX.

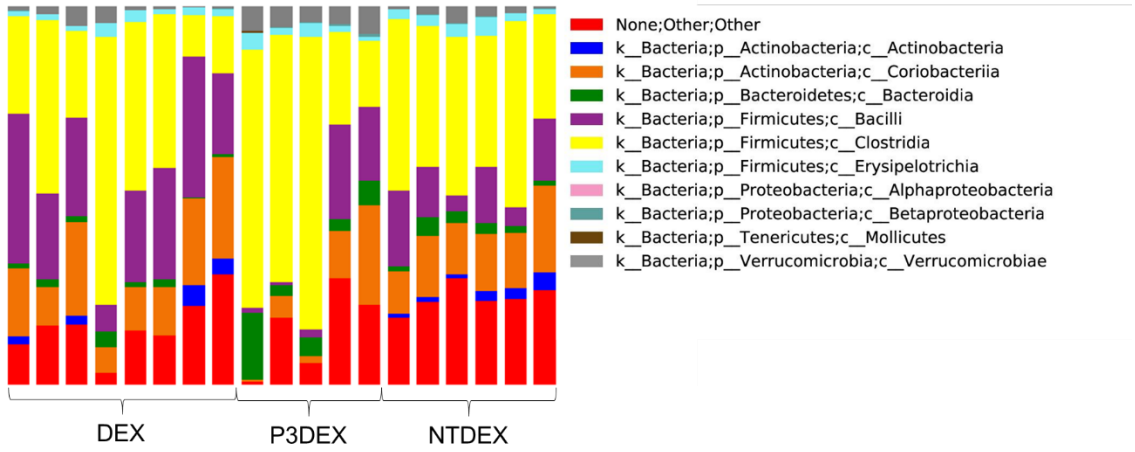

Figure 3.S2: Composition bar plots of all classes present. Color-coded bar plot shows the distribution of bacterial classes in the gut of DIO mice treated with DEX, P3DEX, or NTDEX.

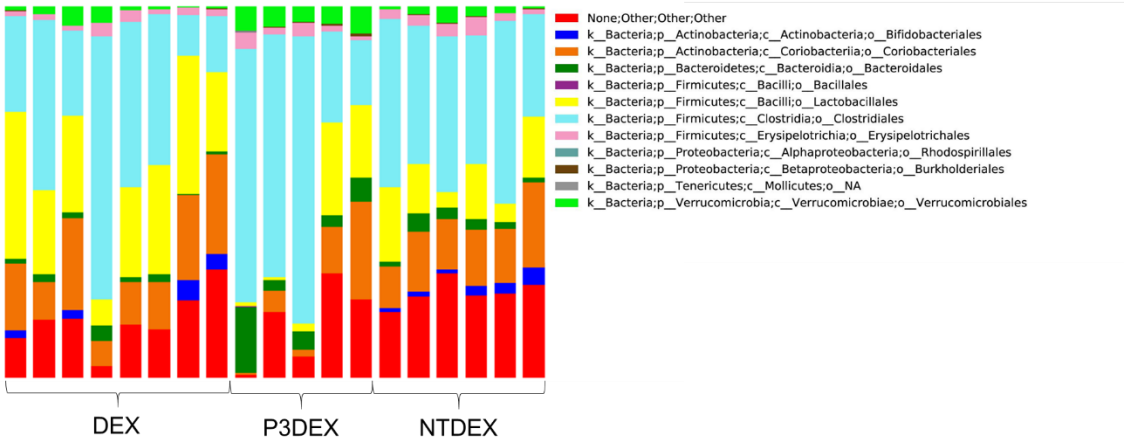

Figure 3.S3: Composition bar plots of all orders present. Color-coded bar plot shows the distribution of bacterial orders in the gut of DIO mice treated with DEX, P3DEX, or NTDEX.

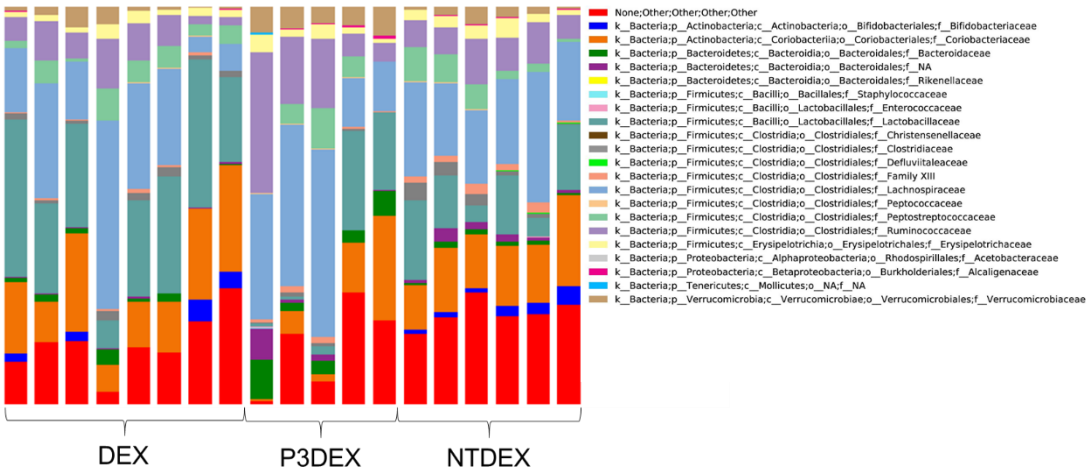

Figure 3.S4: Composition bar plots of all families present. Color-coded bar plot shows the distribution of bacterial families in the gut of DIO mice treated with DEX, P3DEX, or NTDEX.

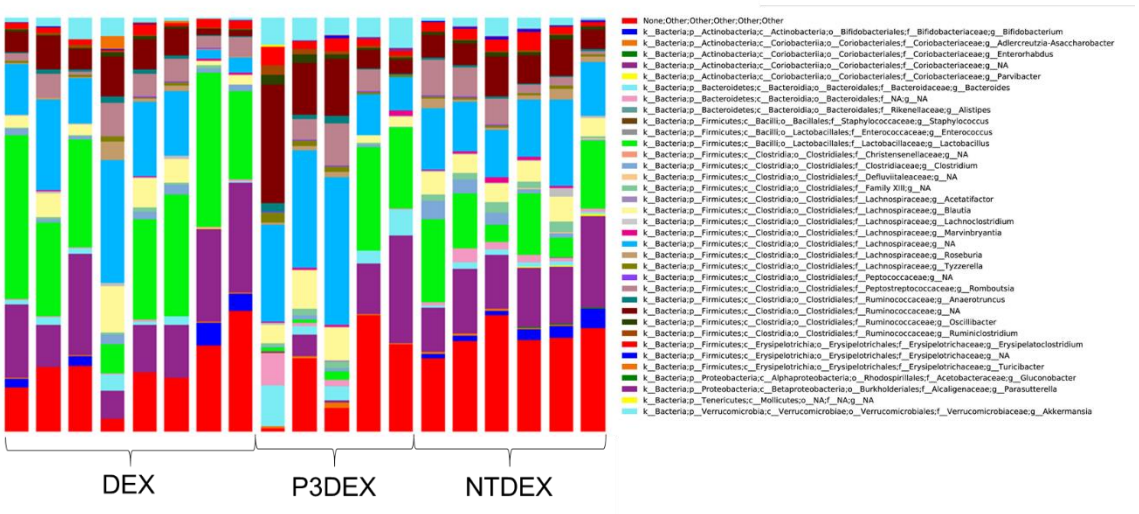

Figure 3.S5: Composition bar plots of all genera present. Color-coded bar plot shows the distribution of bacterial genera in the gut of DIO mice treated with DEX, P3DEX, or NTDEX.

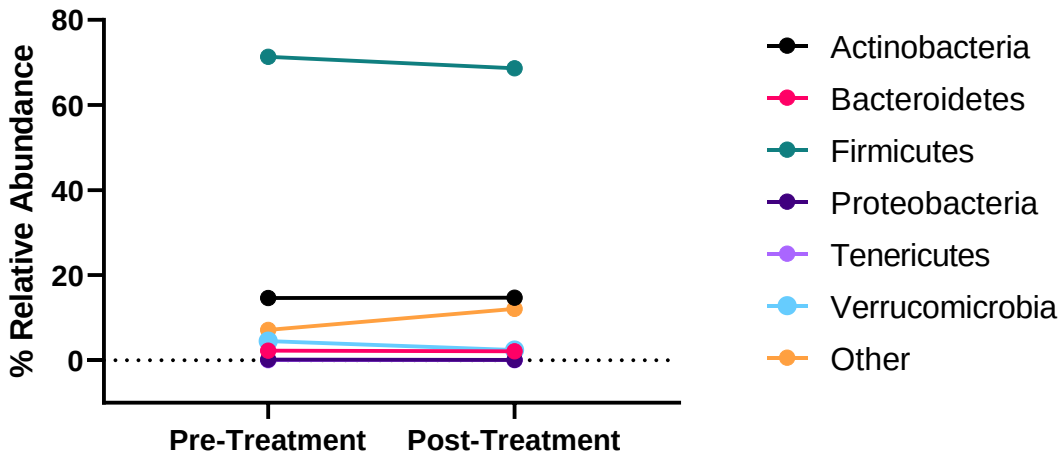

Figure 3.S6: Relative abundances at the phylum level of DIO mice treated with DEX control. DEX treatment of DIO mice had no significant effect on the microbiome at the phylum level.

CHAPTER 4

MONOCLONAL ANTIBODIES GENERATED AGAINST GLYCOCONJUGATES RECOGNIZE CHEMICAL LINKERS[1]

[1] Ramadhin et al. (2021). *Antibodies (Basel).*15;9(3):48.
Reprinted here with permission of the publisher.

4.1 Abstract

Monoclonal antibodies (mAbs) that recognize glycans are useful tools to assess carbohydrates' structure and function. We sought to produce IgG mAbs to the human milk oligosaccharide (HMO), lacto-N-fucopentaose III (LNFPIII). LNFPIII contains the Lewis^x antigen, which is found on the surface of schistosome parasites. mAbs binding the Lewis^x antigen are well-reported in the literature, but mAbs recognizing HMO structures are rare. To generate mAbs, mice were immunized with LNFPIII-DEX (P3DEX) plus CpGs in VacSIM®, a novel vaccine/drug delivery platform. Mice were boosted with LNFPIII-HSA (P3HSA) plus CpGs in Incomplete Freund's Adjuvant (IFA). Splenocytes from immunized mice were used to generate hybridomas and were screened against LNFPIII conjugates via enzyme-linked immunosorbent assay (ELISA). Three positive hybridomas were expanded, and one hybridoma, producing IgG and IgM antibodies, was cloned via flow cytometry. Clone F1P2H4D8D5 was selected because it produced IgG1 mAbs, but rescreening unexpectedly showed binding to both LNFPIII and lacto-N-neotetraose (LNnT) conjugates. To further assess the specificity of the mAb, we screened it on two glycan microarrays and found no significant binding. This finding suggests that the mAb binds to the acetylphenylenediamine (APD) linker-spacer structure of the conjugate. We present the results herein, suggesting that our new mAb could be a useful probe for conjugates using similar linker spacer structures.

4.2 Introduction

Glycans are considered core biological building blocks. Glycans are ubiquitous in nature and exert their effects via their own properties or via the modification of proteins and lipids. Their presence on cell surfaces provide strength and protection, and they also

serve as ligands for receptors (i.e., selectins, galectins, C-type lectins, Siglecs, etc.) to modulate signaling [322]. Glycans are crucial for communication between microbial and more complex species (i.e., plants, animals, humans) and are heavily involved in the innate and adaptive immune responses. The biological roles of glycans have been extensively reviewed in Varki (2016) [323].

The field of glycobiology lacks well-developed tools that facilitate a functional analysis. In terms of structure, glycans are more complex than nucleic acids and proteins because of the assortment of known monosaccharides and their ability to be linked in various numbers and fashions (i.e., branched, anomeric) [324]. In this regard, glycan-binding proteins (GBPs) have become fundamental for assessing carbohydrates' structure and function. Currently, the two most widely used tools for the quantification and/or localization of specific glycans include lectins and glycan-binding antibodies [325]. Various plant and animal lectins have been well-characterized in terms of sequences and binding specificities and are typically available at a low cost [326, 327]. Microarrays containing lectins have been developed, being simpler and more sensitive than traditional mass spectrometry (MS) methods [328-332]. The drawback is that lectins bind their determinants with differing affinities that depend on the glycan in question. For example, concanavalin A (ConA) recognizes oligomannose-type-N-glycans with a much higher affinity than more complex biantennary N-glycans [333].

In contrast to lectins, GBPs bind to specific determinants and do not discriminate between O-glycans, N-glycans, or glycolipids [333]. Several approaches have been utilized to generate glycan-binding antibodies and include generating hybridomas using the splenocytes of mice immunized with whole cells or glycan-protein conjugates or mice

that have been infected with pathogens [334]. A specific example of this is the generation of the anti-glycan mAb (E.5) from mice immunized with living schistosome eggs or soluble egg antigens (SEA). The E.5 mAb binds the Lewis^x trisaccharide, α-L-Fuc-(1→3)-[β-D-Gal-(1→4)]-D-GlcNAc, present on the surface of schistosome eggs, adult tissues, and cancerous tumors [335-338]. E.5 also binds to the human milk oligosaccharide (HMO) and pre-implantation antigen, lacto-N-fucopentaose III (LNFPIII; β-D-Gal-(1→4)-[α-L-Fuc-(1→3)]-β-D-GlcNAc-(1→3)-β-D-Gal-(1→4)-D-Glc) [338]. A drawback of the E.5. mAb is that it is IgM, which makes it difficult to purify [339]. Herein, we sought to produce IgG mAbs against LNFPIII, which contains the Lewis^x antigen. mAbs against the Lewis^x antigen are well-reported in the literature, but mAbs recognizing HMO structures are rare [334, 338, 340]. Previous studies suggest that Lewis^x must be presented on adjacent molecules or in a multimeric form to bind to or activate cells [341]. HMOs, such as LNFPIII and Lacto-N-neotetraose (LNnT; β-D-Gal-(1→4)-β-D-GlcNAc-(1→3)-β-D-Gal-(1→4)-D-Glc), are detected in human breastmilk in their free form or are attached to proteins and lipids, and do not induce a mAb response to our knowledge [342].

Here, we report the development and characterization of a novel IgG mAb (F1P2H4D8D5) generated from the splenocytes of mice immunized with LNFPIII glycan conjugates. LNFPIII conjugates are composed of 10–12 molecules of LNFPIII conjugated to a 40 kDa dextran (P3DEX) or to human serum albumin (P3HSA) via an acetylphenylenediamine (APD) linker. The combined use of a carrier (DEX or HSA) and this linker method increases the concentration of LNFPIII in the conjugates and allows each molecule to rotate in space to bind to cellular receptors. Unlike free LNFPIII, these

LNFPIII conjugates have been shown to act on B cells, macrophages, dendritic cells, hepatocytes, and adipocytes *in vivo* [146, 149, 154, 157, 165].

The initial screening of mAb F1P2H4D8D5 showed binding to LNFPIII conjugates and to conjugates containing the structurally similar tetrasaccharide, LNnT. LNnT conjugates are also conjugated to a 40 kDa dextran (NTDEX) or to human serum albumin (NTHSA). The results of additional screens suggested that the mAb might be binding to the linker spacer of the conjugate and this possibility was partially confirmed when the mAb failed to bind to any glycan structures on both human milk and general glycan structure microarrays. Since APD linkers are used to produce a wide array of conjugates, an anti-APD mAb is valuable to the research community as a probe for any structures produced using the same linker [343, 344]. The advantage of this IgG mAb is that it could be used in laboratory settings as a functional probe for chemically synthesized glycoconjugates.

4.3. Materials and Methods

4.3.1. Chemicals and Parasite Extracts

LNFPIII was synthesized by Dr. George Wang (Georgia State University, Atlanta, GA, USA). LNnT was synthesized by Neose Technologies, Inc. LNFPIII and LNnT were sent to Dr. Thomas Norberg (Uppsala University, Uppsala, Sweden) for conjugation to carriers, dextran from *Leuconostoc mesenteroides* (Sigma Aldrich, St. Louis, MO, USA, Cat. No. D1662), or human serum albumin (Millipore Sigma, St. Louis, MO, USA, Cat. No. A3782) using proprietary APD linker-spacers. On average, each conjugate had 10–12 HMO monomers per 40 kDa dextran or HSA.

Soluble schistosome egg antigen (SEA) was prepared as described previously *[335]*. Briefly, Swiss Webster mice were infected with *Schistosoma mansoni* (PR strain) cercariae obtained from infected snails provided by BEI Resources, the NIAID Schistosomiasis Resource Center. Mice were infected with 100–150 infectious cercariae of S. mansoni via intraperitoneal injection. 7–8 weeks post-infection, parasite eggs were harvested from livers. SEA was prepared by homogenizing purified eggs in phosphate-buffered saline (PBS), pH 7.4, for 1 h at 4 °C. The egg homogenate was then centrifuged at 15,000× *g* for 1 h at 4 °C, and the supernatant was collected as SEA. Protein was quantified via the Pierce™ BCA Protein Assay Kit (Thermofisher Scientific, Waltham, MA, USA, Cat. No. 23227) and stored at −80 °C until use.

Schistosomula membrane protein (SMP) was prepared as described previously *[335]*. In brief, *S. mansoni* cercariae were mechanically transformed into schistosomula using a Vortex mixer. Parasite bodies were then separated from tails via centrifugation on a Percoll gradient and incubated for 24 h in Corning™ Cellgro™ RPMI 1640 (Corning™, Cat. No. 10-040-CV) enriched with 5% Corning™ Regular Fetal Bovine Serum (FBS) (Corning™, Cat. No. 35010CV). Surface extracts of schistosomula were prepared by incubating mechanical schistosomula in 50 mM phosphate buffer, pH 8.0, containing 4 mM deoxycholate in detergent solution on ice for 30 min (100 parasites/µL). Soluble SMP was collected via centrifugation of the detergent extract at 15,000× *g* for 1 h at 4 °C. Deoxycholate was removed from SMP by desalting on Pierce™ Polyacrylamide Spin Desalting Columns, 7K MWCO, 0.7 mL (ThermoFisher Scientific, Waltham, MA, USA, Cat. No. 89849). Protein was quantified via the Pierce™ BCA Protein Assay Kit

(Thermofisher Scientific, Waltham, MA, USA, Cat. No. 23227) and stored at −80 °C until use.

4.3.2. Mouse Immunizations

Glycoconjugates were dissolved in 0.9% sterile saline and stored at −80 °C until use. 200 µg of P3DEX plus 50 µg of CpG ODN 1826 (InvivoGen, San Diego, CA, USA, Cat. No. tlrl-1826) were added to 1% *w/v* VacSIM™ (Vaccine Self-Assembling Immune Matrix) *[345]*, then injected subcutaneously into 4 BALB/c mice at D1. At D21, mice received a second dose containing 200 µg of P3HSA plus 50 µg of CpG ODN 1826 and an equivalent volume of incomplete Freund's adjuvant. A third dose of P3HSA plus 50 µg of CpG ODN 1826 and an equivalent volume of incomplete Freund's adjuvant was injected intraperitoneally three days prior to the removal of spleens (D42). Mice were sacrificed on D45, and the spleens were collected for cell fusion and the production of hybridomas, as described in Section 2.3. Serum was collected at D0, D21, and D35 for screening against LNFPIII conjugates.

4.3.3. Cell Fusion, Hybridoma Selection, & Screening

Mice were sacrificed on D45 for spleen removal and the preparation of splenocytes. Red blood cells (RBCs) were lysed by adding 2 mL of RBC Lysis Buffer (Sigma, St. Louis, MO, USA, Cat. No. R7757) and incubating for 3 min, followed by two washes in HyClone™ Dulbecco's Modified Eagles Medium (DMEM) (HyClone™, Cat. No. SH30081.01). Sp2/0-Ag14 cells (ATCC® CRL-1581™) were grown to 100% confluence in DMEM containing 20% FBS + 8 mM L-glutamine + 100 µg/mL penn/strep at 37 °C in 5% CO_2. Splenocytes were mixed with Sp2/0-Ag14 cells at a ratio of 8:1 splenocytes per Sp2/0-Ag14 cell and then pelleted by centrifugation. The

supernatant was removed, and cells were dislodged by thwacking the tube. Cell fusion was induced by adding 0.7 mL of 50% polyethylene glycol (PEG, MW 1500; Sigma, St. Louis, MO, USA, Cat. No.) for 1 min at 37 °C. Cells were pelleted, the supernatant was removed, and cells were gently resuspended by slow addition of 7 mL of warm (37 °C) DMEM. Then, cells were diluted with an additional 43 mL of hybridoma HAT media (DMEM supplemented with Gibco™ HAT Supplement (50X) (Gibco™, Cat. No. LS21060017)) + 15% FBS + 1% oxaloacetate-pyruvate-insulin (OPI) (Millipore Sigma, St. Louis, MO, USA, Cat. No. O5003-1VL) + 100 µg/mL penn/strep and plated into 96-well plates at 100 µL/well. 7D post-fusion, 100 µL/well of hybridoma HT media (DMEM) supplemented with hypoxanthine-thymidine (HT) + 15% FBS + 1% OPI + 100 µg/mL penn/strep was added. Plates were screened for hybridoma growth and the cell supernatants were tested by ELISA against P3DEX. Hybridomas positive for P3DEX and IgG, but not HSA and DEX, were cloned via flow sorting on a MoFlo Astrios Cell Sorter. In brief, cells were stained using a LIVE/DEAD™ Fixable Near-IR Dead Cell Stain Kit (Invitrogen, Waltham, MA, USA, Cat. No. L10119), resuspended in hybridoma HT media, and sorted into a single cell per well. The determination of Ig subtypes was performed with the SBA Clonotyping System-HRP (Southern Biotech, Birmingham, AL, USA, Cat. No. 5300-05) via indirect ELISA, in order to determine the specific immunoglobulin subclass. Positive hybridomas were propagated and stored in liquid nitrogen.

4.3.4. Enzyme-Linked Immunosorbent Assay (ELISA)

Nunc MaxiSorp™ flat-bottom plates (Invitrogen™, Cat. No. 44-2402-21) were coated at 100 µL/well with one of the following: (1) 5 µg/mL DEX, (2) 5 µg/mL HSA,

(3) 50 µg/mL P3DEX, (4) 100 µg/mL P3HSA, (5) 50 µg/mL NTDEX, (6) 100 µg/mL NTHSA, (7) 5 µg/mL SEA, or (8) 5 µg/mL SMP in 0.05 M carbonate bicarbonate buffer, pH 9.6, and incubated for 16 h at 4 °C. Plates were then washed 6× in PBS with 0.05% Tween-20 (PBST) and blocked via the addition of 300 µL/well of 2.5% milk in PBST at room temperature (RT) for 2 h. After additional washing, 100 µL/well of mice serum (1:100 in PBS) or hybridoma supernatant was added to the plate and incubated at RT for 2 h. Plates were washed and horseradish peroxidase-conjugated anti-mouse IgG (H+L) and IgM (Roche, Cat. No. 0311693001) or a panel of isotyping antibodies (IgG1, IgG2a, IgG2b, IgG3, and IgA; Southern Biotech, Birmingham, AL, USA, Cat. No. 5300-05) were added as required to the wells at a dilution of 1:4000 in PBST at RT for 1 h. Plates were washed four times, and color was developed using 3,3′,5,5′-tetramethylbenzidine (TMB; Sigma, St. Louis, MO, USA, Cat. No. T0440). ELISA reactions were stopped after 10 min of incubation in the dark at RT with 50 µL of sulfuric acid. The optical density (OD) was determined using the SPECTROstar Nano Microplate Reader at 450/570 nm.

4.3.5. mAb Purification

We selected a hybridoma clone secreting IgG1: mAb F1P2H4D8D5 for further analysis. Hybridomas were grown to 80% confluency in DMEM containing 20% FBS + 8 mM L-glutamine + 100 µg/mL penn/strep at 37 °C in 5% CO_2. Supernatants were recovered at 100% confluence and stored at 4 °C until purification. In order to isolate IgG antibodies, hybridoma culture supernatants were purified via ammonium sulfate precipitation according to Fishman and Berg (2018), with some modifications *[346]*. In brief, hybridoma cell culture supernatants were centrifuged at 3000× g for 30 min at 4 °C.

Supernatants were then slowly mixed with saturated ammonium sulfate for a final *w/v* concentration of 25% and incubated at 4 ℃ overnight. The solution was then centrifuged again at 3000× g for 30 min at 4 °C. Saturated ammonium sulfate was then added to reach a final *w/v* concentration of 50% and was incubated at 4 ℃ overnight. The solution then underwent a third round of centrifugation at 3000× g for 30 min at 4 °C. The supernatant was discarded, and the remaining pellet was resuspended in 30% of the original volume of 1×X PBS. The sample was dialyzed against three changes of 1× PBS using 10 K Slide-A-Lyzer™ cassettes (ThermoFisher Scientific, Waltham, MA, USA, Cat. No. 66456). The protein concentration was determined using a Nanodrop 2000 spectrophotometer. Following ammonium sulfate precipitation, eluted proteins were further purified using HiTrap protein G columns (GE Healthcare Life Sciences, Chicago, IL, USA, Cat. No. 29-0485-81) according to the manufacturer's protocol. After protein quantification, 2.5 or 5 µg of purified antibody was loaded into two identical 4–20% SDS-PAGE gels. Gels were run for 2 h at 50 V, 3.00 A, 300 W using the PowerPac™ HC High-Current Power Supply (BioRad, Hercules, CA, USA, Cat. No. 1645052). One gel was stained with Coomassie Brilliant Blue R-250 (Bio-Rad, Hercules, CA, USA, Cat. No. 1610436), and the other was transferred to a PVDF membrane after electrophoresis using the Trans-Blot Turbo RTA Mini 0.45 µm LF PVDF Transfer Kit (BioRad, Hercules, CA, USA, Cat. No. 1704274). Gels were transferred using the Trans-Blot Turbo Transfer System (BioRad, Hercules, CA, USA, Cat. No. 1704150) programmed for mixed molecular weight proteins at 2.5 A and 25 V for 7 min. The membrane was blocked at 4 ℃ for 16 h in 5% milk in tris-buffered saline plus 0.05% Tween (TBST). Subsequently, the membrane was incubated with peroxidase-conjugated anti-mouse IgG

and IgM diluted in 3% milk in TBST at RT for 1 h. The membrane was washed 5× and revealed using the ECL Plus Western Blotting Detection System (GE Healthcare, Chicago, IL, USA, Cat. No.), and images were captured using chemiluminescent detection on a Bio-Rad imager.

4.3.6. RAW 264.7 Cell Culture

RAW 264.7 (ATCC® TIB-71™) cells were grown in DMEM plus 10% FBS, 4 mM L-glutamine, and 100 U/mL + 100 µg/mL penn/strep. For the experiments, 3×10^5 cells/well were plated in a 6-well plate. Once 70–80% confluent, cells were stimulated with (1) sterile saline, (2) 50 µg/mL DEX, (3) 50 µg/mL HSA, (4) 50 µg/mL P3DEX, (5) 50 µg/mL NTDEX, (6) 50 µg/mL P3HSA, or (7) 50 µg/mL NTHSA. Cells were stimulated for 60 s, washed, and lysed using NP-40 buffer (ThermoFisher Scientific, Waltham, MA, USA, Cat. No. FNN0021). Protein was quantified using a Nanodrop, and lysates were stored at −80 °C until use.

4.3.7. Characterization of Monoclonal Antibody

mAbs were characterized in terms of: (1) specificity to different antigen targets in ELISAs and Western blots, and (2) a microarray analysis conducted at Harvard's Center for Functional Glycomics (NCFG). ELISAs were performed according to Section 2.4 with the following modifications. For the characterization of mAb, 100 µL of hybridoma supernatant from clone F1P2H4D8D5 was added to the plate and incubated at RT for 2 h. Plates were washed and Goat Anti-Mouse Ig, Human ads-HRP (Southern Biotech, Birmingham, AL, USA, Cat. No. 1010-05) was added to the wells at a dilution of 1:4000 in PBST at RT for 1 h. For Western blots, 5 or 10 µg of treated RAW 264.7 cell lysates were run on a 4–20% Mini-PROTEAN® TGX™ Precast Protein Gel (BioRad, Hercules,

CA, USA, Cat. No. 4561096) and transferred to a PVDF membrane, as described in Section 2.5, with the following modifications. After the protein transfer, the membrane was incubated with peroxidase-conjugated anti-mouse IgG and IgM diluted in 3% milk in TBST at RT for 1 h. For the microarray analysis, purified mAb F1P2H4D8D5 was sent to Harvard's NCFG, and 200 µg was run on both the Human Milk Glycan and NCFG arrays. The methods and structures present on these arrays are found at https://ncfg.hms.harvard.edu/microarrays and are described in *[347]*.

4.4 Results

4 *BALB/c* mice were immunized using the prime-boost regimen depicted in Figure 1a. Mice were primed via the subcutaneous route with 200 µg P3DEX plus 50 µg of CpG ODN 1826 delivered in VacSIM™ (Vaccine Self-Assembling Immune Matrix) *w/v* [27]. At D21, mice were boosted with 200 µg of P3HSA plus 50 µg of CpG ODN 1826 and an equivalent volume of incomplete Freund's adjuvant to enhance the mAb response. Mice were boosted again on D42 using the same formula. Serum was collected on D0, D21, and D35, and screened via ELISA. Anti-P3 conjugate responses were detected in sera post-prime and post-boost. The anti-P3 conjugate immunoglobulin (Ig) levels were significantly higher post-prime and post-boost ($p < 0.001$) compared to the pre-prime levels (Figure 1b).

Upon sacrifice and 30D post-cellular fusion, 75/384 wells (19.5%) contained hybridomas. The screening of hybridomas generated from one mouse yielded three hybridomas (3/75) producing antibodies to LNFPIII conjugates. We isotyped these hybridomas and determined that F1P2C8 was IgG subclass, while F1P2D8 and F1P2H4 were both IgG and IgM (Figure 2). F1P2H4 was cloned via flow cytometry and screened

again, yielding mAbs F1P2H4D8A7 (IgM) and F1P2H4D8D5 (IgG1) (Figure 3). Supernatants from clone F1P2H4D8D5 were picked for purification and subsequent experiments.

Following ammonium sulfate precipitation and protein G column purification, supernatants from clone F1P2H4D8D5 were run via SDS-PAGE electrophoresis. Table 1 lists the protein concentrations and 260/280 ratios following each purification step. Figure 4a presents an SDS-PAGE gel stained with Coomassie Blue, demonstrating that we were able to eliminate various protein contaminants using protein G column purification. Figure 4b depicts a Western blot of purified F1P2H4D8D5 probed with anti-mouse IgG (H+L). This particular Western blot shows the heavy (~50 kDa) and light (~25 kDa) IgG chains of the purified antibody detected post-protein G column purification. Overall, this demonstrates that we were able to successfully purify and concentrate mAb F1P2H4D8D5.

Next, we performed another screen of the purified mAb via ELISA against each of the sugar conjugates, the carrier structures (DEX and HSA), as well as against schistosome egg antigen (SEA) and schistosomula membrane protein (SMP). In this ELISA, our positive control mAb E.5 recognized P3DEX, P3HSA, SEA, and SMP (as expected) and did not bind to NTDEX or the carriers. The sole difference between LNFPIII and LNnT is the presence/absence of an α1,3-linked fucose residue, as depicted in the chemical structures shown in Figure 5a. The structure of the conjugates is given in Figure 5b, where 10–12 molecules of LNFPIII or LNnT are conjugated to DEX or HSA via the APD linker. Unexpectedly, purified mAb F1P2H4D8D5 recognized P3DEX and NTDEX, as well as P3HSA via ELISA (Figure 6a). Therefore, we initially believed that

mAb F1P2H4D8D5 bound to a smaller structure within LNFPIII and LNnT. mAb F1P2H4D8D5 did not bind to DEX or HSA carriers, supporting this initial hypothesis. To further characterize mAb F1P2H4D8D5, RAW 264.7 cells were treated with HSA, P3HSA, or NTHSA. Lysates of the treated RAW 264.7 cells were prepared, run on an SDS-PAGE gel, and then transferred to a PVDF membrane, where they were probed with the mAb.

In Figure 6b, we found that, unlike proteins, the dextran conjugates did not run properly on an SDS-PAGE, nor could they be visualized. mAb F1P2H4D8D5 recognized both P3HSA and NTHSA on the Western blot, while it did not recognize NTHSA via ELISA. This led us to believe that the denaturing and reducing conditions generated via the use of β-mercaptoethanol and SDS-PAGE exposed specific epitopes on NTHSA, which allowed it to be recognized by mAb F1P2H4D8D5. Nonetheless, mAb F1P2H4D8D5 recognized both sugars in both conjugate forms. At this point, we altered our hypothesis, suggesting that mAb F1P2H4D8D5 potentially binds the APD linker of the conjugate.

To further characterize mAb F1P2H4D8D5 and determine if it recognized any common glycan structures, we sent aliquots of purified mAb to Harvard's National Center for Functional Glycomics to be tested for binding on a Human Milk Glycan Microarray [347]. Surprisingly, mAb F1P2H4D8D5 did not bind to any of the glycans (1–34) present on the Human Milk Glycan Microarray (Figure 7a). mAb F1P2H4D8D5 was then tested for binding to the NCFG Defined Glycan Array (Figure 7b). This array contains various glycan structures, including the Lewis^{x} trisaccharide. Again, we were surprised to see that mAb F1P2H4D8D5 did not bind to any of the glycans (1–159)

present on the array. This result supported our hypothesis that mAb F1P2H4D8D5 likely binds to the APD linker, since it did not recognize DEX (ELISA), HSA (ELISA/Western blot), or the sugar monomer/structures (LNnT, Lewis^{x}).

4.5 Discussion

We attempted to produce mAbs binding to LNFPIII by immunizing mice with LNFPIII conjugates. We detected anti-LNFPIII conjugate antibodies in the sera of immunized mice after the prime. We boosted with the aim of generating IgG antibodies (Figure 1). Initial screens suggested that 3/75 hybridomas produced mAbs that bound to LNFPIII conjugates. It is important to note that the generation of antibodies to LNFPIII and other glycans is difficult. This is expected, as saccharide antigens are known to induce short-lived B cells that produce IgM antibodies independent of T cell help. This is in contrast to protein antigens, which stimulate long-lived B cells that produce IgG antibodies and lead to affinity maturation and memory B cells [339]. In this regard, we believe that the immunization of mice with LNFPIII conjugates, which present multiple LNFPIIIs in a manner that can cross-link cellular receptors, may be responsible for the observed anti-LNFPIII conjugate antibody responses, as B cells mature and develop an increased affinity for highly immunogenic antigens with multivalent displays. Unfortunately, despite a strong antibody binding to LNFPIII conjugates from the sera of immunized mice, mAb F1P2H4D8D5 did not bind to LNFPIII, but rather seemed to be specific for the APD linker spacer that was used to produce conjugates. We initially chose to clone F1P2H4, as it produced the highest IgG and IgM mAb responses. We have yet to screen in detail the other two hybridomas that were positive for binding to LNFPIII: F1P2C8 and F1P2D8 (Figure 2). However, we hypothesize that, as the majority

of anti-Lewis^x antibodies are IgM and hybridoma F1P2D8 contained IgM mAbs, this hybridoma is more likely to be specific for LNFPIII (Figure 3). This could also be the case for clone F1P2H4D8A7 (Figure 3). Future studies will further investigate these hybridomas and clones.

The lack of available tools in glycan biology presents some important limitations. Based on our findings, we deduce that F1P2H4D8D5 binds to the linker spacer of the conjugate because it does not recognize the 40 kDa dextran or HSA carrier (Figure 6a,b) or any related glycan structure present on both the Human Milk Glycan Array (Figure 7a) or the NCFG Defined Glycan Array (Figure 7b) available via Harvard's National Center for Functional Glycomics. While the arrays did not specifically contain LNFPIII, we were able to rule out that F1P2H4D8D5 did not bind to LNnT or LNFPI on the Human Milk Glycan Array. F1P2H4D8D5 also did not bind to the structures present on the NCFG Defined Glycan Array, including Lewis^x. Taken together, these results further led to the conclusion that F1P2H4D8D5 binds to the linker spacer of the glycan conjugates.

Overall, this is important because mAb F1P2H4D8D5 recognized LNFPIII and LNnT conjugates internalized by RAW 264.7 cells. This mAb can be used as an immunological probe for ELISA, Western blot, immunoprecipitation, etc. to recognize conjugates that use this linker-spacer technology. Furthermore, it is important because the in vivo generation of antibodies to drug conjugates can result in drug clearance prior to therapeutic effects. While it is known that mAbs can be generated to the Lewis^x trisaccharide, there are few reports of antibodies specific to the HMOs, LNFPIII, or LNnT.

4.6 Conclusions

It is difficult to generate mAbs to carbohydrate moieties. We sought to produce mAbs to the HMO LNFPIII, but appear to have generated mAbs to the APD linker of LNFPIII and LNnT conjugates. We immunized with these conjugates, given that LNFPIII and LNnT do not appear to be antigenic in their free form. The conjugation to this APD linker allows the glycoconjugate to cross-link multiple receptors and bind multiple cell types [146, 148, 155-157, 159, 348]. LNFPIII conjugates have been shown to be therapeutic in murine models of inflammation-based conditions, such as psoriasis, multiple sclerosis, cardiac allograft survival, and nonalcoholic hepatic steatosis [162-165]. In this regard, it is important to investigate these conjugates further via the development of a mAb that can be used as a probe for mechanistic studies. This mAb would not only be useful for our studies, but also useful for determining the mechanism of other conjugates that utilize the APD linker.

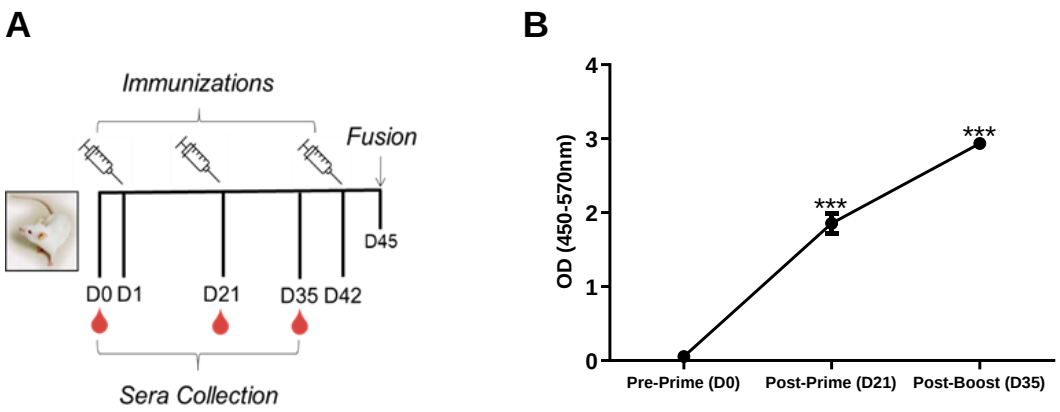

Figure 4.1: Experimental timeline and anti-P3 conjugate response following immunization. A. *BALB/c* mice were primed with 200 µg P3DEX plus 50 µg of CpG ODN 1826 delivered in VacSIM™ (Vaccine Self-Assembling Immune Matrix) w/v on D1 and boosted with 200 µg P3HSA plus 50 µg of CpG ODN 1826 and an equivalent volume of incomplete Freund's adjuvant on D21 and D42. Blood was collected pre-prime (D0), post-prime (D21), and post-boost (D35) **B.** Sera collected on D0, D21, and D35 were evaluated via ELISA to evaluate specific antibody responses against LNFPIII conjugates. *** $p < 0.001$ (t-test, CI: 95%).

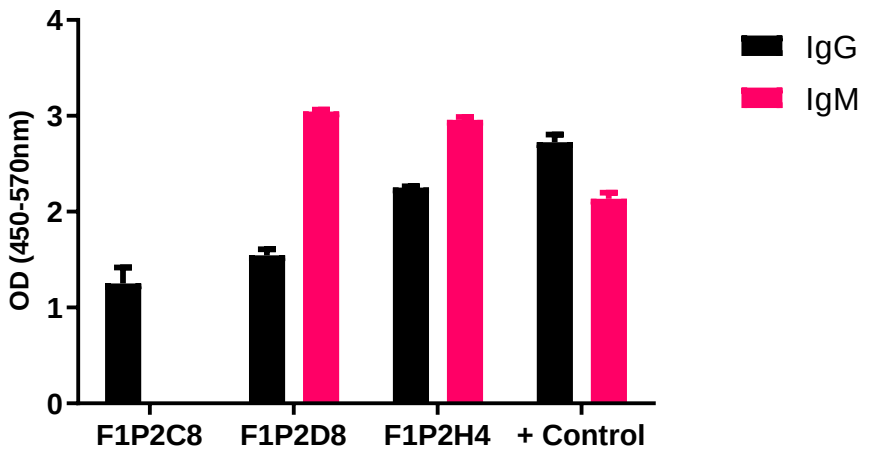

Figure 4.2: IgG and IgM antibodies produced by hybridomas. Hybridomas were screened 15−30 D post-fusion. Supernatants were screened by ELISA against P3DEX to assess the specific IgG and IgM levels. Hybridomas were positive for P3DEX, but not for the carriers DEX and HSA. Sera from immunized mice were used as a positive control.

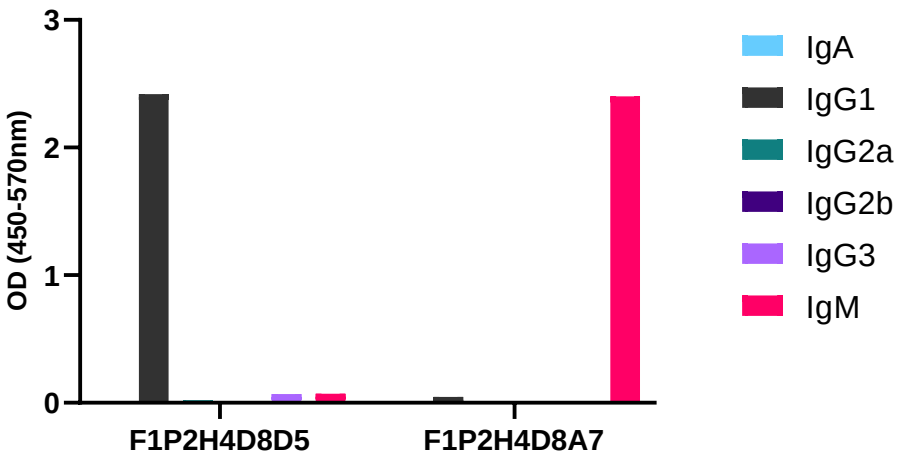

Figure 4.3: Specific class and subclass of selected clones secreting anti-P3 antibodies. Supernatants from clones were screened via ELISA using P3DEX and the carriers DEX and HSA as the antigenic targets.

Table 4.1: mAb Purification Table. Protein concentrations and 260/280 ratios following each purification step.

Purification Step	Protein [mg/mL]	260/280 Ratio
Pre-Ammonium Sulfate	4.93	0.83
Post-25% Ammonium Sulfate	3.76	0.83
Post-50% Ammonium Sulfate	3.19	0.96
Post-Dialysis	2.64	0.85
Post-G Column Purification	1.79	0.57

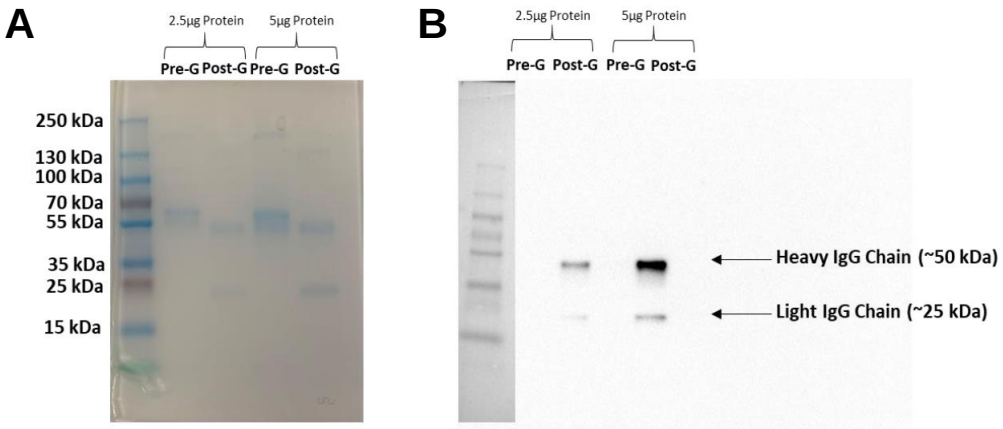

Figure 4.4: Purification and enrichment of mAb F1P2H4D8D5. mAb was run on two SDS-PAGE gels and was **A.** stained with Coomassie Blue or **B.** transferred to a PVDF membrane and probed with horseradish peroxidase-conjugated anti-mouse IgG. The SDS-PAGE stained with Coomassie showed the elimination of contaminating proteins post-G column purification. The membrane showed the enrichment of IgG post-G column purification.

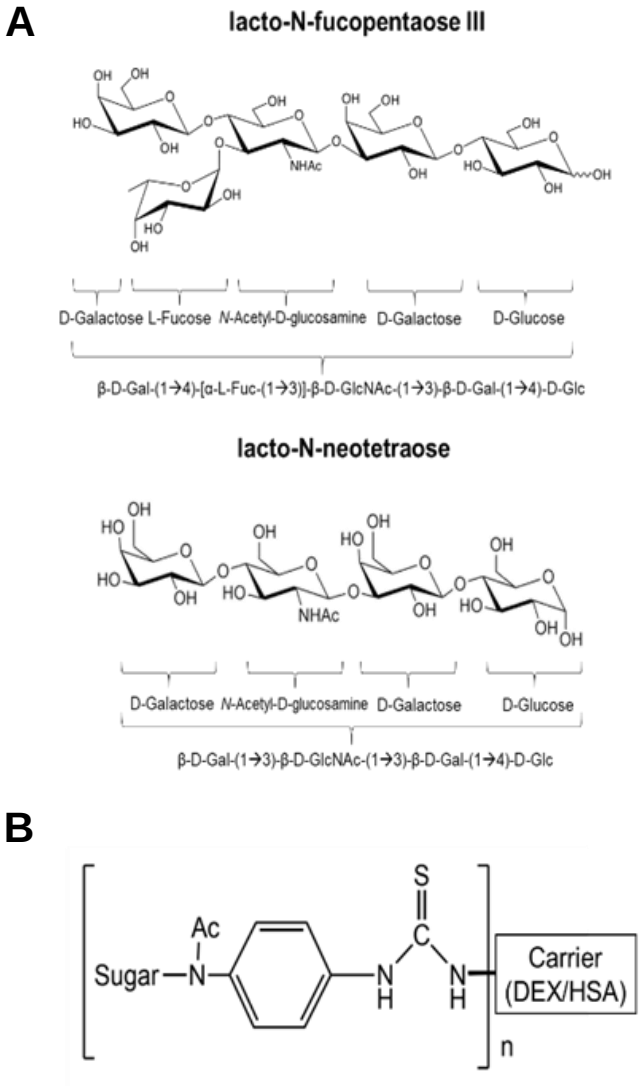

Figure 4.5: Structure of LNFPIII, LNnT, and conjugates. A. Chemical structure of LNFPIII and LNnT. **B.** Chemical structure of LNFPIII and LNnT conjugates. 10–12 molecules of LNFPIII or LNnT were conjugated to DEX or HSA via an APD linker.

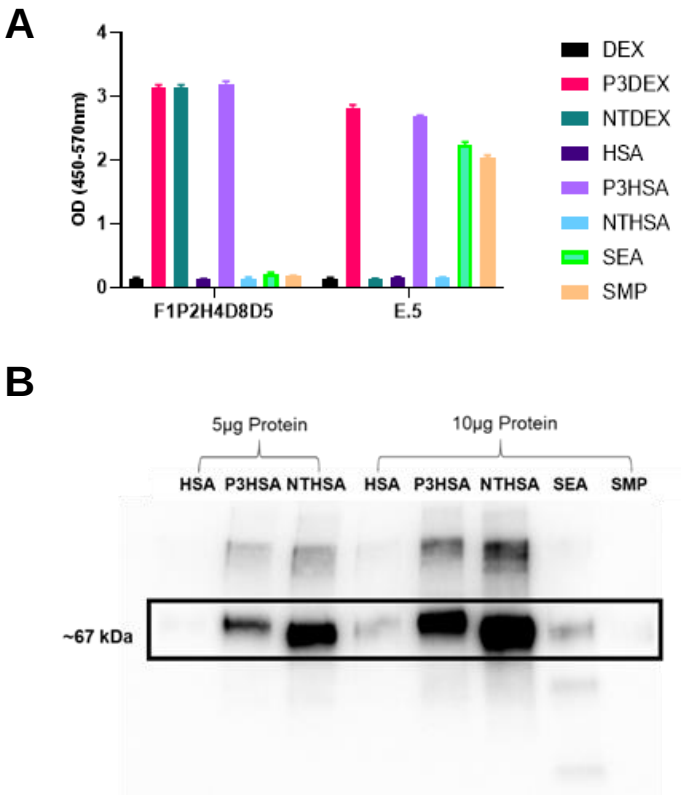

Figure 4.6: Binding of mAb F1P2H4D8D5 to sugar structures in ELISA and Western blots. A. mAb F1P2H4D8D5 was screened against sugar conjugates (P3DEX/P3HSA, NTDEX/NTHSA), carriers (DEX/HSA) and positive controls (SEA/SMP) via ELISA. F1P2H4D8D5 recognized P3DEX, P3HSA, and NTDEX via ELISA. **B.** RAW 264.7 lysates treated with sugar conjugates (P3HSA/NTHSA) or carrier (HSA) were run via SDS-PAGE, transferred to PVDF membranes, and probed with F1P2H4D8D5 via Western blot. F1P2H4D8D5 recognized both P3HSA and NTHSA via Western blot.

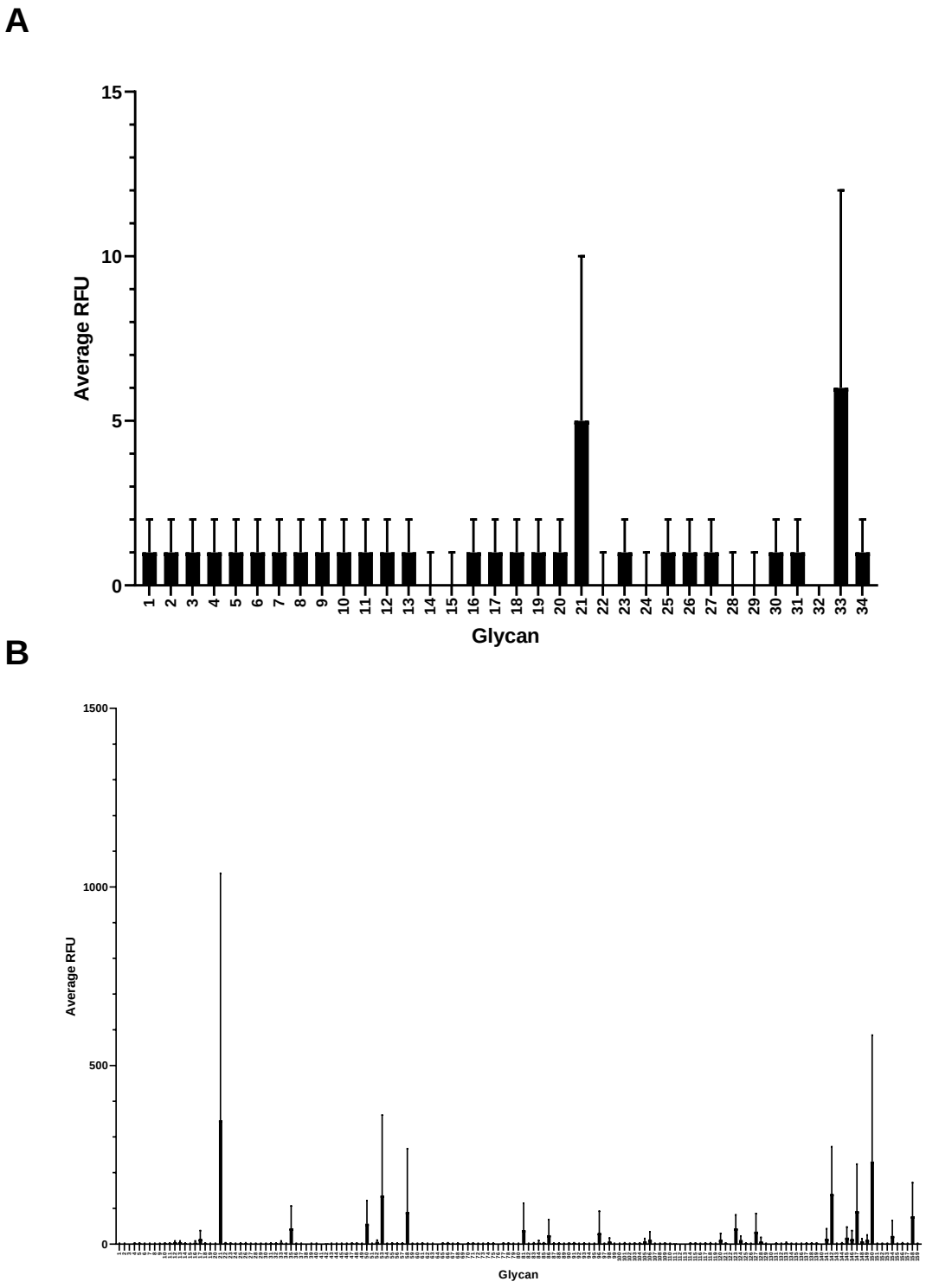

Figure 4.7 Screening of mAb F1P2H4D8D5 against glycan microarrays. A. Human Milk Glycan Array and **B.** NCFG Defined Glycan Array. Binding is depicted as average relative fluorescence units (RFU). Error bars represent standard deviation (SD).

CHAPTER 5

IMMUNOPRECIPITATION OF HMO CONJUGATES AND THEIR PUTATIVE RECEPTORS (PRELIMINARY DATA)

5.1 Introduction

HMOs bind C-type lectins (CTLs) and Toll-like receptors (TLRs) on innate immune cells, adipocytes, and hepatocytes to modulate signaling and consequent gene expression. Both CTLs and TLRs are crucial to immune function. CTLs are calcium-dependent, endocytic receptors that bind sugar motifs [349]. In most cases, sugar uptake is clathrin-dependent and travel occurs from early to late endosomes [349]. Siglecs, galectins, and selectins are examples of CTLs. There 14 Siglecs encoded in the genome, which are predominantly present on hematopoietic cells and bind carbohydrates containing sialic acid [350]. Galectins are found on the surface of various cell types, such as epithelial, adipocyte, and immune cells and tend to bind Galβ1-4GlcNAc structures [351]. Galectins bind several HMOs, including 2'FL, LNnT and LNFPI [352]. P-, E- and L-selectins are present on endothelial and immune cells and are involved in cell trafficking and adhesion [349]. They are also known to bind Lewis^x (α-L-Fuc-(1→3)-[β-D-Gal-(1→4)]-D-GlcNAc), a trisaccharide present within LNFPIII [349]. Other CTLs exist and are reviewed elsewhere [349].

TLRs bind numerous pathogen-associated molecular patterns (PAMPs) to trigger activation of inflammatory signaling (i.e. NFκB, ERK1/2, p38, JNK) [353]. HMOs have been shown to both enhance and suppress TLR signaling [354]. Treatment with a combination of HMOs in a model of necrotizing enterocolitis reduced *tlr4* expression and NFκB signaling in intestinal cells [355]. Mixtures of HMOs also increased IL-10, IL-6, and IL-27 in dendritic cells and enhanced differentiation of T regulatory cells through TLR4 and DC-SIGN [130]. In *in vitro* and *in vivo* models of *Escherichia coli* infection, 2'FL suppressed CD14 to reduce inflammation [356]. In contrast, 3'-SL increased inflammation via TLR4 in a model of colitis, but this was later debunked as a result of lipopolysaccharide (LPS) contamination [357, 358]. In this regard, signaling induced by HMOs through TLRs tends to suppress inflammation overall.

In line with the aforementioned studies, LNFPIII and LNnT conjugates are also anti-inflammatory compounds. LNFPIII conjugates induce secretion of prostaglandin E_2 and IL-10 from B cells [148]. LNFPIII conjugates also promote M2 and DC2 polarization of antigen-presenting cells (APCs) [146, 156, 157]. This is postulated to occur via CTLs and TLRs. LNFPIII conjugates are taken into the cell via clathrin/dynamin-dependent, caveolin-independent endocytic pathway that requires Ca^{2+} [159]. Once internalized, LNFPIII conjugates activate NFκB and ERK signaling via TLR4-Ras-Raf1-Syk-Tpl2-MEK [160]. This also requires CD14 [160]. LNnT conjugates are less-studied in terms of mechanism, but they do promote M2 macrophage polarization and stimulate adipocytes (unpublished) [161]. The individual effect of specific HMOs is less-studied in general, due to difficulties in terms of HMO isolation and chemical synthesis. Therefore, it is

probable that each HMO exerts different functions and should be studied as a single component versus a heterogenous mixture.

As technologies improve, individual synthesis of HMOs is becoming more widespread. This is exemplified by initial inabilities to acquire LNFPIII early on in the studies presented here. Now, LNFPIII can be synthesized in its monomer form by both of our collaborators, Dr. George Wang and Dr. Thomas Norberg [143, 185]. Other studies have reported novel and wide-scale methods to produce various HMOs [238, 239, 359]. While HMOs have been notoriously difficult to synthesize, analysis methods have been equally challenging. At current, glycan microarrays are the most useful technique for identifying HMO binding to glycan-binding proteins (GBPs) [322, 360, 361]. We reported the use of two glycan microarrays, the Human Milk Glycan and National Center for Functional Glycomic arrays, in Chapter 4.

Herein, we utilize the monoclonal antibody (mAb) produced in Chapter 4 to perform initial immunoprecipitation experiments and identify specific receptors for LNFPIII and LNnT conjugates. This work is incomplete, but reported here as a baseline for future studies. We hypothesize that immunoprecipitation and bioinformatic analyses will identify specific CTLs or TLRs that bind LNFPIII and LNnT conjugates on macrophages, adipocytes, and hepatocytes. If successful, we plan to silence putative receptors for LNFPIII and LNnT conjugates in loss-of-function studies to confirm that we have identified the appropriate receptor(s).

5.2 Materials and Methods

5.2.1 Conjugates and Reagents

Dr. George Wang (Georgia State University, Atlanta, GA) synthesized LNFPIII monomers. Dr. Thomas Norberg (Uppsala University, Uppsala, Sweden) conjugated LNFPIII to both 40 kDa dextran from *Leuconostoc mesenteroides* (Sigma Aldrich, Cat. No. D1662) and human serum albumin (Millipore Sigma, Cat. No. A3782) using proprietary acetylphenylenediamine (APD) linker-spacers. On average, each conjugate had 10-12 HMO monomers per 40 kDa dextran or HSA. Prepared buffers for immunoprecipitation experiments are described in Table 1.

5.2.2 RAW 264.7 Cell Culture

RAW 264.7 (ATCC® TIB-71™) cells were maintained in High-Glucose Dulbecco's Minimal Essential Medium (DMEM) plus 10% FBS, 4mM L-glutamine, and 100U/mL + 100µg/mL penn/strep. For experiments, cells were plated at $3x10^5$ cells/well in 6-well plates. Once 70-80% confluent, cells were stimulated for 60 seconds with: 1) 0.9% saline (negative control), 2) 50µg/mL 40 kDa dextran (DEX; negative carrier control), 3) 50µg/mL human serum albumin (HAS; negative carrier control), 4) 50µg/mL P3DEX, or 5) 50µg/mL P3HSA. All treatments were diluted in DMEM. After 60 seconds, we removed treatments and cells were washed twice with ice-cold phosphate-buffered saline (PBS). Cells were removed using a cell scraper and collected in NP-40 lysis buffer plus HALT protease inhibitor (Fisher, Cat. No. 78429). Cells were lysed for 30 minutes, on ice, with vortexing performed at 10-minute intervals. Next, cells were centrifuged at 13,000 RPM for 10 minutes at 4°C. Protein was quantified using a Nanodrop and stored at -80°C until immunoprecipitation.

5.2.3 Immunoprecipitation Experiments

Immunoprecipitation experiments were performed by binding cell lysates to Dynabeads™ Protein G (Fisher, Cat. No. 10004D) with bound and cross-linked mAb. To bind and cross-link mAb, 50µL of Dynabeads™ Protein G were added to a round-bottom tube and placed on a magnetic stand to capture the beads. Storage buffer was then removed and discarded. Next, we added 100µL IgG Binding Buffer plus 1µL of HALT protease inhibitor to the beads and vortexed for 10 seconds. Beads were re-captured, buffer was removed, and this step was repeated 2 more times. Next, beads were re-suspended in 100µL PBST containing 6µL of 1mg/mL mAb. The mAb was allowed to bind to the beads for 30 minutes at room temperature with continuous mixing. After incubation and mixing, the buffer was removed and retained for later analysis. These were called "unbound" samples, which we could later use to determine how much mAb actually bound to the beads and/or was left in solution. Beads were washed 3 times by re-suspending in 100µL PBST and vortexing for 10 seconds. Next, PBST was removed and 500µL Coupling Buffer was added to each tube and vortexed for 60 seconds. This step was repeated a total of 3 times. After we bound the mAb to the beads, we cross-linked it using a BS3 crosslinker (CovaChem, Cat. No. 13306). First, we prepared a 100mM BS3 stock solution by dissolving 5mg of BS3 in 135µL DMSO. Once dissolved, we diluted to 10mM by adding 1215µL Coupling Buffer. Next, 250µL of 10mM BS3 solution was added to each tube and incubated with end-over-end mixing for 30 minutes at room temperature. The reaction was quenched using 12.5µL of Quench Buffer to each tube and incubated again for 30 minutes with end-over-end mixing. The Quench Buffer was discarded and beads were washed with 500µL 0.2M Glycine HCL (pH = 2.5) to remove

any non-crosslinked antibody. Beads were washed 3 times for 1 minute using 500µL PBST. At this point, beads were ready for use.

Cell lysates were prepared by adding 7.5µL 10% NP-40 and 1.5uL HALT protease inhibitor to 150µL Extraction Buffer. 150uL of prepared buffer was then added to each sample and incubated on ice for 5 minutes. Samples were sonicated three times at 10% amplitude for 5 seconds with 1 minute rest periods between each pulse. Samples were then spun at 13,000 rpm for 15 minutes at 4°C. 30µl of supernatant was then saved as an "input" sample. This sample represented the proteins present prior to mixing with the mAb-bead complex. The prepared cell lysate was then added to the prepared mAb-bead complexes and incubated for 1 hour at room temperature with rocking. We collected 3µL of the "unbound" samples to represent proteins that did not bind to the mAb-bead complex. Beads were washed 3 times in 300µL IgG Binding Buffer plus HALT protease inhibitor for 10 minutes each with rocking at 4°C. Beads were then saved at -80°C until elution and SDS-PAGE analysis.

5.2.4 SDS-PAGE

To elute protein from beads, we added 30µL Laemmli Buffer (Bio-Rad, Cat. No. 160747) diluted to 1X plus β-mercaptoethanol (Bio-Rad, Cat. No. 1610710). Samples were boiled at 95°C for 5 minutes with 10µL sample plus 3.5µL 4X Laemmli Buffer. Samples were spun at 13,000 RPM For 10 minutes and then loaded on an 4-20% Mini-Protean TGX SDS-PAGE gel (Bio-Rad, Cat. No. 4561093). Samples were run for 1h at 100V, 3.00A, 300W.

2.5 Silver Stain

Gels were stained using the Pierce™ Silver Stain Kit (ThermoFisher Scientific, Cat. No. 24612), according to manufacturer's instructions.

5.3 Results

Thus far, we have performed IP experiments twice with conflicting results. Figure 1a depicts the silver-stained gel for the first run of untreated, DEX, and P3DEX samples. Here, we see an abundance of protein in all "input" lanes, showing that the cell lysates contained protein prior to bead-binding. In the "unbound" lanes, we still see various proteins within the cell lysate that did not bind to the mAb-bead complex. In the "IP" lanes, we see several bands that appear across all three treatment groups. We cannot visualize any unique bands for the P3DEX-treated samples here, but it is possible that they are present. This can only be determined using mass spectrometric analyses of the bands. For the HSA treatment group in Figure 1b, we observed similar results to the untreated, DEX, and P3DEX "IP" lanes shown in Figure 1a. Again, this suggests that there is some non-specific binding of the mAb to proteins present in the cell lysate. We saw multiple unique bands in the P3HSA "IP" lane, suggesting that we were able to successfully pull-down a protein to which P3HSA was bound. We expected differences in immunoprecipitation results for P3DEX and P3HSA conjugates, given that we identified differences in mAb specificity in Chapter 4.

When we repeated this experiment, we still observed bands in the "input" and "unbound" lanes for each treatment group as expected (Figure 2). However, we saw differences in our "IP" lanes compared to the first experiment. We did not see bands in the untreated or DEX "IP" lanes, but we did see bands in the P3DEX "IP" lane (Figure 2a). Again, this suggests that we were able to pull-down unknown proteins associated

with P3DEX in this experiment. We observed a single band in the HSA-IP lane, indicating the presence of some non-specific binding (Figure 2b). We did not observe bands in the P3HSA "IP" lane, suggesting that we failed to pull-down associated proteins in this experiment.

Between the two IP experiments, there were no known differences in technique and protocol. The silver-stained SDS-PAGE gel from the first experiment, however, was developed much more than the second. This could be the reason for the appearance of these non-specific bands. Nonetheless, these experiments need to be repeated and optimized to acquire consistent bands specific for P3DEX and P3HSA.

5.4 Discussion

We proposed to identify the putative receptors for LNFPIII and LNnT conjugates using a mAb described in Ramadhin et al. (2020). P3DEX and NTDEX induce direct and indirect effects on multiple cell types (i.e. macrophages, adipocytes, and hepatocytes), but the receptors responsible for these effects are unknown. The objective here was to use immunoprecipitation techniques to identify the putative receptors for P3DEX and NTDEX on these three cell types. We hypothesized that P3DEX and NTDEX would bind to CTLs or TLRs to mediate their effects.

Once we are able obtain consistent IP results, we plan to send samples for mass spectrometric and bioinformatic analyses to identify putative receptors. If successful with macrophages, we will also perform these studies using murine 3T3-L1 adipocytes and human HepG2 hepatocytes. Once we identify plausible receptors, we plan to silence them in each cell type to confirm loss-of-function. We propose to transfect cells with Lipofectamine RNAiMAX reagent (Invitrogen Cat. No. 13778-500) containing

Invitrogen™ Ambion™ Silencer™ Select siRNA against the receptor gene of interest. Successful silencing of the appropriate receptor will be confirmed via real-time quantitative polymerase chain reaction (RT-qPCR) or Western blot. Transfected cells will be treated in triplicate with 1) 0.9% saline, 2) 50μg/ml 40 kDa dextran, 3) 50μg/ml LNFPIII monomer, 4) 50μg/ml LNnT monomer, 5) 50μg/ml P3DEX, or 6) 50μg/ml NTDEX for various time points to assess cytokine and catecholamine secretion via RT-qPCR and enzyme-linked immunosorbent assay (ELISA). We will then perform these studies on adipocytes and human HepG2 hepatocytes. We will test for loss-of-function by evaluating M2 macrophage polarization and catecholamine secretion. This is because P3DEX induces expression of *il10* and upregulates M2 markers *arg1*, *ym1*, and *mgl1* in macrophages [11]. NTDEX also induces expression of *il10* and *tgfb* in macrophages [14]. Both P3DEX and NTDEX drive catecholamine secretion in RAW 264.7 macrophages and enhance lipolytic activity in 3T3-L1 cells (unpublished). Macrophage conditioned medium (MCM) from macrophages treated with P3DEX also improves insulin responsiveness and increases expression of *insr*, *irs2*, and *cebpa* and decreases *il1b* and *tnfa* in 3T3-L1 adipocytes [11]. P3DEX also activates FXRα to decrease lipogenesis and increase fatty acid oxidation in hepatocytes. We do not know if NTDEX acts on hepatocytes [11]. Loss of any of these functions will mean that we have identified the relevant receptors, which will be crucial to progressing either P3DEX or NTDEX as therapeutics.

Table 5.1 Buffers for Immunoprecipitation

Extraction Buffer: 40mM Tris-HCl (pH=7.5), 150mM KCl, 1mM EDTA
IgG Binding Buffer: 20mM Tris-HCl (pH=7.5), 150mM KCl, 1mM EDTA, 0.1% NP-40
Coupling Buffer: 1X PBS
Wash Buffer: PBS + 0.01% Tween (PBST)
Quench Buffer: 1M Tris-HCl (pH=7.5)

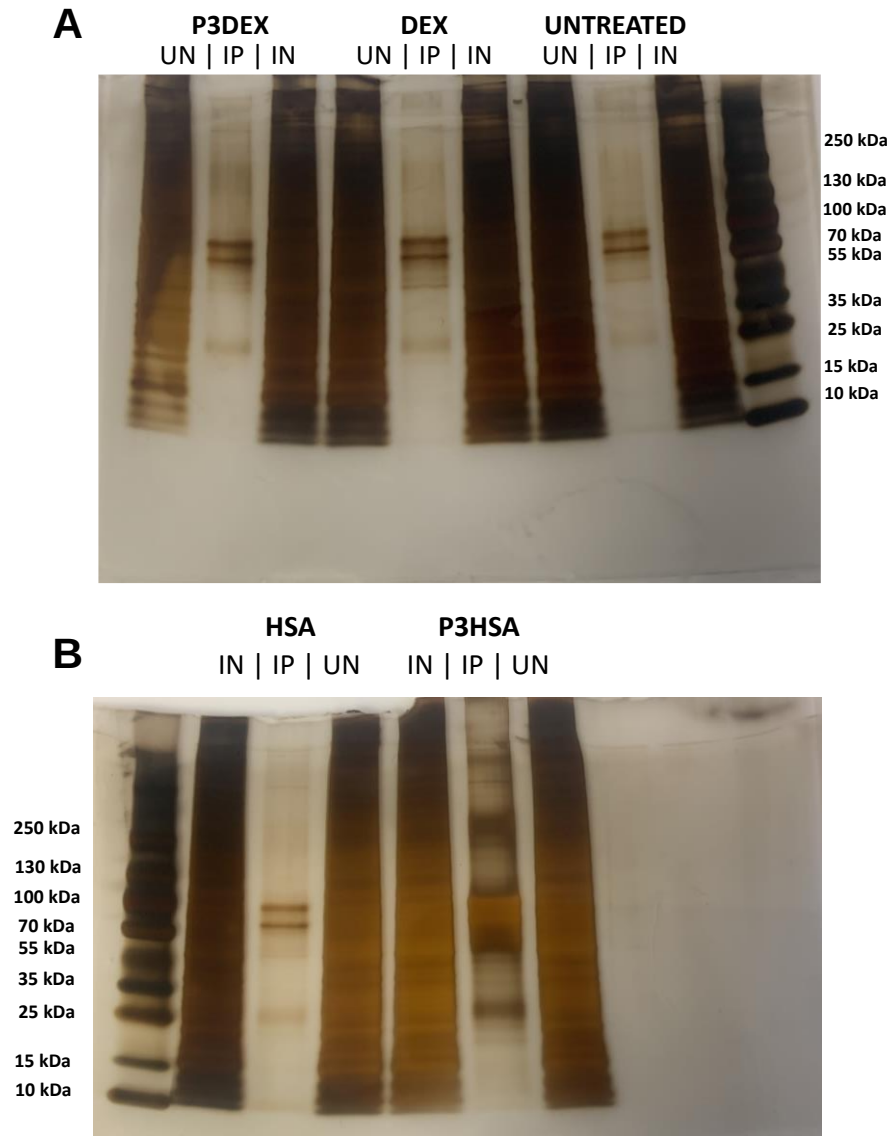

Figure 5.1: Silver-stain of 1st immunoprecipitation experiments. Silver-stained SDS-PAGE gels depicting controls and IP results for **A.** untreated, DEX, and P3DEX treatment groups and **B.** HSA and P3HSA treatment groups. **IN:** Input Control, **IP:** Immunoprecipitation, **UN:** Unbound Control.

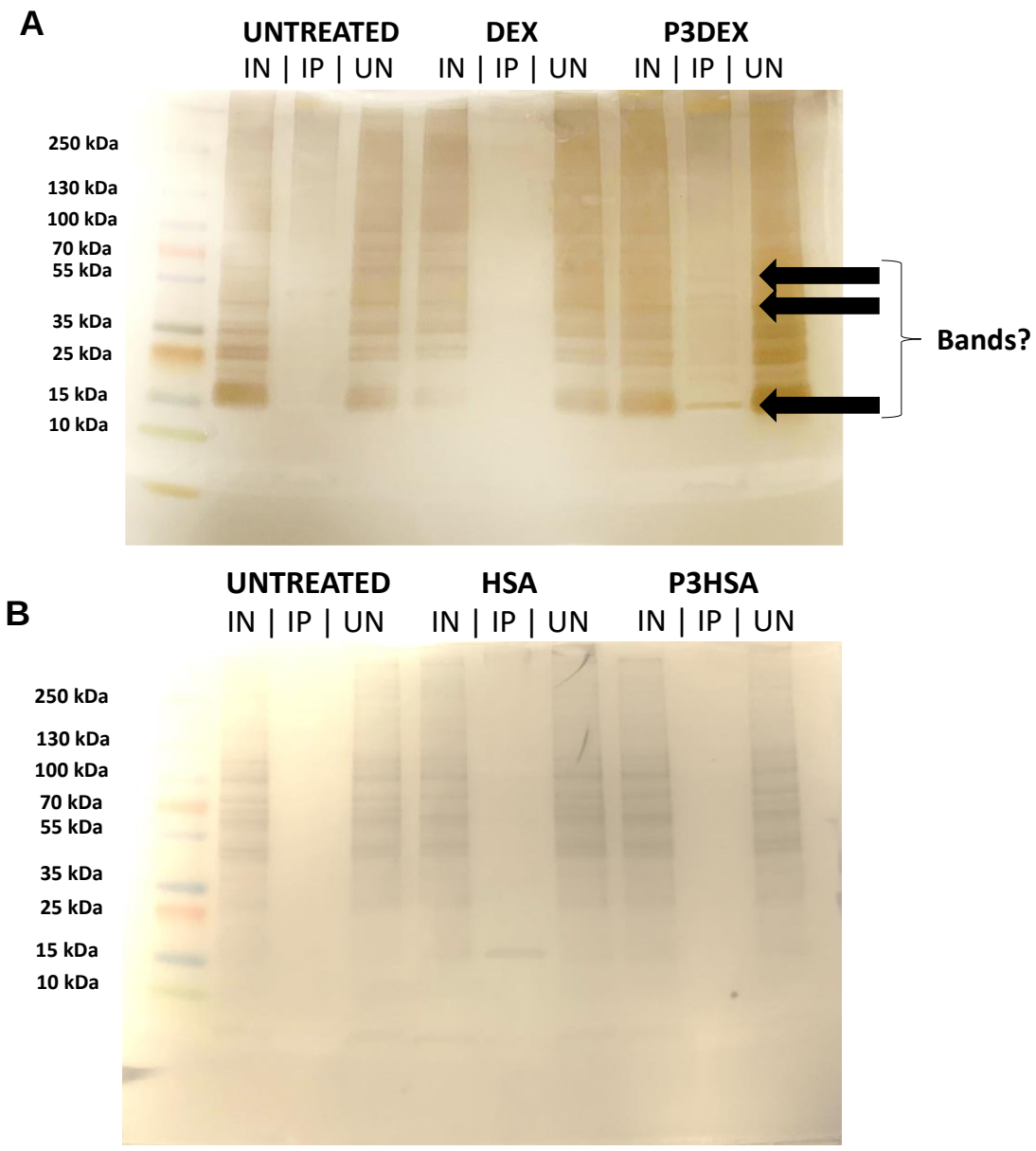

Figure 5.2 Silver-stain of 2nd immunoprecipitation experiments. Silver-stained SDS-PAGE gels depicting controls and IP results for **A.** untreated, DEX, and P3DEX treatment groups and **B.** untreated, HSA and P3HSA treatment groups. **IN:** Input Control, **IP:** Immunoprecipitation, **UN:** Unbound Control.

CHAPTER 6

CONCLUSIONS AND FUTURE DIRECTIONS

LNFPIII conjugates induce direct effects on B cells, antigen presenting cells (APCs; macrophages & dendritic cells), adipocytes, and hepatocytes [146, 148, 150, 151, 156, 157]. LNFPIII conjugates also exert indirect effects on NK cells, $CD4^+$ T cells, $CD8^+$ T cells, and memory T cells [153, 155, 158]. In contrast, LNnT conjugates have only been shown to wield direct effects on macrophages and adipocytes [161]. Table 1 summarizes the cellular studies performed using LNFPIII and LNnT conjugates to date.

More in-depth studies have been performed on LNFPIII conjugates in terms of intracellular mechanism. What do we know about the intracellular mechanism of LNFPII conjugates? It is a receptor-mediated process, which undergoes clathrin-dependent endocytosis [159]. Internalization does not require TLR4 or MyD88, but does require CD14. Signaling continues via CD14/TLR4-Ras-Raf1-TPL2-MEK to induce ERK and NFκB signaling. This results in production of anti-inflammatory mediators, such as IL-4, IL-10, MMP9, and CCL22. LNnT conjugates do not activate antigen-presenting cells (APCs) via TLR4/MD2/CD14, so it is probable that the fucose residue on LNFPII is vital for signaling [160]. It is also likely that, while anti-inflammatory *in vivo*, LNnT conjugates might induce effects that differ from LNFPIII conjugates.

Prior to this work, *in vivo* studies focused on the therapeutic implications of LNFPIII conjugates. As reviewed in Chapter 1, LNFPIII conjugates prolong cardiac allograft survival, reduce skin lesions during psoriasis, decrease brain inflammation during EAE, prevent neurological perturbations during GWI, ameliorate hepatic steatosis, and improve insulin signaling during obesity [162-166]. This is the first direct comparison of LNFPIII and LNnT conjugates *in vivo* and the first investigation of LNnT conjugates in DIO mice.

In Chapter 2, we compared LNFPIII and LNnT conjugates as therapeutics in DIO mice. This expanded on the work published in Bhargava et. al (2012), in which LNFPIII conjugates were shown to decrease crown-like structures and macrophages in WAT depots and increase insulin signaling in adipocytes, as well as decrease hepatic lipid accumulation, reduce lipogenesis, and increase fatty acid β-oxidation in the liver [165]. We showed that treatment with LNFPIII conjugates decreased body weight and total weight gain over time, in contrast to DEX and NTDEX-treated mice. This corresponded to a trending decrease in scWAT and a significant decrease in vWAT. We saw no differences in BAT, liver, heart, spleen, or kidney weights. Bhargava et al. (2012) did not report decreased body weight, total weight gain, or AT depots in response to LNFPIII conjugate treatment [165]. This could be attributed to differences in experimental design, in which DIO mice in Bhargava et al. (2012) were subject to treatment for a total of 4 weeks [165]. In the experiments presented herein, we treated DIO mice for a total of 8 weeks. In this regard, it is possible that this longer timeframe led us to the observed decreases.

While Bhargava et al. (2012) did not report fasting blood glucose levels, we can deduce from their glucose tolerance test (GTT) data that P3DEX-treated DIO mice had lower fasting blood glucose levels than the DEX-treated control [165]. We report that DEX, P3DEX, and NTDEX-treated DIO mice had fasting blood glucose levels within normal range (88.5-154.9mg/dL) at W0 and these became elevated in all groups after W6 of HFD. P3DEX treatment prevented a further increase in fasting blood glucose levels, whereas DEX and NTDEX treatment did not. In agreement with Bhargava et al. (2012), P3DEX treatment improved both glucose tolerance and insulin responses compared to the DEX control. In addition, we report that NTDEX had no effect during GTTs and insulin tolerance tests (ITTs).

We evaluated changes in circulating mediators using a comprehensive panel of chemokines, cytokines, and adipokines. We observed that both conjugates reduced markers involved in hematopoiesis, which indicated a decrease in the overactive immune response seen during obesity and MetS. While both conjugates had an effect on hematopoiesis, only LNFPIII conjugates significantly reduced markers associated with chemotaxis (KC, MCP-1, RANTES). We also investigated a series of innate and adaptive cytokines, observing specific effects for each conjugate treatment. The most notable and interesting, however, was the virtual elimination of circulating IL-6 in response to NTDEX treatment. In the context of DIO, IL-6 is controversial. IL-6 has both immunomodulating and pro-inflammatory functions during DIO, so there is no consensus on its overall effect [362, 363]. Bhargava et al. (2012) reported no differences in IL-4 during P3DEX treatment, whereas we noted a trending decrease in our own studies [165]. Another interesting observation was that we did not see a considerable increase in

circulating IL-10 in response to P3DEX treatment. Again, these differences could be attributed to differences in experimental timeline or even to differences in microbiome composition. We discussed microbiome alterations in Chapter 3. Nonetheless, it is clear that increases in circulating IL-10 are not the driving force for the LNFPIII conjugates' therapeutic abilities *in vivo*. While it appears that P3DEX treatment does need to increase circulating IL-10, it does need to be present. In Bhargava et al. (2012), 3T3-L1 adipocytes cultured with macrophage-condition medium (MCM) from macrophages treated with P3DEX exhibited improved insulin signaling, but culturing with MCM from *il10*$^{-/-}$ macrophages treated with P3DEX did not [165]. Furthermore, P3DEX could not improve insulin signaling and reduce WAT inflammation in *il10*$^{-/-}$ mice [165]. The immunoregulation functions of IL-10 are well-regarded in DIO mice, so it is possible that the absence of IL-10 causes a more severe phenotype that cannot be remedied via P3DEX treatment.

LNFPIII conjugate treatment did not alter leptin or resistin in Bhargava et al. (2012), but we observed significant decreases in our studies [165]. Given that circulating leptin correlates with adipose tissue content, it makes sense that we see significant differences here [250, 364]. It seems like the extended 8-week treatment period was long enough to observe weight changes and corresponding decreases in adipokines. While NTDEX did not alter adipokine secretion to the extent of P3DEX, we observed significant changes in incretin effect hormones. NTDEX treatment decreased circulating GIP and glucagon, which can have negative effects on insulin synthesis and secretion in pancreatic islets and can increase glucose production in the liver [234]. This could explain how or why LNnT conjugates do not improve obesity and MetS.

At the tissue level, P3DEX treatment reduced WAT inflammation and hepatic lipid accumulation in alignment with Bhargava et al. (2012) [165]. NTDEX, however, seemed to exacerbate WAT inflammation and lipid accumulation in comparison to the DEX control. This exacerbation of disease was corroborated by the noted increase in the ratio of AST:ALT. We can conclude that LNFPIII conjugates remain therapeutic for obesity and MetS, but LNnT conjugates are not.

As with all studies, there are limitations to these *in vivo* experiments. First, the DIO model is variable and susceptible to changes as a result of numerous factors, such as rodent manufacturer, age, HFD composition, fasting duration, cage position, single versus co-housing, technical abilities, room temperature, cage bedding, etc. [365]. To mitigate these effects, we purchased all male *C57BL/6* mice from Jackson Laboratories Inc. and started experiments between 6-7 weeks of age. We housed rodents at 3 per cage, in order to prevent excessive feeding shown in single-housed animals and also to encourage social behavior. We used a 6-hour fast for all metabolic tests, which has been shown to be more physiologically relevant than longer fasting periods [187, 189]. Cotton bedding was provided to prevent mice from consuming corn bedding in lieu of the HFD. We used the 60% kcal from fat diet used in Bhargava et al. (2012) to replicate those experiments as much as possible, given that HFD composition often varies between published studies [165]. We did not include chow-fed, lean mice as our control. Studies have shown inherent issues with this control in DIO mouse models, due to the fact that it is difficult to see differences in weight gain. Control mice are often inactive, overweight, and glucose intolerant to begin with, making them poor controls for HFD studies [365].

Using chow-fed animals would have also introduced diet as a second independent variable.

The magnitude of these experiments allows for a plethora of suggestions for future directions. In relation to the data presented in Chapter 2, it would be informative to determine the source of the altered cytokines. This would involve investigating metabolic tissues, such as adipose tissue or the liver, for chemokine, cytokine, or adipokine (AT only) transcripts. Determining the source of these cytokines would more specifically tell us which tissues were affected by conjugate treatment. We could also stain for immune cell markers in WAT depots to further investigate the inflammation shown via histology. This would also be useful in the liver. We could also measure AST and ALT in the liver directly, instead of in circulation.

Banked tissue includes blood, brain, scWAT, vWAT, BAT, iLN, mLN, small intestine, colon, spleen, kidney, liver, heart, and muscle. Appendix B provides a detailed overview of available tissues and preservation techniques used, in order to inform future studies.

In Chapter 3, we studied the microbiome changes induced in DIO mice in response to LNFPIII and LNnT conjugates. Observational and correlational studies have associated HMOs with microbiome alterations. However, studies with purified or specific HMOs are lacking. Furthermore, HMO synthesis techniques are just now advancing to produce more complex (i.e. branched chain, fucosylated, sialylated) HMOs. In our studies, we investigated the specific bacterial changes induced by purified HMO conjugates (LNFPII & LNnT). We showed that HMO conjugates tended to decrease absolute abundance and increase species richness. We noted that the DEX control was

enriched for *Lactobacillus*, which was also reported by Mote et al. (2020) in a model of GWI [167]. We showed that LNFPIII conjugates increased the ratio of Bacteroidetes to Firmicutes and promoted outgrowth of bacteria with both HMO- and fucose-metabolizing capabilities, such as *Bacteroidaceae* and *Verrucomicrobiae*. The most specific enrichment we observed was in *Bacteroides thetaiotamicron* and *Akkermansia muciniphila*. Mote et al. (2020) also observed an increase in *Akkermansia* in control mice treated with LNFPIII conjugates alone [273]. In the GWI model, LNFPIII conjugate treatment increased *Ruminococcus*, which aligned with our reported results as well [167]. An unpublished experiment using DIO dams also observed an increase in the order *Bacteroidales* after LNFPIII conjugate treatment.

LNnT conjugates induced expected changes in the context of HMO treatment, increasing *Bifidobacteria* and *Bifidobacterium pseudolongum* in particular. We saw outgrowth of other bacterial species with pathogenic potential. It is possible that the fucose residue on LNFPIII prevented growth of these species, while LNnT fed them or failed to inhibit them.

Microbiome studies have inherent limitations. For instance, numerous factors can affect the microbiome, such as rodent manufacturer, housing conditions, handling, etc. The first limitation involves distinguishing correlative vs. causative changes. Herein, we introduce two variables that are known to alter the microbiome: 1) HFD feeding and 2) HMO conjugate treatment. Studies that look at changes induced via these two variables are often correlative. For example, HFD feeding is most often associated with an increase in Firmicutes related to Bacteroidetes [71]. However, there are other correlative studies that suggest the opposite. From a mechanistic perspective, Firmicutes increase because

they are more efficient at extracting calories from excess nutrients [257]. However, there is little consensus within the field and bacterial functions can differ down to the species level to have different effects on a host. HMOs have been shown to increase Bifidobacteria in breastfeeding infants, but according to our studies, it is clear that not all HMOs do this [280]. Changes in the microbiome can occur as a result of factors that lead to disease, during the disease course itself, or after disease progression. In addition, these is no concrete definition of a "healthy" microbiome and this might differ amongst individuals depending on a variety of lifestyle factors. More studies need to be performed to elucidate the functions of specific species of bacteria and their interactions with other bacteria. This is a tremendous task, given the sheer number of bacterial species and incidence of mutualism. Many microbiome studies are conducted using different healthy and diseased models, making it difficult to draw overall conclusions.

Sampling also introduces variation in microbiome data. We performed 16S sequencing on fecal samples from DIO mice collected at W14 of our experiments. However, we do not have 16S sequencing data throughout development of disease and prior to treatment. In addition, the use of feces is limiting in itself because it does not provide specific information about different communities that exist along the entire gastrointestinal tract. It would be informational to run 16S sequencing on samples collected at W0 and W6 timepoints to determine what the microbiome looked like prior to HFD and after 6W of HFD, but prior to treatment.

In Chapter 4, we report generation of a mAb that recognizes both LNFPIII and LNnT conjugates. While Dr. Harn had previously generated a mAb against Lewis^x that recognizes the trisaccharide within LNFPIII, we had no method to probe for both

conjugates. We sought to generate a new mAb to LNFPIII, but this led to a new mAb that recognized the acetylphenylenediamine (APD) linker of both conjugates. APD linkers are used in standard technologies to produce drug conjugates, so therefore, an anti-APD mAb is beneficial to the research community as a probe. While we could not define the exact binding site of the new mAb, it recognized both conjugates, but not the DEX, HSA, LNFPIII, or LNnT components in monomer form. This mAb was used for our initial IP experiments described in Chapter 5.

In Chapter 5, we used the mAb described in Chapter 4 to perform initial immunoprecipitation experiments involving LNFPIII and LNnT conjugates. While we have observed numerous downstream effects of the conjugates on multiple cell types, we have not identified the receptor(s) responsible for these events. Receptor identification is crucial to understanding a potential drug's mechanism of action, including dosage and side effects. We show preliminary data for immunoprecipitation experiments, in hopes that these studies will continue to pinpoint a specific conjugate receptor. Once a putative receptor is identified via immunoprecipitation, mass spectrometry, and bioinformatics, it can then be silenced for confirmed loss-of-function studies. A potential limitation for these studies is how strongly our mAb binds to LNFPIII or LNnT conjugates. We have also observed different results based on whether these HMOs are bound to dextran or HSA. If successful, we hope to perform these experiments on macrophages, adipocytes, and hepatocytes.

Completion of this dissertation involved comparative studies of LNFPIII and LNnT conjugates in a DIO model (Chapters 2 & 3), as well as molecular studies aimed to generate a conjugate probe (mAb) used for receptor identification (Chapters 4 & 5). We

demonstrated that LNFPIII, but not LNnT conjugates, lessens total weight gain, reduces AT depots, improves glucose tolerance and insulin tolerance, decreases WAT inflammation, and diminishes hepatic lipid accumulation. Both conjugates had differential effects on circulating cytokines, chemokines, and adipokines, as well as the microbiome. We then produced a mAb that recognized both LNFPIII and LNnT conjugates, which we used in initial immunoprecipitation experiments. This work opens limitless possibilities for future studies, including advancing LNFPIII conjugates as therapeutics for diet-induced obesity and identifying its mechanism of action.

Table 6.1 LNFPIII and LNnT Conjugates Act on Different Cell Types and Differ in Mechanism.

LNFPIII Conjugates		**LNnT Conjugates**
Direct Effects	**Indirect Effects**	**Direct Effects (Indirect Effects Unknown)**
B Cells - IL-10 Production [148, 150, 151]	**NK Cells** - Activated Upon Exposure to Treated M2 Macrophages [155]	**Macrophages** - M2 Polarization [161]
Macrophages - M2 Polarization [156, 157, 159, 160, 165]	**$CD4^+$ T Cells** - T_H2 Response [153]	**Adipocytes** - Increased Lipolysis (Unpublished)
Dendritic Cells - DC2 Polarization [146]	**$CD8^+$ T Cells** - No Impairment Upon Different Antigen Exposure [158]	
Adipocytes - Increased Insulin Signaling [165] - Increased Lipolysis [165]	**Memory T Cells** - No Impairment Upon Different Antigen Exposure [158]	
Hepatocytes - Decreased Lipogenesis [165] - FXRα Activation [165]		

REFERENCES

1. Cildir, G., S.C. Akincilar, and V. Tergaonkar, *Chronic adipose tissue inflammation: all immune cells on the stage.* Trends Mol Med, 2013. **19**(8): p. 487-500.
2. Brestoff, J.R. and D. Artis, *Immune regulation of metabolic homeostasis in health and disease.* Cell, 2015. **161**(1): p. 146-60.
3. Organization, W.H., *Obesity: preventing and managing the global epidemic.* 2000.
4. Afshin, A., et al., *Health Effects of Overweight and Obesity in 195 Countries over 25 Years.* N Engl J Med, 2017. **377**(1): p. 13-27.
5. Hales, C.M., et al., *Prevalence of Obesity and Severe Obesity Among Adults: United States, 2017-2018.* NCHS Data Brief, 2020(360): p. 1-8.
6. Institute, I.F.P.R., *Global Nutrition Report 2016. From Promise to Impact: Ending Malnutrition by 2030.* 2016.
7. Cawley, J., et al., *Direct medical costs of obesity in the United States and the most populous states.* J Manag Care Spec Pharm, 2021: p. 1-13.
8. Djalalinia, S., et al., *Health impacts of Obesity.* Pakistan journal of medical sciences, 2015. **31**(1): p. 239-242.
9. *Clinical Guidelines on the Identification, Evaluation, and Treatment of Overweight and Obesity in Adults--The Evidence Report. National Institutes of Health.* Obes Res, 1998. **6 Suppl 2**: p. 51s-209s.
10. Reaven, G.M., *Role of Insulin Resistance in Human Disease.* Diabetes, 1988. **37**(12): p. 1595.
11. Alberti, K.G., P. Zimmet, and J. Shaw, *The metabolic syndrome--a new worldwide definition.* Lancet, 2005. **366**(9491): p. 1059-62.
12. Alberti, K.G.M.M. and P.Z. Zimmet, *Definition, diagnosis and classification of diabetes mellitus and its complications. Part 1: diagnosis and classification of diabetes mellitus. Provisional report of a WHO consultation.* Diabetic medicine, 1998. **15**(7): p. 539-553.
13. Balkau, B. and M.A. Charles, *Comment on the provisional report from the WHO consultation. European Group for the Study of Insulin Resistance (EGIR).* Diabet Med, 1999. **16**(5): p. 442-3.
14. Alberti, G., et al., *The IDF consensus worldwide definition of the metabolic syndrome.* Brussels: International Diabetes Federation, 2006. **23**(5): p. 469-80.
15. Kakkar, A.K. and N. Dahiya, *Drug treatment of obesity: current status and future prospects.* Eur J Intern Med, 2015. **26**(2): p. 89-94.
16. Daneschvar, H.L., M.D. Aronson, and G.W. Smetana, *FDA-Approved Anti-Obesity Drugs in the United States.* Am J Med, 2016.

17. Hotamisligil, G.S., N.S. Shargill, and B.M. Spiegelman, *Adipose expression of tumor necrosis factor-alpha: direct role in obesity-linked insulin resistance.* Science, 1993. **259**(5091): p. 87-91.
18. Ofei, F., et al., *Effects of an engineered human anti–TNF-α antibody (CDP571) on insulin sensitivity and glycemic control in patients with NIDDM.* Diabetes, 1996. **45**(7): p. 881-885.
19. Paquot, N., et al., *No increased insulin sensitivity after a single intravenous administration of a recombinant human tumor necrosis factor receptor: Fc fusion protein in obese insulin-resistant patients.* The Journal of Clinical Endocrinology & Metabolism, 2000. **85**(3): p. 1316-1319.
20. Stanley, T.L., et al., *TNF-α antagonism with etanercept decreases glucose and increases the proportion of high molecular weight adiponectin in obese subjects with features of the metabolic syndrome.* The Journal of Clinical Endocrinology & Metabolism, 2011. **96**(1): p. E146-E150.
21. Maedler, K., et al., *Glucose-induced β cell production of IL-1β contributes to glucotoxicity in human pancreatic islets.* The Journal of clinical investigation, 2002. **110**(6): p. 851-860.
22. Larsen, C.M., et al., *Interleukin-1–receptor antagonist in type 2 diabetes mellitus.* New England Journal of Medicine, 2007. **356**(15): p. 1517-1526.
23. Cavelti-Weder, C., et al., *Effects of Gevokizumab on Glycemia and Inflammatory Markers in Type 2 Diabetes.* Diabetes Care, 2012. **35**(8): p. 1654.
24. Jack, D.B., *One hundred years of aspirin.* The Lancet, 1997. **350**(9075): p. 437-439.
25. Anderson, K., et al., *Salsalate, an old, inexpensive drug with potential new indications: a review of the evidence from 3 recent studies.* Am Health Drug Benefits, 2014. **7**(4): p. 231-5.
26. Hundal, R.S., et al., *Mechanism by which high-dose aspirin improves glucose metabolism in type 2 diabetes.* J Clin Invest, 2002. **109**(10): p. 1321-6.
27. Kim, J.K., et al., *Prevention of fat-induced insulin resistance by salicylate.* J Clin Invest, 2001. **108**(3): p. 437-46.
28. Goldfine, A.B., et al., *Salicylate (salsalate) in patients with type 2 diabetes: a randomized trial.* Ann Intern Med, 2013. **159**(1): p. 1-12.
29. Fleischman, A., et al., *Salsalate improves glycemia and inflammatory parameters in obese young adults.* Diabetes care, 2008. **31**(2): p. 289-294.
30. Koska, J., et al., *The effect of salsalate on insulin action and glucose tolerance in obese non-diabetic patients: results of a randomised double-blind placebo-controlled study.* Diabetologia, 2009. **52**(3): p. 385-93.
31. Faghihimani, E., et al., *Reduction of insulin resistance and plasma glucose level by salsalate treatment in persons with prediabetes.* Endocr Pract, 2012. **18**(6): p. 826-33.
32. Yki-Järvinen, H., *Thiazolidinediones.* New England Journal of Medicine, 2004. **351**(11): p. 1106-1118.
33. Pfützner, A., et al., *Improvement of Cardiovascular Risk Markers by Pioglitazone Is Independent From Glycemic Control.* Journal of the American College of Cardiology, 2005. **45**(12): p. 1925-1931.

34. Hattori, Y., et al., *Metformin inhibits cytokine-induced nuclear factor κB activation via AMP-activated protein kinase activation in vascular endothelial cells.* Hypertension, 2006. **47**(6): p. 1183-1188.
35. Huang, N.-L., et al., *Metformin inhibits TNF-α-induced IκB kinase phosphorylation, IκB-α degradation and IL-6 production in endothelial cells through PI3K-dependent AMPK phosphorylation.* International journal of cardiology, 2009. **134**(2): p. 169-175.
36. De Jager, J., et al., *Effects of short-term treatment with metformin on markers of endothelial function and inflammatory activity in type 2 diabetes mellitus: a randomized, placebo-controlled trial.* Journal of internal medicine, 2005. **257**(1): p. 100-109.
37. Caballero, A.E., et al., *The differential effects of metformin on markers of endothelial activation and inflammation in subjects with impaired glucose tolerance: a placebo-controlled, randomized clinical trial.* The Journal of Clinical Endocrinology & Metabolism, 2004. **89**(8): p. 3943-3948.
38. Wernstedt Asterholm, I., et al., *Adipocyte Inflammation Is Essential for Healthy Adipose Tissue Expansion and Remodeling.* Cell Metabolism, 2014. **20**(1): p. 103-118.
39. Hellman, B., *Studies in obese-hyperglycemic mice.* Annals of the New York Academy of Sciences, 1965. **131**(1): p. 541-558.
40. Hausberger, F.X., *Pathological changes in adipose tissue of obese mice.* The Anatomical Record, 1966. **154**(3): p. 651-660.
41. Pekala, P., et al., *Studies of insulin resistance in adipocytes induced by macrophage mediator.* The Journal of experimental medicine, 1983. **157**(4): p. 1360-1365.
42. Mahoney, J., et al., *Lipopolysaccharide-treated RAW 264.7 cells produce a mediator that inhibits lipoprotein lipase in 3T3-L1 cells.* The Journal of Immunology, 1985. **134**(3): p. 1673-1675.
43. Beutler, B., et al., *Identity of tumour necrosis factor and the macrophage-secreted factor cachectin.* Nature, 1985. **316**(6028): p. 552-554.
44. Feingold, K.R., et al., *Effect of tumor necrosis factor (TNF) on lipid metabolism in the diabetic rat. Evidence that inhibition of adipose tissue lipoprotein lipase activity is not required for TNF-induced hyperlipidemia.* The Journal of clinical investigation, 1989. **83**(4): p. 1116-1121.
45. Lang, C.H., C. Dobrescu, and G.J. Bagby, *Tumor necrosis factor impairs insulin action on peripheral glucose disposal and hepatic glucose output.* Endocrinology, 1992. **130**(1): p. 43-52.
46. Hotamisligil, G.S., et al., *Increased adipose tissue expression of tumor necrosis factor-alpha in human obesity and insulin resistance.* J Clin Invest, 1995. **95**(5): p. 2409-15.
47. Feinstein, R., et al., *Tumor necrosis factor-alpha suppresses insulin-induced tyrosine phosphorylation of insulin receptor and its substrates.* Journal of Biological Chemistry, 1993. **268**(35): p. 26055-26058.

48. Hotamisligil, G.S., et al., *Tumor necrosis factor alpha inhibits signaling from the insulin receptor.* Proceedings of the National Academy of Sciences, 1994. **91**(11): p. 4854-4858.
49. Uysal, K.T., et al., *Protection from obesity-induced insulin resistance in mice lacking TNF-alpha function.* Nature, 1997. **389**(6651): p. 610-4.
50. Fève, B. and J.-P. Bastard, *The role of interleukins in insulin resistance and type 2 diabetes mellitus.* Nature Reviews Endocrinology, 2009. **5**(6): p. 305-311.
51. Hotamisligil, G.S., *Inflammation, metaflammation and immunometabolic disorders.* Nature, 2017. **542**(7640): p. 177-185.
52. Sell, H., C. Habich, and J. Eckel, *Adaptive immunity in obesity and insulin resistance.* Nat Rev Endocrinol, 2012. **8**(12): p. 709-16.
53. Weisberg, S.P., et al., *Obesity is associated with macrophage accumulation in adipose tissue.* J Clin Invest, 2003. **112**(12): p. 1796-808.
54. Xu, H., et al., *Chronic inflammation in fat plays a crucial role in the development of obesity-related insulin resistance.* J Clin Invest, 2003. **112**(12): p. 1821-30.
55. Cinti, S., et al., *Adipocyte death defines macrophage localization and function in adipose tissue of obese mice and humans.* J Lipid Res, 2005. **46**(11): p. 2347-55.
56. Strissel, K.J., et al., *Adipocyte death, adipose tissue remodeling, and obesity complications.* Diabetes, 2007. **56**(12): p. 2910-8.
57. Lumeng, C.N., J.L. Bodzin, and A.R. Saltiel, *Obesity induces a phenotypic switch in adipose tissue macrophage polarization.* J Clin Invest, 2007. **117**(1): p. 175-84.
58. Hill, A.A., W. Reid Bolus, and A.H. Hasty, *A decade of progress in adipose tissue macrophage biology.* Immunol Rev, 2014. **262**(1): p. 134-52.
59. Rosen, E.D. and O.A. MacDougald, *Adipocyte differentiation from the inside out.* Nat Rev Mol Cell Biol, 2006. **7**(12): p. 885-96.
60. Romacho, T., et al., *Adipose tissue and its role in organ crosstalk.* Acta Physiol (Oxf), 2014. **210**(4): p. 733-53.
61. Younossi, Z.M., et al., *Global epidemiology of nonalcoholic fatty liver disease—meta-analytic assessment of prevalence, incidence, and outcomes.* Hepatology, 2016. **64**(1): p. 73-84.
62. Eslam, M., et al., *A new definition for metabolic associated fatty liver disease: an international expert consensus statement.* Journal of hepatology, 2020.
63. Eslam, M., et al., *MAFLD: a consensus-driven proposed nomenclature for metabolic associated fatty liver disease.* Gastroenterology, 2020. **158**(7): p. 1999-2014. e1.
64. Donnelly, K.L., et al., *Sources of fatty acids stored in liver and secreted via lipoproteins in patients with nonalcoholic fatty liver disease.* The Journal of clinical investigation, 2005. **115**(5): p. 1343-1351.
65. Makri, E., A. Goulas, and S.A. Polyzos, *Epidemiology, Pathogenesis, Diagnosis and Emerging Treatment of Nonalcoholic Fatty Liver Disease.* Archives of Medical Research, 2021. **52**(1): p. 25-37.
66. Kirpich, I.A., L.S. Marsano, and C.J. McClain, *Gut–liver axis, nutrition, and non-alcoholic fatty liver disease.* Clinical biochemistry, 2015. **48**(13-14): p. 923-930.
67. Le Chatelier, E., et al., *Richness of human gut microbiome correlates with metabolic markers.* Nature, 2013. **500**(7464): p. 541-6.

68. Kong, L.C., et al., *Gut microbiota after gastric bypass in human obesity: increased richness and associations of bacterial genera with adipose tissue genes.* Am J Clin Nutr, 2013. **98**(1): p. 16-24.
69. Palleja, A., et al., *Roux-en-Y gastric bypass surgery of morbidly obese patients induces swift and persistent changes of the individual gut microbiota.* Genome Med, 2016. **8**(1): p. 67.
70. Turnbaugh, P.J., et al., *A core gut microbiome in obese and lean twins.* Nature, 2009. **457**(7228): p. 480-4.
71. Magne, F., et al., *The Firmicutes/Bacteroidetes Ratio: A Relevant Marker of Gut Dysbiosis in Obese Patients?* Nutrients, 2020. **12**(5): p. 1474.
72. Ley, R.E., et al., *Obesity alters gut microbial ecology.* Proc Natl Acad Sci U S A, 2005. **102**(31): p. 11070-5.
73. Wong, C. and T.H. Marwick, *Obesity cardiomyopathy: pathogenesis and pathophysiology.* Nature Clinical Practice Cardiovascular Medicine, 2007. **4**(8): p. 436-443.
74. Ying, W., et al., *The role of macrophages in obesity-associated islet inflammation and β-cell abnormalities.* Nature Reviews Endocrinology, 2020. **16**(2): p. 81-90.
75. D'Agati, V.D., et al., *Obesity-related glomerulopathy: clinical and pathologic characteristics and pathogenesis.* Nat Rev Nephrol, 2016. **12**(8): p. 453-71.
76. Chait, A. and L.J. den Hartigh, *Adipose Tissue Distribution, Inflammation and Its Metabolic Consequences, Including Diabetes and Cardiovascular Disease.* Front Cardiovasc Med, 2020. **7**: p. 22.
77. Ben-Ami Shor, D., et al., *The hygiene theory harnessing helminths and their ova to treat autoimmunity.* Clin Rev Allergy Immunol, 2013. **45**(2): p. 211-6.
78. CDC, *Parasites - Schistosomiasis.* 2012.
79. O'Garra, A., *Cytokines induce the development of functionally heterogeneous T helper cell subsets.* Immunity, 1998. **8**(3): p. 275-83.
80. Jankovic, D., A. Sher, and G. Yap, *Th1/Th2 effector choice in parasitic infection: decision making by committee.* Curr Opin Immunol, 2001. **13**(4): p. 403-9.
81. Colley, D.G. and W.E. Secor, *Immunology of human schistosomiasis.* Parasite Immunol, 2014. **36**(8): p. 347-57.
82. Caldas, I.R., et al., *Human schistosomiasis mansoni: immune responses during acute and chronic phases of the infection.* Acta Trop, 2008. **108**(2-3): p. 109-17.
83. Urban, J.F., Jr., et al., *Local TH1 and TH2 responses to parasitic infection in the intestine: regulation by IFN-gamma and IL-4.* Vet Immunol Immunopathol, 1996. **54**(1-4): p. 337-44.
84. Finkelman, F.D. and J.F. Urban, Jr., *The other side of the coin: the protective role of the TH2 cytokines.* J Allergy Clin Immunol, 2001. **107**(5): p. 772-80.
85. La Flamme, A.C., et al., *IL-4 plays a crucial role in regulating oxidative damage in the liver during schistosomiasis.* J Immunol, 2001. **166**(3): p. 1903-11.
86. Patton, E.A., et al., *Central role for interleukin-4 in regulating nitric oxide-mediated inhibition of T-cell proliferation and gamma interferon production in schistosomiasis.* Infect Immun, 2002. **70**(1): p. 177-84.
87. Brunet, L.R., et al., *IL-4 protects against TNF-alpha-mediated cachexia and death during acute schistosomiasis.* J Immunol, 1997. **159**(2): p. 777-85.

88. Fairfax, K., et al., *Th2 responses in schistosomiasis.* Semin Immunopathol, 2012. **34**(6): p. 863-71.
89. Okano, M., et al., *Induction of Th2 responses and IgE is largely due to carbohydrates functioning as adjuvants on Schistosoma mansoni egg antigens.* J Immunol, 1999. **163**(12): p. 6712-7.
90. Tawill, S., et al., *Both free-living and parasitic nematodes induce a characteristic Th2 response that is dependent on the presence of intact glycans.* Infect Immun, 2004. **72**(1): p. 398-407.
91. Zaccone, P., et al., *Schistosoma mansoni antigens modulate the activity of the innate immune response and prevent onset of type 1 diabetes.* Eur J Immunol, 2003. **33**(5): p. 1439-49.
92. Zaccone, P., et al., *Immune modulation by Schistosoma mansoni antigens in NOD mice: effects on both innate and adaptive immune systems.* J Biomed Biotechnol, 2010. **2010**: p. 795210.
93. Hussaarts, L., et al., *Chronic helminth infection and helminth-derived egg antigens promote adipose tissue M2 macrophages and improve insulin sensitivity in obese mice.* FASEB J, 2015. **29**(7): p. 3027-39.
94. Guigas, B. and A.B. Molofsky, *A worm of one's own: how helminths modulate host adipose tissue function and metabolism.* Trends Parasitol, 2015. **31**(9): p. 435-41.
95. Osada, Y. and T. Kanazawa, *Parasitic helminths: new weapons against immunological disorders.* J Biomed Biotechnol, 2010. **2010**: p. 743758.
96. Osada, Y., et al., *Schistosoma mansoni infection reduces severity of collagen-induced arthritis via down-regulation of pro-inflammatory mediators.* Int J Parasitol, 2009. **39**(4): p. 457-64.
97. La Flamme, A.C., K. Ruddenklau, and B.T. Backstrom, *Schistosomiasis decreases central nervous system inflammation and alters the progression of experimental autoimmune encephalomyelitis.* Infect Immun, 2003. **71**(9): p. 4996-5004.
98. Mangan, N.E., et al., *Helminth-modified pulmonary immune response protects mice from allergen-induced airway hyperresponsiveness.* J Immunol, 2006. **176**(1): p. 138-47.
99. Harrison, J. and D.S. Ridley, *Heterologous reactions involving parasites, blood group antibodies and tissue components.* Trans R Soc Trop Med Hyg, 1975. **69**(3): p. 312-7.
100. Nash, T.E., E.A. Ottesen, and A.W. Cheever, *Antibody response to a polysaccharide antigen present in the schistosome gut. II. Modulation of antibody response.* Am J Trop Med Hyg, 1978. **27**(5): p. 944-50.
101. Nash, T.E., *Antibody response to a polysaccharide antigen present in the schistosome gut. I. Sensitivity and specificity.* Am J Trop Med Hyg, 1978. **27**(5): p. 939-43.
102. Richter, D., R.N. Incani, and D.A. Harn, *Lacto-N-fucopentaose III (Lewis x), a target of the antibody response in mice vaccinated with irradiated cercariae of Schistosoma mansoni.* Infect Immun, 1996. **64**(5): p. 1826-31.

103. van Die, I., et al., *The dendritic cell-specific C-type lectin DC-SIGN is a receptor for Schistosoma mansoni egg antigens and recognizes the glycan antigen Lewis x.* Glycobiology, 2003. **13**(6): p. 471-8.
104. Gringhuis, S.I., et al., *Carbohydrate-specific signaling through the DC-SIGN signalosome tailors immunity to Mycobacterium tuberculosis, HIV-1 and Helicobacter pylori.* Nat Immunol, 2009. **10**(10): p. 1081-8.
105. Victora, C.G., et al., *Breastfeeding in the 21st century: epidemiology, mechanisms, and lifelong effect.* The Lancet, 2016. **387**(10017): p. 475-490.
106. Stuebe, A., *The risks of not breastfeeding for mothers and infants.* Reviews in obstetrics & gynecology, 2009. **2**(4): p. 222-231.
107. Plaza-Díaz, J., L. Fontana, and A. Gil, *Human Milk Oligosaccharides and Immune System Development.* Nutrients, 2018. **10**(8): p. 1038.
108. Orczyk-Pawiłowicz, M. and J. Lis-Kuberka, *The Impact of Dietary Fucosylated Oligosaccharides and Glycoproteins of Human Milk on Infant Well-Being.* Nutrients, 2020. **12**(4).
109. Coppa, G.V., et al., *Oligosaccharides in human milk during different phases of lactation.* Acta Paediatr Suppl, 1999. **88**(430): p. 89-94.
110. Ninonuevo, M.R., et al., *A Strategy for Annotating the Human Milk Glycome.* Journal of Agricultural and Food Chemistry, 2006. **54**(20): p. 7471-7480.
111. Totten, S.M., et al., *Comprehensive profiles of human milk oligosaccharides yield highly sensitive and specific markers for determining secretor status in lactating mothers.* J Proteome Res, 2012. **11**(12): p. 6124-33.
112. Kunz, C., et al., *Influence of Gestational Age, Secretor, and Lewis Blood Group Status on the Oligosaccharide Content of Human Milk.* J Pediatr Gastroenterol Nutr, 2017. **64**(5): p. 789-798.
113. Oriol, R., et al., *Divergent evolution of fucosyltransferase genes from vertebrates, invertebrates, and bacteria.* Glycobiology, 1999. **9**(4): p. 323-334.
114. Engfer, M.B., et al., *Human milk oligosaccharides are resistant to enzymatic hydrolysis in the upper gastrointestinal tract.* Am J Clin Nutr, 2000. **71**(6): p. 1589-96.
115. Gnoth, M.J., et al., *Human milk oligosaccharides are minimally digested in vitro.* J Nutr, 2000. **130**(12): p. 3014-20.
116. Rudloff, S., et al., *Urinary excretion of lactose and oligosaccharides in preterm infants fed human milk or infant formula.* Acta Paediatrica, 1996. **85**(5): p. 598-603.
117. Rudloff, S., et al., *Urinary excretion of in vivo 13 C-labelled milk oligosaccharides in breastfed infants.* British Journal of Nutrition, 2012. **107**(7): p. 957-963.
118. Albrecht, S., et al., *CE-LIF-MSn profiling of oligosaccharides in human milk and feces of breast-fed babies.* Electrophoresis, 2010. **31**(7): p. 1264-1273.
119. Albrecht, S., et al., *Occurrence of oligosaccharides in feces of breast-fed babies in their first six months of life and the corresponding breast milk.* Carbohydrate Research, 2011. **346**(16): p. 2540-2550.
120. Pickard, J.M. and A.V. Chervonsky, *Intestinal fucose as a mediator of host-microbe symbiosis.* J Immunol, 2015. **194**(12): p. 5588-93.

121. Yu, Z.T., N.N. Nanthakumar, and D.S. Newburg, *The Human Milk Oligosaccharide 2'-Fucosyllactose Quenches Campylobacter jejuni-Induced Inflammation in Human Epithelial Cells HEp-2 and HT-29 and in Mouse Intestinal Mucosa.* J Nutr, 2016. **146**(10): p. 1980-1990.
122. Weichert, S., et al., *Bioengineered 2'-fucosyllactose and 3-fucosyllactose inhibit the adhesion of Pseudomonas aeruginosa and enteric pathogens to human intestinal and respiratory cell lines.* Nutrition research, 2013. **33**(10): p. 831-838.
123. Lin, A.E., et al., *Human milk oligosaccharides protect bladder epithelial cells against uropathogenic Escherichia coli invasion and cytotoxicity.* J Infect Dis, 2014. **209**(3): p. 389-98.
124. Triantis, V., L. Bode, and R. Van Neerven, *Immunological effects of human milk oligosaccharides.* Frontiers in pediatrics, 2018. **6**: p. 190.
125. Kuntz, S., S. Rudloff, and C. Kunz, *Oligosaccharides from human milk influence growth-related characteristics of intestinally transformed and non-transformed intestinal cells.* British Journal of Nutrition, 2008. **99**(3): p. 462-471.
126. Kuntz, S., C. Kunz, and S. Rudloff, *Oligosaccharides from human milk induce growth arrest via G2/M by influencing growth-related cell cycle genes in intestinal epithelial cells.* British Journal of Nutrition, 2009. **101**(9): p. 1306-1315.
127. Lane, J.A., et al., *Transcriptional response of HT-29 intestinal epithelial cells to human and bovine milk oligosaccharides.* Br J Nutr, 2013. **110**(12): p. 2127-37.
128. Rudloff, S., et al., *Detection of ligands for selectins in the oligosaccharide fraction of human milk.* European journal of nutrition, 2002. **41**(2): p. 85-92.
129. Koning, N., et al., *Human milk blocks DC-SIGN–pathogen interaction via MUC1.* Frontiers in immunology, 2015. **6**: p. 112.
130. Xiao, L., et al., *Human milk oligosaccharides promote immune tolerance via direct interactions with human dendritic cells.* European journal of immunology, 2019. **49**(7): p. 1001-1014.
131. György, P., R.F. Norris, and C.S. Rose, *Bifidus factor. I. A variant of Lactobacillus bifidus requiring a special growth factor.* Archives of Biochemistry and Biophysics, 1954. **48**(1): p. 193-201.
132. Ward, R.E., et al., *In vitro fermentation of breast milk oligosaccharides by Bifidobacterium infantis and Lactobacillus gasseri.* Appl Environ Microbiol, 2006. **72**(6): p. 4497-9.
133. Ward, R.E., et al., *In vitro fermentability of human milk oligosaccharides by several strains of bifidobacteria.* Mol Nutr Food Res, 2007. **51**(11): p. 1398-405.
134. Sakanaka, M., et al., *Varied Pathways of Infant Gut-Associated Bifidobacterium to Assimilate Human Milk Oligosaccharides: Prevalence of the Gene Set and Its Correlation with Bifidobacteria-Rich Microbiota Formation.* Nutrients, 2019. **12**(1).
135. Marcobal, A., et al., *Bacteroides in the infant gut consume milk oligosaccharides via mucus-utilization pathways.* Cell Host Microbe, 2011. **10**(5): p. 507-14.
136. Marcobal, A., et al., *Consumption of human milk oligosaccharides by gut-related microbes.* J Agric Food Chem, 2010. **58**(9): p. 5334-40.

137. Lewis, Z.T., et al., *Maternal fucosyltransferase 2 status affects the gut bifidobacterial communities of breastfed infants.* Microbiome, 2015. **3**: p. 13.
138. Smith-Brown, P., et al., *Mothers Secretor Status Affects Development of Childrens Microbiota Composition and Function: A Pilot Study.* PLoS One, 2016. **11**(9): p. e0161211.
139. Steenhout, P., et al., *Term Infant Formula Supplemented with Human Milk Oligosaccharides (2' Fucosyllactose and Lacto-N-neotetraose) Shifts Stool Microbiota and Metabolic Signatures Closer to that of Breastfed Infants.* The FASEB Journal, 2016. **30**: p. 275.7-275.7.
140. Thurl, S., et al., *Systematic review of the concentrations of oligosaccharides in human milk.* Nutrition reviews, 2017. **75**(11): p. 920-933.
141. Murata, T., et al., *Facile enzymatic conversion of lactose into lacto-N-tetraose and lacto-N-neotetraose.* Glycoconj J, 1999. **16**(3): p. 189-95.
142. Renaudie, L., et al., *Enzymatic supported synthesis of lacto-N-neotetraose using dendrimeric polyethylene glycol.* Carbohydr Res, 2004. **339**(3): p. 693-8.
143. Chen, C., et al., *Sequential one-pot multienzyme (OPME) synthesis of lacto-N-neotetraose and its sialyl and fucosyl derivatives.* Chem Commun (Camb), 2015. **51**(36): p. 7689-92.
144. Coulet, M., et al., *Pre-clinical safety assessment of the synthetic human milk, nature-identical, oligosaccharide Lacto-N-neotetraose (LNnT).* Food Chem Toxicol, 2013. **62**: p. 528-37.
145. Bode, L., et al., *Overcoming the limited availability of human milk oligosaccharides: challenges and opportunities for research and application.* Nutr Rev, 2016. **74**(10): p. 635-44.
146. Thomas, P.G., et al., *Maturation of dendritic cell 2 phenotype by a helminth glycan uses a Toll-like receptor 4-dependent mechanism.* J Immunol, 2003. **171**(11): p. 5837-41.
147. Hokke, C.H. and A.M. Deelder, *Schistosome glycoconjugates in host-parasite interplay.* Glycoconj J, 2001. **18**(8): p. 573-87.
148. Velupillai, P. and D.A. Harn, *Oligosaccharide-specific induction of interleukin 10 production by B220+ cells from schistosome-infected mice: a mechanism for regulation of CD4+ T-cell subsets.* Proc Natl Acad Sci U S A, 1994. **91**(1): p. 18-22.
149. Palanivel, V., et al., *B-cell outgrowth and ligand-specific production of IL-10 correlate with Th2 dominance in certain parasitic diseases.* Exp Parasitol, 1996. **84**(2): p. 168-77.
150. Velupillai, P., et al., *B-1 cell (CD5+B220+) outgrowth in murine schistosomiasis is genetically restricted and is largely due to activation by polylactosamine sugars.* J Immunol, 1997. **158**(1): p. 338-44.
151. Velupillai, P., J. Sypek, and D.A. Harn, *Interleukin-12 and -10 and gamma interferon regulate polyclonal and ligand-specific expansion of murine B-1 cells.* Infect Immun, 1996. **64**(11): p. 4557-60.
152. Velupillai, P., et al., *Lewis(x)-containing oligosaccharide attenuates schistosome egg antigen-induced immune depression in human schistosomiasis.* Hum Immunol, 2000. **61**(3): p. 225-32.

153. Okano, M., et al., *Lacto-N-fucopentaose III found on Schistosoma mansoni egg antigens functions as adjuvant for proteins by inducing Th2-type response.* J Immunol, 2001. **167**(1): p. 442-50.
154. Atochina, O., et al., *A schistosome-expressed immunomodulatory glycoconjugate expands peritoneal Gr1(+) macrophages that suppress naive CD4(+) T cell proliferation via an IFN-gamma and nitric oxide-dependent mechanism.* J Immunol, 2001. **167**(8): p. 4293-302.
155. Atochina, O. and D. Harn, *LNFPIII/LeX-stimulated macrophages activate natural killer cells via CD40-CD40L interaction.* Clin Diagn Lab Immunol, 2005. **12**(9): p. 1041-9.
156. Atochina, O., et al., *The immunomodulatory glycan LNFPIII initiates alternative activation of murine macrophages in vivo.* Immunology, 2008. **125**(1): p. 111-21.
157. Thomas, P.G., et al., *A helminth glycan induces APC maturation via alternative NF-kappa B activation independent of I kappa B alpha degradation.* J Immunol, 2005. **175**(4): p. 2082-90.
158. Wang, Y., et al., *Dendritic cells activated by an anti-inflammatory agent induce CD4(+) T helper type 2 responses without impairing CD8(+) memory and effector cytotoxic T-lymphocyte responses.* Immunology, 2010. **129**(3): p. 406-17.
159. Srivastava, L., et al., *Immunomodulatory glycan lacto-N-fucopentaose III requires clathrin-mediated endocytosis to induce alternative activation of antigen-presenting cells.* Infect Immun, 2014. **82**(5): p. 1891-903.
160. Tundup, S., et al., *A Neoglycoconjugate Containing the Human Milk Sugar LNFPIII Drives Anti-Inflammatory Activation of Antigen Presenting Cells in a CD14 Dependent Pathway.* PLoS One, 2015. **10**(9): p. e0137495.
161. Terrazas, L.I., et al., *The schistosome oligosaccharide lacto-N-neotetraose expands Gr1(+) cells that secrete anti-inflammatory cytokines and inhibit proliferation of naive CD4(+) cells: a potential mechanism for immune polarization in helminth infections.* J Immunol, 2001. **167**(9): p. 5294-303.
162. Dutta, P., et al., *Lacto-N-fucopentaose III, a pentasaccharide, prolongs heart transplant survival.* Transplantation, 2010. **90**(10): p. 1071-8.
163. Atochina, O. and D. Harn, *Prevention of psoriasis-like lesions development in fsn/fsn mice by helminth glycans.* Exp Dermatol, 2006. **15**(6): p. 461-8.
164. Zhu, B., et al., *Immune modulation by Lacto-N-fucopentaose III in experimental autoimmune encephalomyelitis.* Clin Immunol, 2012. **142**(3): p. 351-61.
165. Bhargava, P., et al., *Immunomodulatory glycan LNFPIII alleviates hepatosteatosis and insulin resistance through direct and indirect control of metabolic pathways.* Nat Med, 2012. **18**(11): p. 1665-72.
166. Carpenter, J.M., et al., *Neurochemical and neuroinflammatory perturbations in two Gulf War Illness models: Modulation by the immunotherapeutic LNFPIII.* Neurotoxicology, 2020. **77**: p. 40-50.
167. Mote, R.S., et al., *Assessing the Beneficial Effects of the Immunomodulatory Glycan LNFPIII on Gut Microbiota and Health in a Mouse Model of Gulf War Illness.* International Journal of Environmental Research and Public Health, 2020. **17**(19): p. 7081.

168. Weir, C.B. and A. Jan, *BMI Classification Percentile And Cut Off Points*, in *StatPearls*. 2020, StatPearls Publishing

169. Godoy-Matos, A.F., W.S. Silva Júnior, and C.M. Valerio, *NAFLD as a continuum: from obesity to metabolic syndrome and diabetes.* Diabetol Metab Syndr, 2020. **12**: p. 60.
170. Zimmet, P., et al., *The metabolic syndrome: a global public health problem and a new definition.* J Atheroscler Thromb, 2005. **12**(6): p. 295-300.
171. Hirsch, J. and P.W. Han, *Cellularity of rat adipose tissue: effects of growth, starvation, and obesity.* J Lipid Res, 1969. **10**(1): p. 77-82.
172. Faust, I.M., et al., *Diet-induced adipocyte number increase in adult rats: a new model of obesity.* Am J Physiol, 1978. **235**(3): p. E279-86.
173. Spalding, K.L., et al., *Dynamics of fat cell turnover in humans.* Nature, 2008. **453**(7196): p. 783-7.
174. Tang, W., et al., *White fat progenitor cells reside in the adipose vasculature.* Science, 2008. **322**(5901): p. 583-6.
175. Wang, Q.A., et al., *Tracking adipogenesis during white adipose tissue development, expansion and regeneration.* Nat Med, 2013. **19**(10): p. 1338-44.
176. Vishvanath, L., et al., *Pdgfrβ+ Mural Preadipocytes Contribute to Adipocyte Hyperplasia Induced by High-Fat-Diet Feeding and Prolonged Cold Exposure in Adult Mice.* Cell Metab, 2016. **23**(2): p. 350-9.
177. Hosogai, N., et al., *Adipose tissue hypoxia in obesity and its impact on adipocytokine dysregulation.* Diabetes, 2007. **56**(4): p. 901-11.
178. Halberg, N., et al., *Hypoxia-inducible factor 1alpha induces fibrosis and insulin resistance in white adipose tissue.* Mol Cell Biol, 2009. **29**(16): p. 4467-83.
179. Salans, L.B., J.L. Knittle, and J. Hirsch, *The role of adipose cell size and adipose tissue insulin sensitivity in the carbohydrate intolerance of human obesity.* J Clin Invest, 1968. **47**(1): p. 153-65.
180. Dandona, P., et al., *Tumor necrosis factor-alpha in sera of obese patients: fall with weight loss.* J Clin Endocrinol Metab, 1998. **83**(8): p. 2907-10.
181. Maury, E. and S.M. Brichard, *Adipokine dysregulation, adipose tissue inflammation and metabolic syndrome.* Mol Cell Endocrinol, 2010. **314**(1): p. 1-16.
182. Thurl, S., et al., *Systematic review of the concentrations of oligosaccharides in human milk.* Nutr Rev, 2017. **75**(11): p. 920-933.
183. Bode, L., *Human milk oligosaccharides: every baby needs a sugar mama.* Glycobiology, 2012. **22**(9): p. 1147-62.
184. Elison, E., et al., *Oral supplementation of healthy adults with 2'-O-fucosyllactose and lacto-N-neotetraose is well tolerated and shifts the intestinal microbiota.* Br J Nutr, 2016. **116**(8): p. 1356-1368.
185. Xiao, Z., et al., *Chemoenzymatic Synthesis of a Library of Human Milk Oligosaccharides.* J Org Chem, 2016. **81**(14): p. 5851-65.
186. Beguinot, F. and C. Nigro, *Measurement of glucose homeostasis in vivo: glucose and insulin tolerance tests.* Methods Mol Biol, 2012. **933**: p. 219-28.

187. Ayala, J.E., et al., *Standard operating procedures for describing and performing metabolic tests of glucose homeostasis in mice.* Dis Model Mech, 2010. **3**(9-10): p. 525-34.
188. Bowe, J.E., et al., *Metabolic phenotyping guidelines: assessing glucose homeostasis in rodent models.* J Endocrinol, 2014. **222**(3): p. G13-25.
189. Andrikopoulos, S., et al., *Evaluating the glucose tolerance test in mice.* Am J Physiol Endocrinol Metab, 2008. **295**(6): p. E1323-32.
190. Whary, M.T., et al., *Chapter 3 - Biology and Diseases of Mice*, in *Laboratory Animal Medicine (Third Edition)*, J.G. Fox, et al., Editors. 2015, Academic Press: Boston. p. 43-149.
191. Huttunen, R. and J. Syrjänen, *Obesity and the outcome of infection.* Lancet Infect Dis, 2010. **10**(7): p. 442-3.
192. Huttunen, R. and J. Syrjänen, *Obesity and the risk and outcome of infection.* Int J Obes (Lond), 2013. **37**(3): p. 333-40.
193. Ogawa, M., *Differentiation and proliferation of hematopoietic stem cells.* Blood, 1993. **81**(11): p. 2844-53.
194. Bohnsack, B.L. and K.K. Hirschi, *Nutrient regulation of cell cycle progression.* Annu Rev Nutr, 2004. **24**: p. 433-53.
195. Ihle, J.N., *Interleukin-3 and hematopoiesis.* Chem Immunol, 1992. **51**: p. 65-106.
196. Choi, K.D., M. Vodyanik, and Slukvin, II, *Hematopoietic differentiation and production of mature myeloid cells from human pluripotent stem cells.* Nat Protoc, 2011. **6**(3): p. 296-313.
197. Pratley, R.E., C. Wilson, and C. Bogardus, *Relation of the white blood cell count to obesity and insulin resistance: effect of race and gender.* Obes Res, 1995. **3**(6): p. 563-71.
198. Herishanu, Y., et al., *Leukocytosis in obese individuals: possible link in patients with unexplained persistent neutrophilia.* Eur J Haematol, 2006. **76**(6): p. 516-20.
199. Dixon, J.B. and P.E. O'Brien, *Obesity and the white blood cell count: changes with sustained weight loss.* Obes Surg, 2006. **16**(3): p. 251-7.
200. Farhangi, M.A., et al., *White blood cell count in women: relation to inflammatory biomarkers, haematological profiles, visceral adiposity, and other cardiovascular risk factors.* J Health Popul Nutr, 2013. **31**(1): p. 58-64.
201. Nanji, A.A. and J.B. Freeman, *Relationship between body weight and total leukocyte count in morbid obesity.* Am J Clin Pathol, 1985. **84**(3): p. 346-7.
202. Ryder, E., et al., *Association of obesity with leukocyte count in obese individuals without metabolic syndrome.* Diabetes Metab Syndr, 2014. **8**(4): p. 197-204.
203. Xue, W., et al., *The chemokine system and its role in obesity.* J Cell Physiol, 2019. **234**(4): p. 3336-3346.
204. Vasudevan, A.R., et al., *Eotaxin and obesity.* J Clin Endocrinol Metab, 2006. **91**(1): p. 256-61.
205. Lee, E.H., et al., *Eosinophils support adipocyte maturation and promote glucose tolerance in obesity.* Sci Rep, 2018. **8**(1): p. 9894.
206. Nunemaker, C.S., et al., *Increased serum CXCL1 and CXCL5 are linked to obesity, hyperglycemia, and impaired islet function.* J Endocrinol, 2014. **222**(2): p. 267-76.

207. Sajadi, S.M., et al., *Plasma levels of CXCL1 (GRO-alpha) and CXCL10 (IP-10) are elevated in type 2 diabetic patients: evidence for the involvement of inflammation and angiogenesis/angiostasis in this disease state.* Clin Lab, 2013. **59**(1-2): p. 133-7.
208. De Filippo, K., et al., *Mast cell and macrophage chemokines CXCL1/CXCL2 control the early stage of neutrophil recruitment during tissue inflammation.* Blood, 2013. **121**(24): p. 4930-7.
209. Christiansen, T., B. Richelsen, and J.M. Bruun, *Monocyte chemoattractant protein-1 is produced in isolated adipocytes, associated with adiposity and reduced after weight loss in morbid obese subjects.* Int J Obes (Lond), 2005. **29**(1): p. 146-50.
210. Weisberg, S.P., et al., *CCR2 modulates inflammatory and metabolic effects of high-fat feeding.* J Clin Invest, 2006. **116**(1): p. 115-24.
211. Kanda, H., et al., *MCP-1 contributes to macrophage infiltration into adipose tissue, insulin resistance, and hepatic steatosis in obesity.* J Clin Invest, 2006. **116**(6): p. 1494-505.
212. Jiao, P., et al., *Obesity-related upregulation of monocyte chemotactic factors in adipocytes: involvement of nuclear factor-kappaB and c-Jun NH2-terminal kinase pathways.* Diabetes, 2009. **58**(1): p. 104-15.
213. Huber, J., et al., *CC chemokine and CC chemokine receptor profiles in visceral and subcutaneous adipose tissue are altered in human obesity.* J Clin Endocrinol Metab, 2008. **93**(8): p. 3215-21.
214. Chawla, A., K.D. Nguyen, and Y.P. Goh, *Macrophage-mediated inflammation in metabolic disease.* Nat Rev Immunol, 2011. **11**(11): p. 738-49.
215. Meier, C.A., et al., *IL-1 receptor antagonist serum levels are increased in human obesity: a possible link to the resistance to leptin?* J Clin Endocrinol Metab, 2002. **87**(3): p. 1184-8.
216. Um, J.Y., et al., *Association of interleukin-1beta gene polymorphism with body mass index in women.* Clin Chem, 2004. **50**(3): p. 647-50.
217. Di Renzo, L., et al., *Interleukin-1 (IL-1) receptor antagonist gene polymorphism in normal weight obese syndrome: relationship to body composition and IL-1 alpha and beta plasma levels.* Pharmacol Res, 2007. **55**(2): p. 131-8.
218. Wensveen, F.M., et al., *The "Big Bang" in obese fat: Events initiating obesity-induced adipose tissue inflammation.* Eur J Immunol, 2015. **45**(9): p. 2446-56.
219. Goswami, R. and M.H. Kaplan, *A brief history of IL-9.* J Immunol, 2011. **186**(6): p. 3283-8.
220. Gee, K., et al., *The IL-12 family of cytokines in infection, inflammation and autoimmune disorders.* Inflamm Allergy Drug Targets, 2009. **8**(1): p. 40-52.
221. Darkhal, P., et al., *Blocking high-fat diet-induced obesity, insulin resistance and fatty liver by overexpression of Il-13 gene in mice.* Int J Obes (Lond), 2015. **39**(8): p. 1292-9.
222. Yanagi, S., et al., *The Homeostatic Force of Ghrelin.* Cell Metab, 2018. **27**(4): p. 786-804.

223. Toshinai, K., et al., *Upregulation of Ghrelin expression in the stomach upon fasting, insulin-induced hypoglycemia, and leptin administration.* Biochem Biophys Res Commun, 2001. **281**(5): p. 1220-5.
224. Cummings, D.E., et al., *Plasma ghrelin levels after diet-induced weight loss or gastric bypass surgery.* N Engl J Med, 2002. **346**(21): p. 1623-30.
225. Shiiya, T., et al., *Plasma ghrelin levels in lean and obese humans and the effect of glucose on ghrelin secretion.* J Clin Endocrinol Metab, 2002. **87**(1): p. 240-4.
226. Dixit, V.D., et al., *Ghrelin inhibits leptin- and activation-induced proinflammatory cytokine expression by human monocytes and T cells.* J Clin Invest, 2004. **114**(1): p. 57-66.
227. Moreno, M., et al., *Ghrelin attenuates hepatocellular injury and liver fibrogenesis in rodents and influences fibrosis progression in humans.* Hepatology, 2010. **51**(3): p. 974-85.
228. Myers, M.G., Jr., et al., *Obesity and leptin resistance: distinguishing cause from effect.* Trends Endocrinol Metab, 2010. **21**(11): p. 643-51.
229. Weigle, D.S., et al., *Effect of fasting, refeeding, and dietary fat restriction on plasma leptin levels.* J Clin Endocrinol Metab, 1997. **82**(2): p. 561-5.
230. Keim, N.L., J.S. Stern, and P.J. Havel, *Relation between circulating leptin concentrations and appetite during a prolonged, moderate energy deficit in women.* Am J Clin Nutr, 1998. **68**(4): p. 794-801.
231. Ahima, R.S., et al., *Role of leptin in the neuroendocrine response to fasting.* Nature, 1996. **382**(6588): p. 250-2.
232. Morton, G.J., et al., *Central nervous system control of food intake and body weight.* Nature, 2006. **443**(7109): p. 289-95.
233. Nauck, M.A. and J.J. Meier, *Incretin hormones: Their role in health and disease.* Diabetes Obes Metab, 2018. **20 Suppl 1**: p. 5-21.
234. Kim, W. and J.M. Egan, *The role of incretins in glucose homeostasis and diabetes treatment.* Pharmacol Rev, 2008. **60**(4): p. 470-512.
235. Kalra, S. and Y. Gupta, *The Insulin:Glucagon Ratio and the Choice of Glucose-Lowering Drugs.* Diabetes Ther, 2016. **7**(1): p. 1-9.
236. Moukarzel, S. and L. Bode, *Human Milk Oligosaccharides and the Preterm Infant: A Journey in Sickness and in Health.* Clin Perinatol, 2017. **44**(1): p. 193-207.
237. Hegar, B., et al., *The Role of Two Human Milk Oligosaccharides, 2'-Fucosyllactose and Lacto-N-Neotetraose, in Infant Nutrition.* Pediatric gastroenterology, hepatology & nutrition, 2019. **22**(4): p. 330-340.
238. Bandara, M.D., K.J. Stine, and A.V. Demchenko, *The chemical synthesis of human milk oligosaccharides: Lacto-N-neotetraose (Galβ1→4GlcNAcβ1→3Galβ1→4Glc).* Carbohydr Res, 2019. **483**: p. 107743.
239. Agoston, K., et al., *Kilogram scale chemical synthesis of 2'-fucosyllactose.* Carbohydr Res, 2019. **476**: p. 71-77.
240. Ni, Y., et al., *Adipose Tissue Macrophage Phenotypes and Characteristics: The Key to Insulin Resistance in Obesity and Metabolic Disorders.* Obesity, 2020. **28**(2): p. 225-234.

241. Jing, Y., et al., *Metformin improves obesity-associated inflammation by altering macrophages polarization.* Molecular and Cellular Endocrinology, 2018. **461**: p. 256-264.
242. Koppaka, S., et al., *Reduced Adipose Tissue Macrophage Content Is Associated With Improved Insulin Sensitivity in Thiazolidinedione-Treated Diabetic Humans.* Diabetes, 2013. **62**(6): p. 1843.
243. Ellingsgaard, H., et al., *Interleukin-6 enhances insulin secretion by increasing glucagon-like peptide-1 secretion from L cells and alpha cells.* Nat Med, 2011. **17**(11): p. 1481-9.
244. El-Kadre, L.J. and A.C. Tinoco, *Interleukin-6 and obesity: the crosstalk between intestine, pancreas and liver.* Curr Opin Clin Nutr Metab Care, 2013. **16**(5): p. 564-8.
245. Kim, J.H., R.A. Bachmann, and J. Chen, *Interleukin-6 and insulin resistance.* Vitam Horm, 2009. **80**: p. 613-33.
246. Ahmed, M. and S.L. Gaffen, *IL-17 in obesity and adipogenesis.* Cytokine Growth Factor Rev, 2010. **21**(6): p. 449-53.
247. Tschöp, M., et al., *Circulating ghrelin levels are decreased in human obesity.* Diabetes, 2001. **50**(4): p. 707-9.
248. Otto, B., et al., *Weight gain decreases elevated plasma ghrelin concentrations of patients with anorexia nervosa.* Eur J Endocrinol, 2001. **145**(5): p. 669-73.
249. Otto, B., et al., *Postprandial ghrelin release in anorectic patients before and after weight gain.* Psychoneuroendocrinology, 2005. **30**(6): p. 577-81.
250. Frederich, R.C., et al., *Leptin levels reflect body lipid content in mice: evidence for diet-induced resistance to leptin action.* Nat Med, 1995. **1**(12): p. 1311-4.
251. Friedman, J.M. and J.L. Halaas, *Leptin and the regulation of body weight in mammals.* Nature, 1998. **395**(6704): p. 763-70.
252. Huang, X. and Z. Yang, *Resistin's, obesity and insulin resistance: the continuing disconnect between rodents and humans.* J Endocrinol Invest, 2016. **39**(6): p. 607-15.
253. Lehrke, M., et al., *An inflammatory cascade leading to hyperresistinemia in humans.* PLoS Med, 2004. **1**(2): p. e45.
254. Filková, M., et al., *The role of resistin as a regulator of inflammation: Implications for various human pathologies.* Clin Immunol, 2009. **133**(2): p. 157-70.
255. Hales, C.M., Carroll, M.D., Fryaer C.D., Ogden, C.L. . *Prevalence of obesity and severe obesity among adults; United States, 2017-2018.* [NCHS Data Brief] 2020.
256. Ward, Z.J., et al., *Projected U.S. State-Level Prevalence of Adult Obesity and Severe Obesity.* New England Journal of Medicine, 2019. **381**(25): p. 2440-2450.
257. Turnbaugh, P.J., et al., *An obesity-associated gut microbiome with increased capacity for energy harvest.* Nature, 2006. **444**(7122): p. 1027-31.
258. Ridaura, V.K., et al., *Gut microbiota from twins discordant for obesity modulate metabolism in mice.* Science, 2013. **341**(6150): p. 1241214.
259. Vrieze, A., et al., *Transfer of intestinal microbiota from lean donors increases insulin sensitivity in individuals with metabolic syndrome.* Gastroenterology, 2012. **143**(4): p. 913-6.e7.

260. Wu, G.D., et al., *Linking long-term dietary patterns with gut microbial enterotypes.* Science, 2011. **334**(6052): p. 105-8.
261. Carmody, R.N., et al., *Diet dominates host genotype in shaping the murine gut microbiota.* Cell Host Microbe, 2015. **17**(1): p. 72-84.
262. Turnbaugh, P.J., et al., *The effect of diet on the human gut microbiome: a metagenomic analysis in humanized gnotobiotic mice.* Science translational medicine, 2009. **1**(6): p. 6ra14-6ra14.
263. Caesar, R., et al., *Crosstalk between Gut Microbiota and Dietary Lipids Aggravates WAT Inflammation through TLR Signaling.* Cell metabolism, 2015. **22**(4): p. 658-668.
264. Cani, P.D., et al., *Metabolic endotoxemia initiates obesity and insulin resistance.* Diabetes, 2007. **56**(7): p. 1761-72.
265. Walker, A.W., et al., *Dominant and diet-responsive groups of bacteria within the human colonic microbiota.* Isme j, 2011. **5**(2): p. 220-30.
266. David, L.A., et al., *Diet rapidly and reproducibly alters the human gut microbiome.* Nature, 2014. **505**(7484): p. 559-563.
267. Wu, G.D., et al., *Comparative metabolomics in vegans and omnivores reveal constraints on diet-dependent gut microbiota metabolite production.* Gut, 2016. **65**(1): p. 63-72.
268. Cotillard, A., et al., *Dietary intervention impact on gut microbial gene richness.* Nature, 2013. **500**(7464): p. 585-588.
269. *Structure, function and diversity of the healthy human microbiome.* Nature, 2012. **486**(7402): p. 207-14.
270. De Wit, N., et al., *Saturated fat stimulates obesity and hepatic steatosis and affects gut microbiota composition by an enhanced overflow of dietary fat to the distal intestine.* American Journal of Physiology-Gastrointestinal and Liver Physiology, 2012. **303**(5): p. G589-G599.
271. Wang, M., et al., *Fecal microbiota composition of breast-fed infants is correlated with human milk oligosaccharides consumed.* Journal of pediatric gastroenterology and nutrition, 2015. **60**(6): p. 825-833.
272. Asakuma, S., et al., *Physiology of consumption of human milk oligosaccharides by infant gut-associated bifidobacteria.* J Biol Chem, 2011. **286**(40): p. 34583-92.
273. Mote, R.S., et al., *Assessing the Beneficial Effects of the Immunomodulatory Glycan LNFPIII on Gut Microbiota and Health in a Mouse Model of Gulf War Illness.* Int J Environ Res Public Health, 2020. **17**(19).
274. Callahan, B.J., et al., *DADA2: High-resolution sample inference from Illumina amplicon data.* Nature Methods, 2016. **13**(7): p. 581-583.
275. Caporaso, J.G., et al., *QIIME allows analysis of high-throughput community sequencing data.* Nature Methods, 2010. **7**(5): p. 335-336.
276. Segata, N., et al., *Metagenomic biomarker discovery and explanation.* Genome Biology, 2011. **12**(6): p. R60.
277. Chiarucci, A., G. Bacaro, and S.M. Scheiner, *Old and new challenges in using species diversity for assessing biodiversity.* Philosophical Transactions of the Royal Society B: Biological Sciences, 2011. **366**(1576): p. 2426-2437.

278. Hughes, J.B., et al., *Counting the uncountable: statistical approaches to estimating microbial diversity.* Applied and environmental microbiology, 2001. **67**(10): p. 4399-4406.
279. Anderson, M. and T. Willis, *Canonical analysis of principal coordinates: A useful method of constrained ordination for ecology.* Ecology, 2003. **84**: p. 511-525.
280. Turroni, F., et al., *Glycan Utilization and Cross-Feeding Activities by Bifidobacteria.* Trends Microbiol, 2018. **26**(4): p. 339-350.
281. Thomson, P., D.A. Medina, and D. Garrido, *Human milk oligosaccharides and infant gut bifidobacteria: Molecular strategies for their utilization.* Food Microbiology, 2018. **75**: p. 37-46.
282. Lawson, M.A.E., et al., *Breast milk-derived human milk oligosaccharides promote Bifidobacterium interactions within a single ecosystem.* The ISME Journal, 2020. **14**(2): p. 635-648.
283. Drissi, F., D. Raoult, and V. Merhej, *Metabolic role of lactobacilli in weight modification in humans and animals.* Microbial Pathogenesis, 2017. **106**: p. 182-194.
284. Freilich, S., et al., *Competitive and cooperative metabolic interactions in bacterial communities.* Nature Communications, 2011. **2**(1): p. 589.
285. Sivamaruthi, B.S., et al., *A Review on Role of Microbiome in Obesity and Antiobesity Properties of Probiotic Supplements.* BioMed research international, 2019. **2019**: p. 3291367-3291367.
286. Magne, F., et al., *The Firmicutes/Bacteroidetes Ratio: A Relevant Marker of Gut Dysbiosis in Obese Patients?* Nutrients, 2020. **12**(5).
287. Ley, R.E., et al., *Microbial ecology: human gut microbes associated with obesity.* Nature, 2006. **444**(7122): p. 1022-3.
288. Krajmalnik-Brown, R., et al., *Effects of gut microbes on nutrient absorption and energy regulation.* Nutr Clin Pract, 2012. **27**(2): p. 201-14.
289. Turpin, W., et al., *Lactobacilli as multifaceted probiotics with poorly disclosed molecular mechanisms.* International Journal of Food Microbiology, 2010. **143**(3): p. 87-102.
290. Pridmore, R.D., et al., *The genome sequence of the probiotic intestinal bacterium Lactobacillus johnsonii NCC 533.* Proceedings of the National Academy of Sciences of the United States of America, 2004. **101**(8): p. 2512-2517.
291. Armougom, F., et al., *Monitoring bacterial community of human gut microbiota reveals an increase in Lactobacillus in obese patients and Methanogens in anorexic patients.* PloS one, 2009. **4**(9): p. e7125.
292. Crovesy, L., et al., *Effect of Lactobacillus on body weight and body fat in overweight subjects: a systematic review of randomized controlled clinical trials.* Int J Obes (Lond), 2017. **41**(11): p. 1607-1614.
293. Million, M., et al., *Comparative meta-analysis of the effect of Lactobacillus species on weight gain in humans and animals.* Microbial Pathogenesis, 2012. **53**(2): p. 100-108.
294. Dao, M.C., et al., *Akkermansia muciniphila and improved metabolic health during a dietary intervention in obesity: relationship with gut microbiome richness and ecology.* Gut, 2016. **65**(3): p. 426-36.

295. Karlsson, C.L.J., et al., *The Microbiota of the Gut in Preschool Children With Normal and Excessive Body Weight.* Obesity, 2012. **20**(11): p. 2257-2261.
296. Depommier, C., et al., *Supplementation with Akkermansia muciniphila in overweight and obese human volunteers: a proof-of-concept exploratory study.* Nat Med, 2019. **25**(7): p. 1096-1103.
297. Plovier, H., et al., *A purified membrane protein from Akkermansia muciniphila or the pasteurized bacterium improves metabolism in obese and diabetic mice.* Nat Med, 2017. **23**(1): p. 107-113.
298. Zhao, S., et al., *Akkermansia muciniphila improves metabolic profiles by reducing inflammation in chow diet-fed mice.* J Mol Endocrinol, 2017. **58**(1): p. 1-14.
299. Kim, S., et al., *Akkermansia muciniphila Prevents Fatty Liver Disease, Decreases Serum Triglycerides, and Maintains Gut Homeostasis.* Appl Environ Microbiol, 2020. **86**(7).
300. Everard, A., et al., *Cross-talk between Akkermansia muciniphila and intestinal epithelium controls diet-induced obesity.* Proc Natl Acad Sci U S A, 2013. **110**(22): p. 9066-71.
301. Kostopoulos, I., et al., *Akkermansia muciniphila uses human milk oligosaccharides to thrive in the early life conditions in vitro.* Sci Rep, 2020. **10**(1): p. 14330.
302. Ottman, N., et al., *Genome-Scale Model and Omics Analysis of Metabolic Capacities of Akkermansia muciniphila Reveal a Preferential Mucin-Degrading Lifestyle.* Appl Environ Microbiol, 2017. **83**(18).
303. Haro, C., et al., *The gut microbial community in metabolic syndrome patients is modified by diet.* J Nutr Biochem, 2016. **27**: p. 27-31.
304. Liu, R., et al., *Gut microbiome and serum metabolome alterations in obesity and after weight-loss intervention.* Nat Med, 2017. **23**(7): p. 859-868.
305. Yu, Z.-T., C. Chen, and D.S. Newburg, *Utilization of major fucosylated and sialylated human milk oligosaccharides by isolated human gut microbes.* Glycobiology, 2013. **23**(11): p. 1281-1292.
306. Sonnenburg, J.L., et al., *Glycan foraging in vivo by an intestine-adapted bacterial symbiont.* Science, 2005. **307**(5717): p. 1955-9.
307. Martens, E.C., et al., *Complex glycan catabolism by the human gut microbiota: the Bacteroidetes Sus-like paradigm.* J Biol Chem, 2009. **284**(37): p. 24673-7.
308. Xu, J., et al., *A genomic view of the human-Bacteroides thetaiotaomicron symbiosis.* Science, 2003. **299**(5615): p. 2074-6.
309. Reeves, A.R., et al., *A Bacteroides thetaiotaomicron outer membrane protein that is essential for utilization of maltooligosaccharides and starch.* Journal of bacteriology, 1996. **178**(3): p. 823-830.
310. Bjursell, M.K., E.C. Martens, and J.I. Gordon, *Functional Genomic and Metabolic Studies of the Adaptations of a Prominent Adult Human Gut Symbiont, Bacteroides thetaiotaomicron, to the Suckling Period*.* Journal of Biological Chemistry, 2006. **281**(47): p. 36269-36279.
311. Bry, L., et al., *A model of host-microbial interactions in an open mammalian ecosystem.* Science, 1996. **273**(5280): p. 1380-3.

312. Hooper, L.V., et al., *A molecular sensor that allows a gut commensal to control its nutrient foundation in a competitive ecosystem.* Proc Natl Acad Sci U S A, 1999. **96**(17): p. 9833-8.
313. Pham, Tu Anh N., et al., *Epithelial IL-22RA1-Mediated Fucosylation Promotes Intestinal Colonization Resistance to an Opportunistic Pathogen.* Cell Host & Microbe, 2014. **16**(4): p. 504-516.
314. Goodrich, J.K., et al., *Human genetics shape the gut microbiome.* Cell, 2014. **159**(4): p. 789-99.
315. Alemán, J.O., et al., *Fecal microbiota and bile acid interactions with systemic and adipose tissue metabolism in diet-induced weight loss of obese postmenopausal women.* Journal of translational medicine, 2018. **16**(1): p. 244-244.
316. Fu, J., et al., *The Gut Microbiome Contributes to a Substantial Proportion of the Variation in Blood Lipids.* Circ Res, 2015. **117**(9): p. 817-24.
317. Waters, J.L. and R.E. Ley, *The human gut bacteria Christensenellaceae are widespread, heritable, and associated with health.* BMC biology, 2019. **17**(1): p. 83-83.
318. Arboleya, S., et al., *Gut Bifidobacteria Populations in Human Health and Aging.* Frontiers in microbiology, 2016. **7**: p. 1204-1204.
319. Ashida, H., et al., *Two distinct alpha-L-fucosidases from Bifidobacterium bifidum are essential for the utilization of fucosylated milk oligosaccharides and glycoconjugates.* Glycobiology, 2009. **19**(9): p. 1010-7.
320. Agergaard, C.N., et al., *Two Serious Cases of Infection with Clostridium celatum after 40 Years in Hiding?* Journal of clinical microbiology, 2016. **54**(1): p. 236-238.
321. Clavel, T., et al., *Isolation of bacteria from the ileal mucosa of TNFdeltaARE mice and description of Enterorhabdus mucosicola gen. nov., sp. nov.* Int J Syst Evol Microbiol, 2009. **59**(Pt 7): p. 1805-12.
322. Gao, C., et al., *Glycan Microarrays as Chemical Tools for Identifying Glycan Recognition by Immune Proteins.* Front Chem, 2019. **7**: p. 833.
323. Varki, A., *Biological roles of glycans.* Glycobiology, 2016. **27**(1): p. 3-49.
324. Copoiu, L. and S. Malhotra, *The current structural glycome landscape and emerging technologies.* Curr Opin Struct Biol, 2020. **62**: p. 132-139.
325. Haab, B.B. and Z. Klamer, *Advances in Tools to Determine the Glycan-Binding Specificities of Lectins and Antibodies.* Molecular & Cellular Proteomics, 2020. **19**(2): p. 224-232.
326. Nakamura-Tsuruta, S., et al., *Evidence that Agaricus bisporus agglutinin (ABA) has dual sugar-binding specificity.* Biochemical and Biophysical Research Communications, 2006. **347**(1): p. 215-220.
327. Matsumura, K., et al., *Comparative analysis of oligosaccharide specificities of fucose-specific lectins from Aspergillus oryzae and Aleuria aurantia using frontal affinity chromatography.* Analytical biochemistry, 2009. **386**(2): p. 217-221.
328. Liu, X., et al., *Development of a sandwiched microarray platform for studying the interactions of antibiotics with Staphylococcus aureus.* Analytica chimica acta, 2016. **917**: p. 93-100.

329. Hsu, K.-L., K.T. Pilobello, and L.K. Mahal, *Analyzing the dynamic bacterial glycome with a lectin microarray approach.* Nature chemical biology, 2006. **2**(3): p. 153-157.
330. Kilcoyne, M., et al., *Campylobacter jejuni strain discrimination and temperature-dependent glycome expression profiling by lectin microarray.* Carbohydrate research, 2014. **389**: p. 123-133.
331. Yasuda, E., et al., *Lectin microarray reveals binding profiles of Lactobacillus casei strains in a comprehensive analysis of bacterial cell wall polysaccharides.* Appl. Environ. Microbiol., 2011. **77**(13): p. 4539-4546.
332. Dang, K., et al., *Application of Lectin Microarrays for Biomarker Discovery.* ChemistryOpen, 2020. **9**(3): p. 285-300.
333. Cummings, R.D., et al., *Glycan-Recognizing Probes as Tools*, in *Essentials of Glycobiology*, A. Varki, et al., Editors. 2015, Cold Spring Harbor Laboratory Press

Copyright 2015-2017 by The Consortium of Glycobiology Editors, La Jolla, California. All rights reserved.: Cold Spring Harbor (NY). p. 611-25.
334. Mandalasi, M., et al., *Development and characterization of a specific IgG monoclonal antibody toward the Lewis x antigen using splenocytes of Schistosoma mansoni-infected mice.* Glycobiology, 2013. **23**(7): p. 877-92.
335. Harn, D.A., M. Mitsuyama, and J.R. David, *Schistosoma mansoni. Anti-egg monoclonal antibodies protect against cercarial challenge in vivo.* J Exp Med, 1984. **159**(5): p. 1371-87.
336. Ko, A.I. and D.A. Harn, *Characterization of protective and non-protective surface membrane carbohydrate epitopes of Schistosoma mansoni.* Mem Inst Oswaldo Cruz, 1987. **82 Suppl 4**: p. 115-9.
337. Harn, D.A., et al., *Evidence that a protective membrane epitope is involved in early but not late phase immunity in Schistosoma mansoni.* The Journal of Immunology, 1987. **138**(5): p. 1571-1580.
338. Ko, A.I., U.C. Drager, and D.A. Harn, *A Schistosoma mansoni epitope recognized by a protective monoclonal antibody is identical to the stage-specific embryonic antigen 1.* Proc Natl Acad Sci U S A, 1990. **87**(11): p. 4159-63.
339. Heimburg-Molinaro, J. and K. Rittenhouse-Olson, *Development and Characterization of Antibodies to Carbohydrate Antigens*, in *Glycomics: Methods and Protocols*, N.H. Packer and N.G. Karlsson, Editors. 2009, Humana Press: Totowa, NJ. p. 341-357.
340. Solter, D. and B.B. Knowles, *Monoclonal antibody defining a stage-specific mouse embryonic antigen (SSEA-1).* Proceedings of the National Academy of Sciences, 1978. **75**(11): p. 5565-5569.
341. Hokke, C.H. and A.M. Deelder, *Schistosome glycoconjugates in host-parasite interplay.* Glycoconjugate Journal, 2001. **18**(8): p. 573-587.
342. Smilowitz, J.T., et al., *Breast milk oligosaccharides: structure-function relationships in the neonate.* Annual review of nutrition, 2014. **34**: p. 143-169.
343. Tivadar, S.T., et al., *Monoclonal Antibody Targeting Sialyl-di-Lewis^a–Containing Internalizing and Noninternalizing*

Glycoproteins with Cancer Immunotherapy Development Potential. Molecular Cancer Therapeutics, 2020. **19**(3): p. 790-801.
344. de Rougemont, A., et al., *Qualitative and Quantitative Analysis of the Binding of GII.4 Norovirus Variants onto Human Blood Group Antigens.* Journal of Virology, 2011. **85**(9): p. 4057-4070.
345. Grenfell, R.F., et al., *Vaccine self-assembling immune matrix is a new delivery platform that enhances immune responses to recombinant HBsAg in mice.* Clin Vaccine Immunol, 2015. **22**(3): p. 336-43.
346. Fishman, J.B. and E.A. Berg, *Ammonium Sulfate Fractionation of Antibodies.* Cold Spring Harb Protoc, 2018. **2018**(6).
347. Yu, Y., et al., *Functional glycomic analysis of human milk glycans reveals the presence of virus receptors and embryonic stem cell biomarkers.* J Biol Chem, 2012. **287**(53): p. 44784-99.
348. Tundup, S., et al., *CD14 influences host immune responses and alternative activation of macrophages during Schistosoma mansoni infection.* Infect Immun, 2014. **82**(8): p. 3240-51.
349. Cummings, R.D. and R.P. McEver, *C-type Lectins*, in *Essentials of Glycobiology*, A. Varki, et al., Editors. 2009, Cold Spring Harbor Laboratory Press

Copyright © 2009, The Consortium of Glycobiology Editors, La Jolla, California.: Cold Spring Harbor (NY).
350. Bornhöfft, K.F., et al., *Siglecs: a journey through the evolution of sialic acid-binding immunoglobulin-type lectins.* Developmental & Comparative Immunology, 2018. **86**: p. 219-231.
351. Thiemann, S. and L.G. Baum, *Galectins and immune responses—just how do they do those things they do?* Annual review of immunology, 2016. **34**: p. 243-264.
352. Noll, A.J., et al., *Galectins are human milk glycan receptors.* Glycobiology, 2016. **26**(6): p. 655-669.
353. Kawasaki, T. and T. Kawai, *Toll-like receptor signaling pathways.* Frontiers in immunology, 2014. **5**: p. 461-461.
354. He, Y., N.T. Lawlor, and D.S. Newburg, *Human Milk Components Modulate Toll-Like Receptor-Mediated Inflammation.* Advances in nutrition (Bethesda, Md.), 2016. **7**(1): p. 102-111.
355. Wang, C., et al., *Human Milk Oligosaccharides Protect against Necrotizing Enterocolitis by Inhibiting Intestinal Damage via Increasing the Proliferation of Crypt Cells.* Mol Nutr Food Res, 2019. **63**(18): p. e1900262.
356. He, Y., et al., *The human milk oligosaccharide 2'-fucosyllactose modulates CD14 expression in human enterocytes, thereby attenuating LPS-induced inflammation.* Gut, 2016. **65**(1): p. 33-46.
357. Kurakevich, E., et al., *Milk oligosaccharide sialyl(α2,3)lactose activates intestinal CD11c+ cells through TLR4.* Proc Natl Acad Sci U S A, 2013. **110**(43): p. 17444-9.
358. Perdijk, O., et al., *Induction of human tolerogenic dendritic cells by 3'-sialyllactose via TLR4 is explained by LPS contamination.* Glycobiology, 2018. **28**(3): p. 126-130.

359. Craft, K.M. and S.D. Townsend, *Synthesis of lacto-N-tetraose.* Carbohydr Res, 2017. **440-441**: p. 43-50.
360. Blixt, O., et al., *Printed covalent glycan array for ligand profiling of diverse glycan binding proteins.* Proc Natl Acad Sci U S A, 2004. **101**(49): p. 17033-8.
361. Song, X., et al., *Novel fluorescent glycan microarray strategy reveals ligands for galectins.* Chem Biol, 2009. **16**(1): p. 36-47.
362. Vozarova, B., et al., *Circulating interleukin-6 in relation to adiposity, insulin action, and insulin secretion.* Obes Res, 2001. **9**(7): p. 414-7.
363. Eder, K., et al., *The major inflammatory mediator interleukin-6 and obesity.* Inflammation Research, 2009. **58**(11): p. 727.
364. Klein, S., et al., *Adipose tissue leptin production and plasma leptin kinetics in humans.* Diabetes, 1996. **45**(7): p. 984-7.
365. Kleinert, M., et al., *Animal models of obesity and diabetes mellitus.* Nature Reviews Endocrinology, 2018. **14**(3): p. 140-162.

APPENDIX A

COMPLETE MONOMER, CONJUGATE, AND INJECTION ROUTE DATA

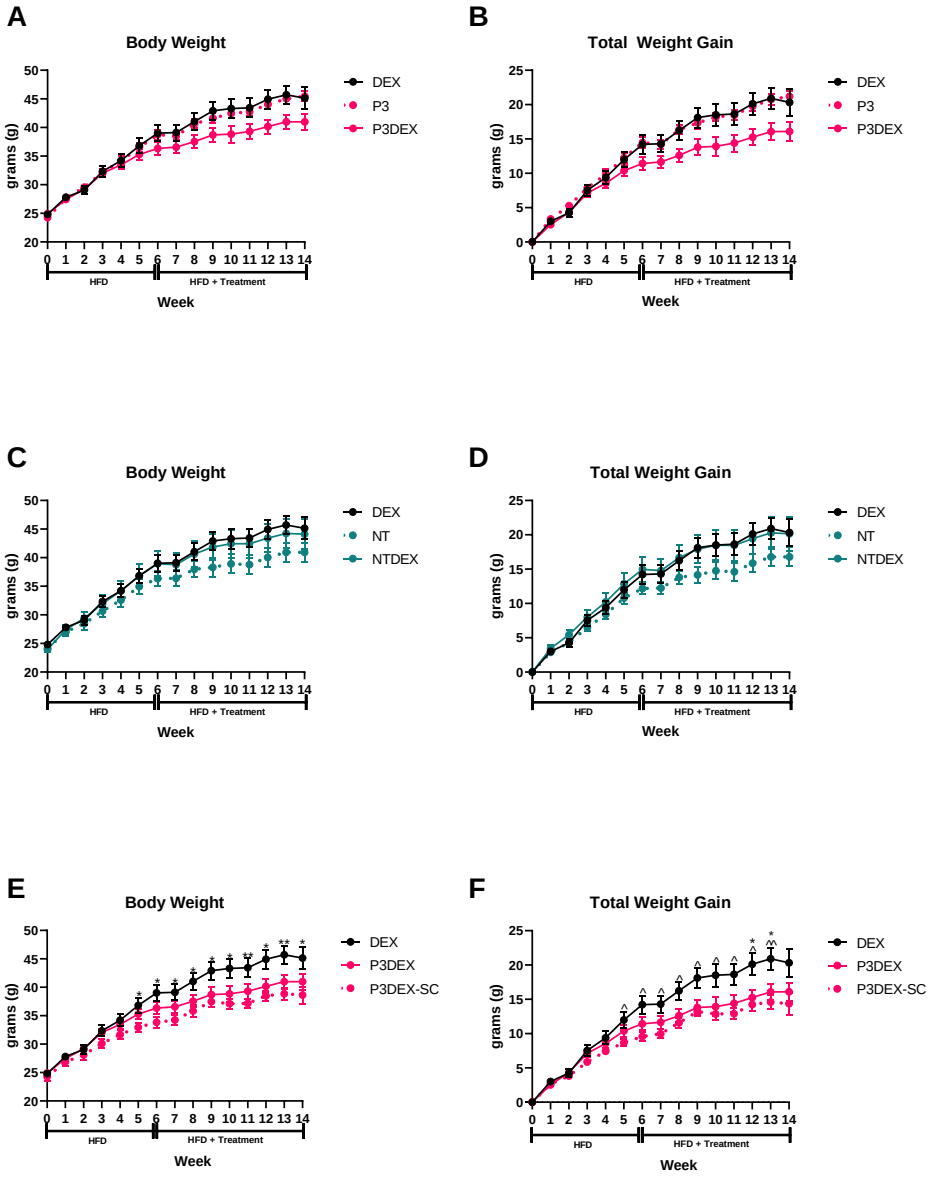

Figure A.1: Effect of LNFPIII and LNnT monomers, as well as injection route, on body weight and total weight gain. Comparison of **A**. body weight and **B.** total weight gain between DIO mice treated with DEX, LNFPIII monomers, or LNFPIII conjugates. Comparison of **C.** body weight and **D.** total weight gain between DIO mice treated **with** DEX, LNnT monomers, or LNnT conjugates**.** Comparison of **E.** body weight and **F.** total weight gain between DIO mice treated with DEX or LNFPIII conjugates (IP vs. SC injection route). One-Way ANOVA with Holm-Sidak's Multiple Comparisons Test. *indicates a significant difference between DEX and P3DEX (*p≤ 0.05; **p≤0.01). ^indicates a significant difference between DEX and P3DEX-SC (^p≤ 0.05; ^^p≤0.01).

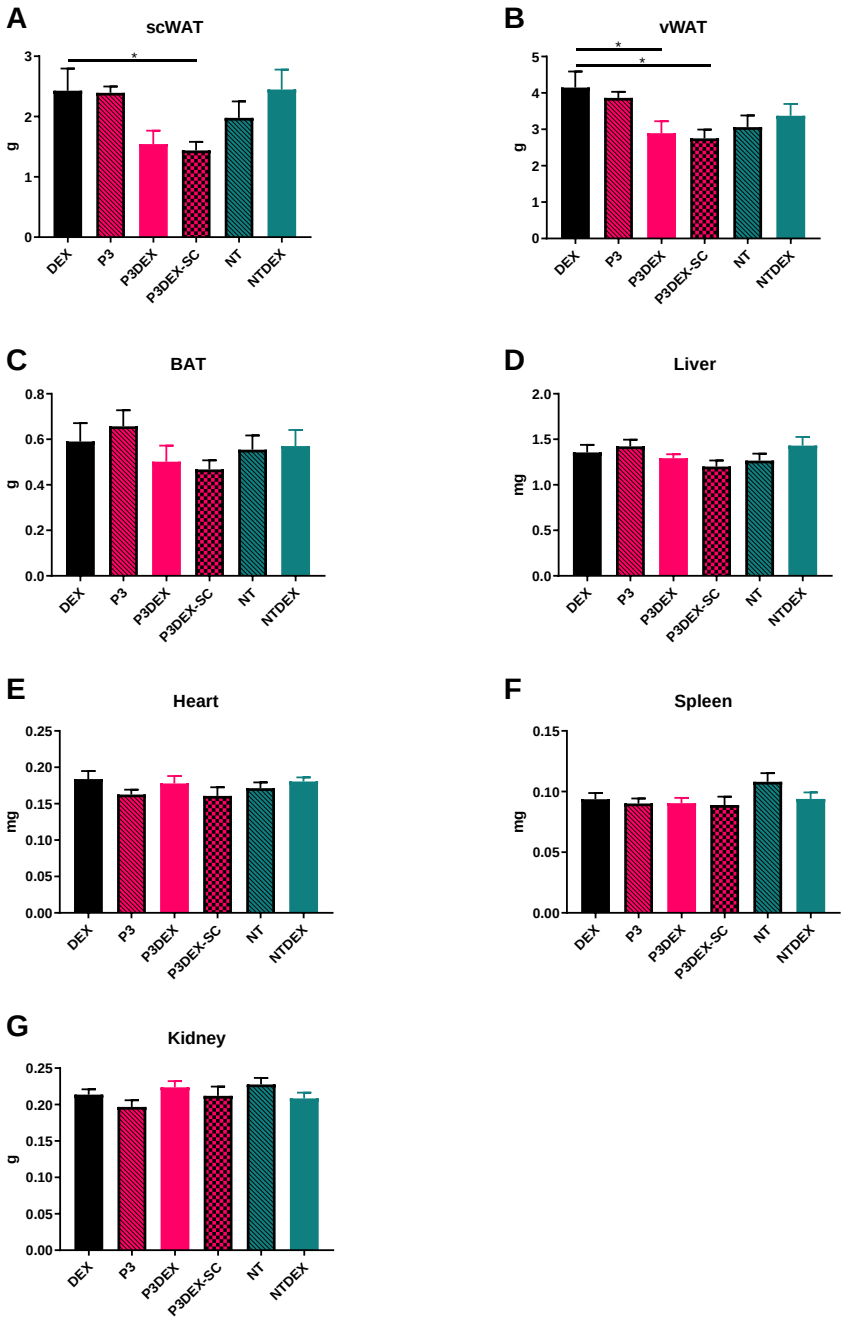

Figure A.2: Effect of LNFPIII and LNnT monomers, as well as injection route, on organ weights. Comparison of **A**. scWAT, **B.** vWAT, **C.** BAT, **D.** liver, **E.** heart, **F.** spleen, and **G.** kidney weights between DIO mice treated with DEX, LNFPIII monomers, LNFPIII conjugates (IP vs. SC injection route), LNnT monomers, or LNnT conjugates. One-Way ANOVA with Holm-Sidak's Multiple Comparisons Test. *indicates a significant difference between DEX and P3DEX (*$p \leq 0.05$)

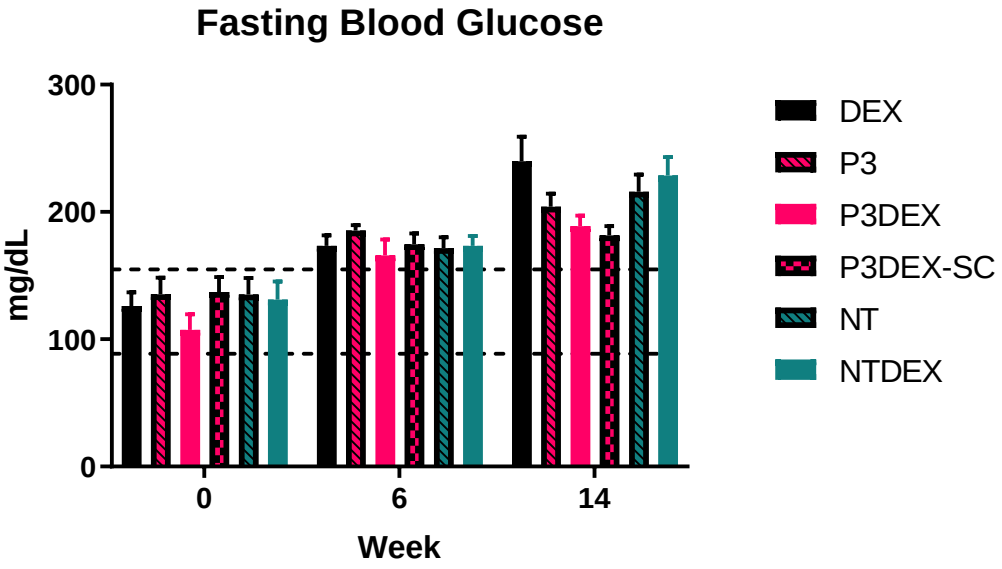

Figure A.3: Effect of LNFPIII and LNnT monomers, as well as injection route, on fasting blood glucose levels. Comparison of fasting blood glucose levels between DIO mice treated with DEX, LNFPIII monomers, LNFPIII conjugates (IP vs. SC injection route), LNnT monomers, or LNnT conjugates. One-Way ANOVA with Holm-Sidak's Multiple Comparisons Test.

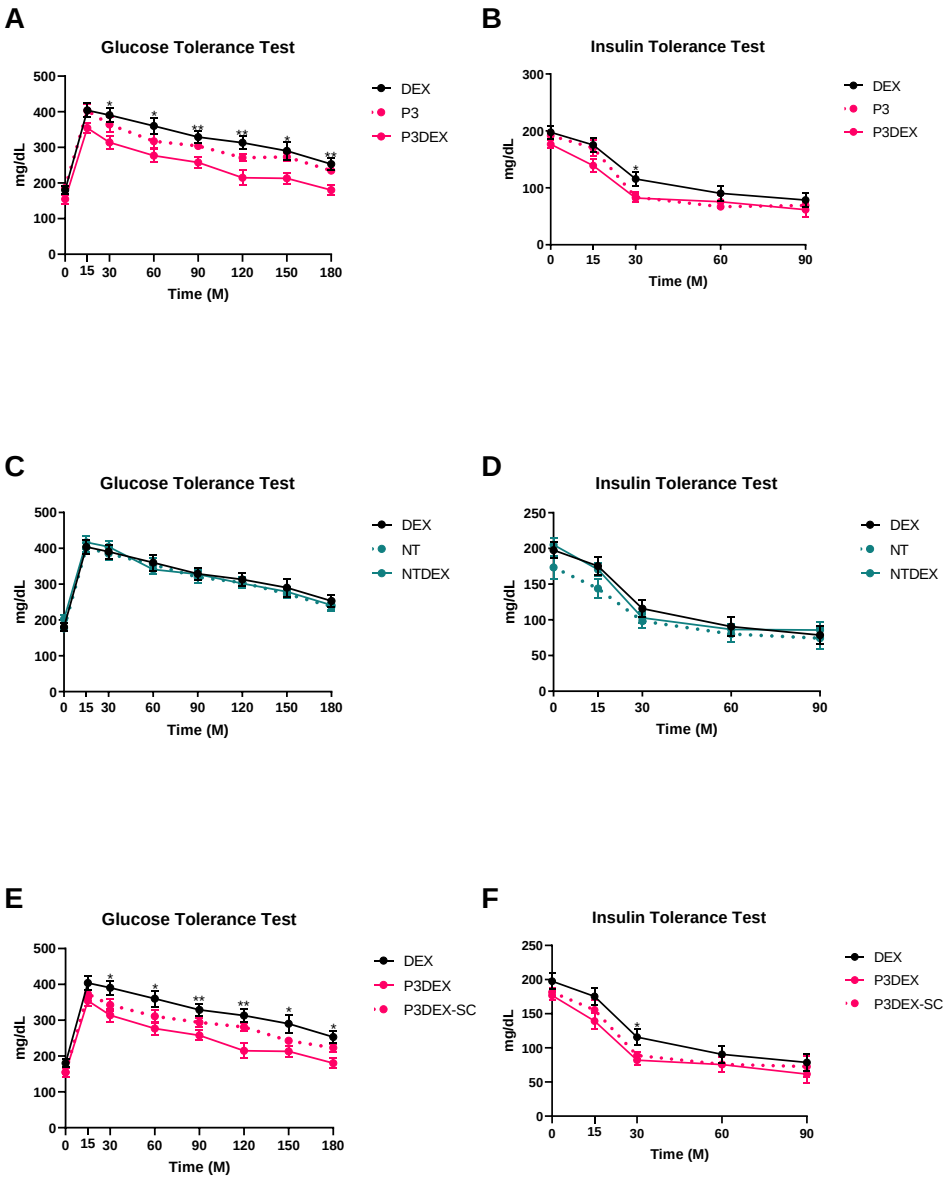

Figure A.4: Effect of LNFPIII and LNnT monomers, as well as injection route, on glucose tolerance and insulin tolerance. Comparison of **A**. glucose tolerance **B.** insulin tolerance between DIO mice treated with DEX, LNFPIII monomers, or LNFPIII conjugates. Comparison of **C.** glucose tolerance and **D.** insulin tolerance between DIO mice treated with DEX, LNnT monomers, or LNnT conjugates**.** Comparison of **E.** glucose tolerance and **F.** insulin tolerance between DIO mice treated with DEX or LNFPIII conjugates (IP vs. SC injection route). One-Way ANOVA with Holm-Sidak's Multiple Comparisons Test. *indicates a significant difference between DEX and P3DEX (*$p \leq 0.05$; **$p \leq 0.01$).

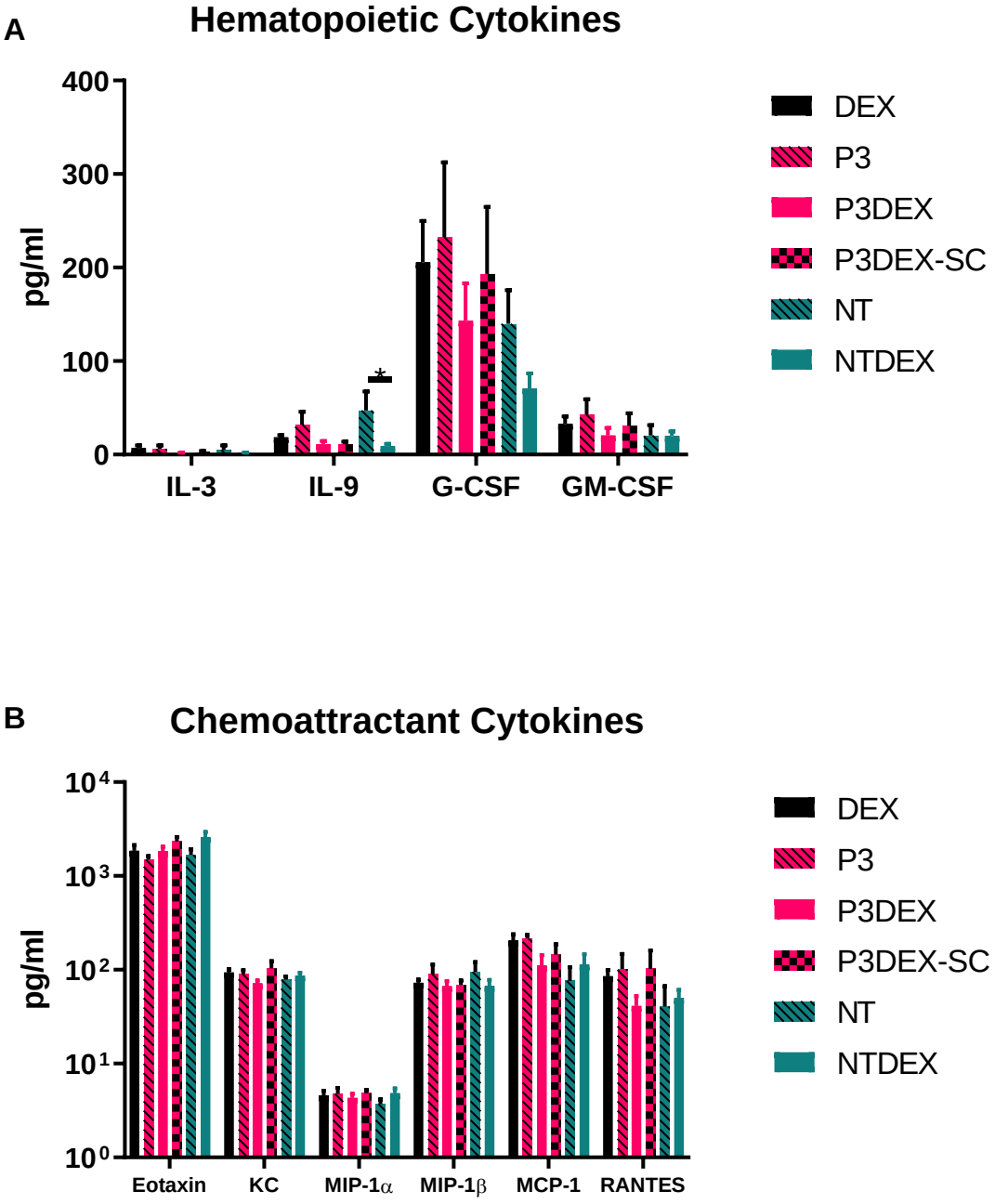

Figure A.5: Effect of LNFPIII and LNnT monomers, as well as injection route, on hematopoietic and chemoattractant cytokines. Measurement of **A**. hematopoietic and **B.** chemoattractant cytokines between DIO mice treated with DEX, LNFPIII monomers, LNFPIII conjugates (IP vs. SC injection route), LNnT monomers, or LNnT conjugates. One-Way ANOVA with Holm-Sidak's Multiple Comparisons Test. *indicates a significant difference (*$p \leq 0.05$).

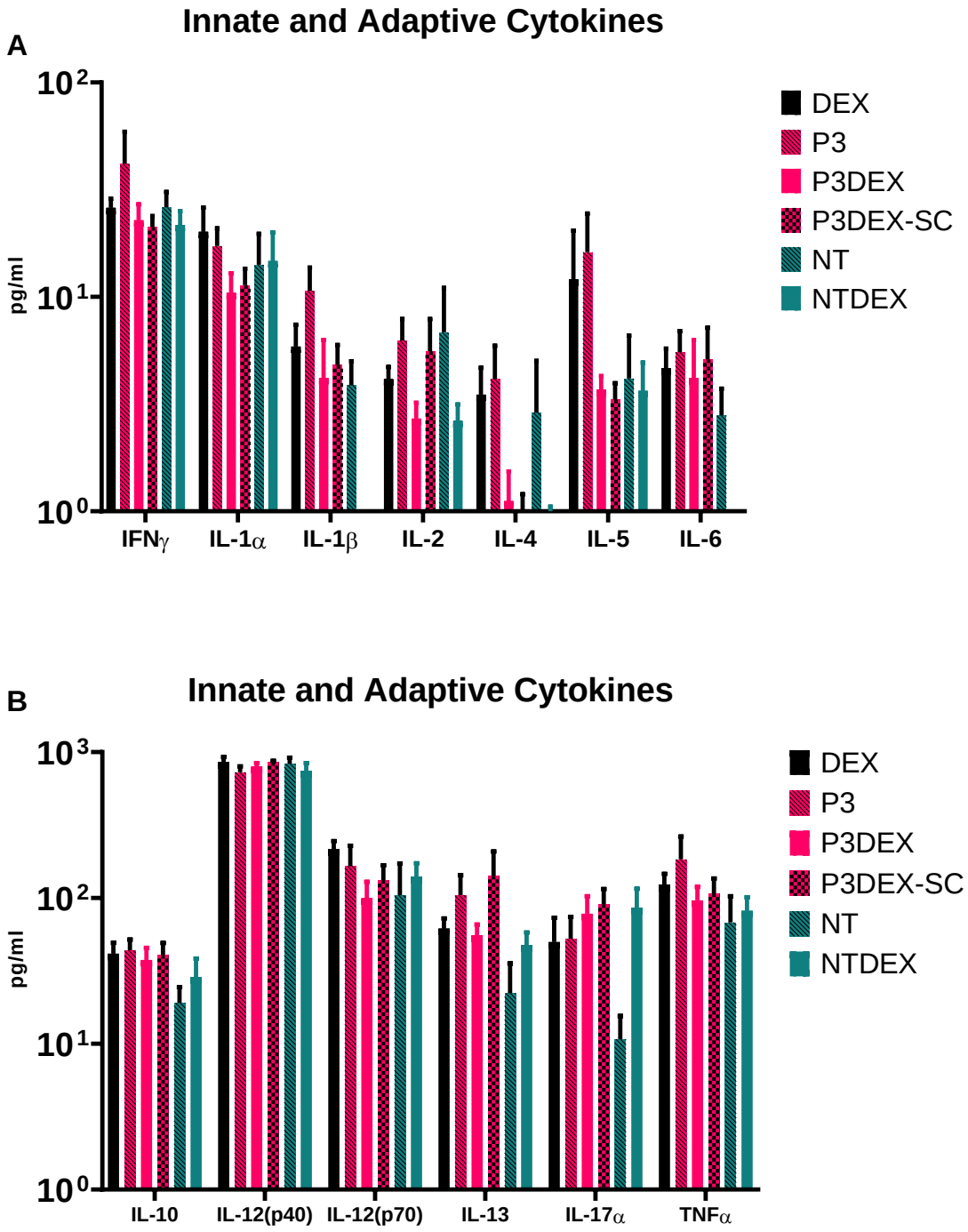

Figure A.6: Effect of LNFPIII and LNnT monomers, as well as injection route, on innate and adaptive cytokines. Measurement of **A-B**. innate and adaptive cytokines between DIO mice treated with DEX, LNFPIII monomers, LNFPIII conjugates (IP vs. SC injection route), LNnT monomers, or LNnT conjugates. One-Way ANOVA with Holm-Sidak's Multiple Comparisons Test.

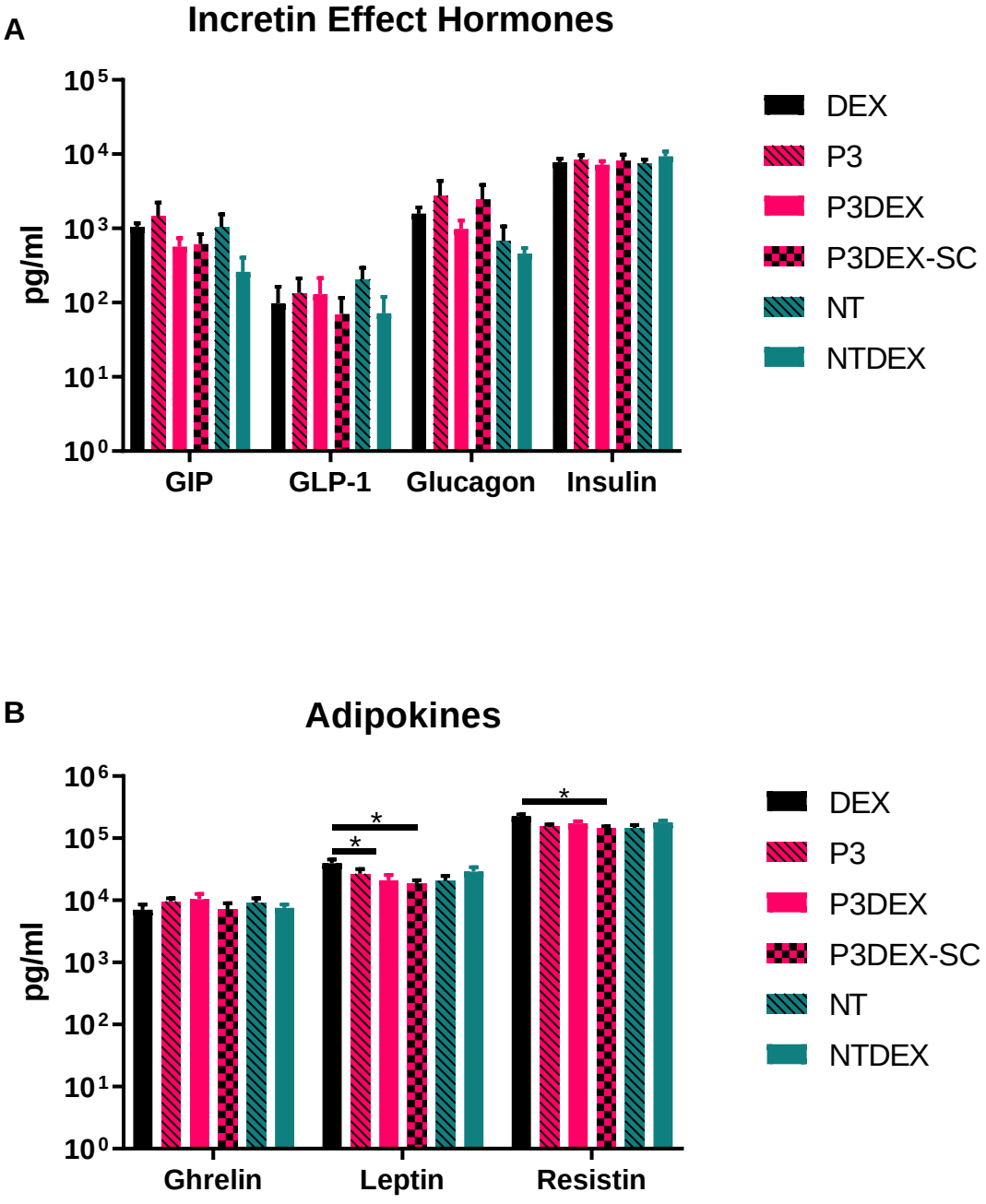

Figure A.7: Effect of LNFPIII and LNnT monomers, as well as injection route, on incretin effect hormones and adipokines. Measurement of **A**. incretin effect hormones **and B.** adipokines between DIO mice treated with DEX, LNFPIII monomers, LNFPIII conjugates (IP vs. SC injection route), LNnT monomers, or LNnT conjugates. One-Way ANOVA with Holm-Sidak's Multiple Comparisons Test. *indicates a significant difference (*$p \leq 0.05$).

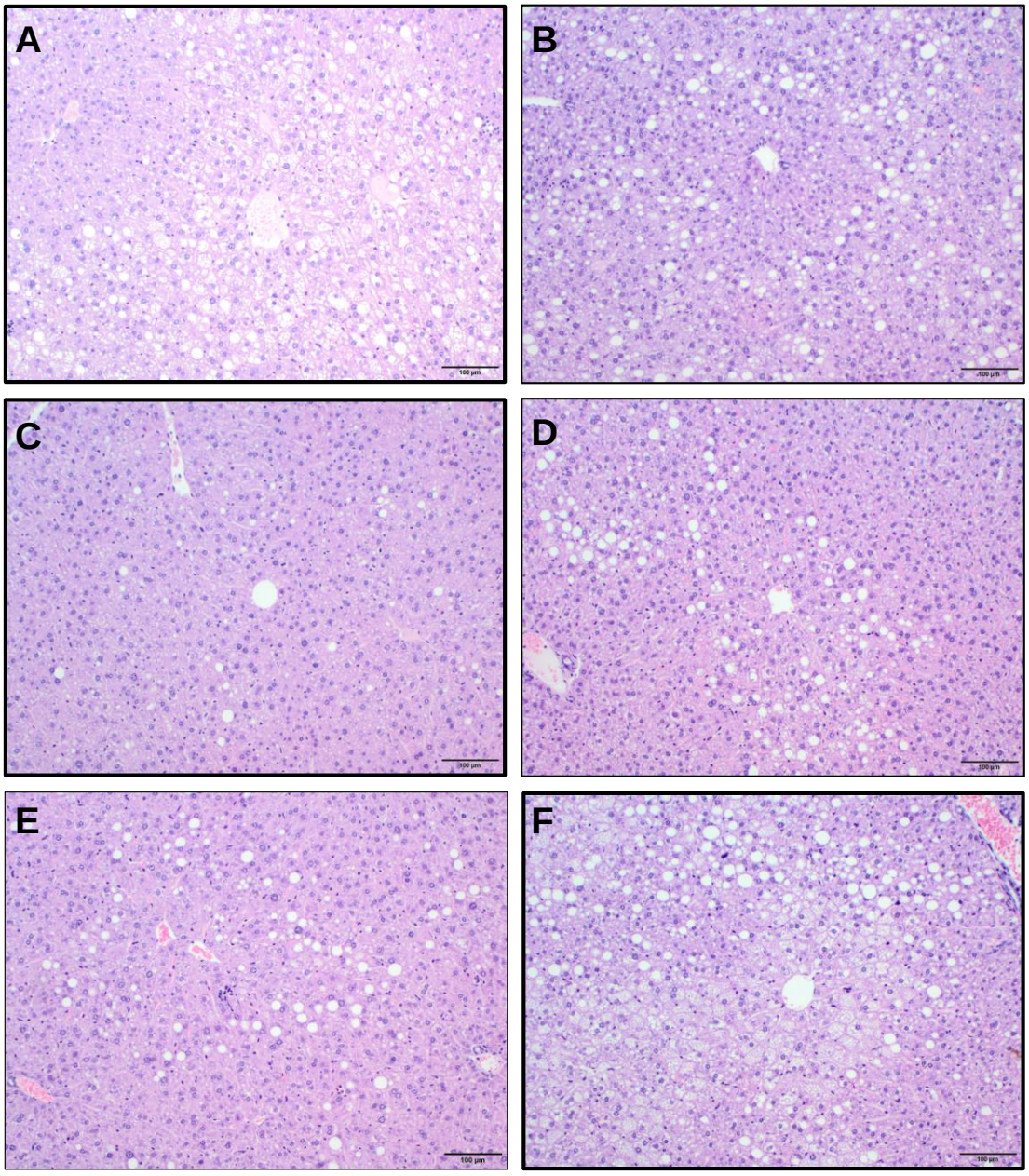

Figure A.8: Effect of LNFPIII and LNnT monomers, as well as injection route, on hepatic lipid accumulation. Liver sections from DO mice treated with **A.** DEX, **B.** P3, **C.** P3DEX, **D.** P3DEX-SC, **E.** NT, and **F.** NTDEX.

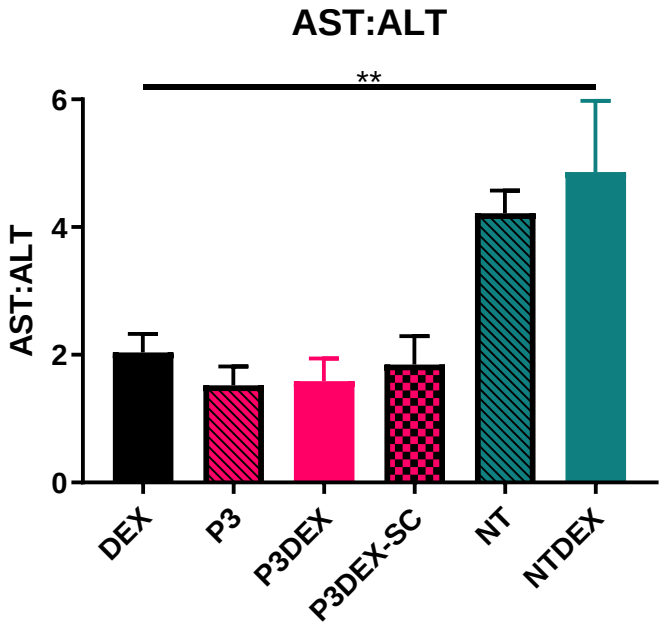

Figure A.9: Effect of LNFPIII and LNnT monomers, as well as injection route, on the ratio of AST:ALT. Comparison of AST:ALT between DIO mice treated with DEX, LNFPIII monomers, LNFPIII conjugates (IP vs. SC injection route), LNnT monomers, or LNnT conjugates. One-Way ANOVA with Holm-Sidak's Multiple Comparisons Test. *indicates a significant difference (**$p \leq 0.01$).

APPENDIX B

ORGAN PRESERVATION METHODS FROM *IN VIVO* EXPERIMENTS

Table B.1 Tissue Preservation

Tissue	Diagram	Preservation
Blood		• Collect in Microvette Tube and store on ice. • Spin @ 10,000 x g for 5 minutes. • Aliquot 30µl of serum into Eppendorf tubes. • Freeze at -80°C.
Brain	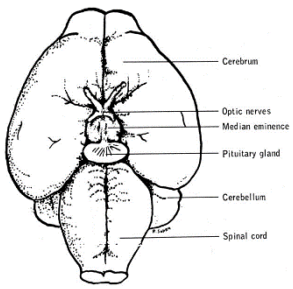	• Freeze on dry ice. • Wrap in foil. • Leave on dry ice until transfer to -80°C.
scWAT	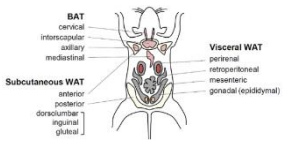	• Weigh scWAT. • Place a small piece of scWAT in formalin. • Place remaining scWAT in foil and snap freeze in liquid nitrogen until storage at -80°C.
vWAT		• Weigh vWAT. • Place a small piece of vWAT in formalin. • Place remaining vWAT in foil and snap freeze in liquid nitrogen until storage at -80°C.
BAT		• Weigh BAT. • Place a small piece of BAT in formalin. • Place remaining BAT in foil and snap freeze in liquid nitrogen until storage at -80°C.
iLN	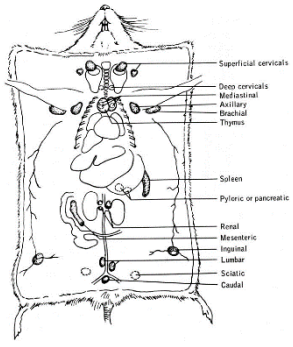	• Place both lymph nodes in formalin.
mLN		• Place all (3) lymph nodes in formalin.

Small Intestine	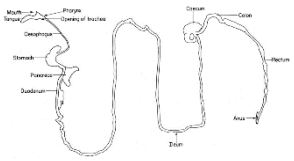	• Cut below stomach and above cecum to isolate small intestine. • Place a small piece (a few centimeters) in an Eppendorf tube and snap freeze in dry ice/methanol until storage at -80°C. • Mince a small piece (a few centimeters) and place in Eppendorf tube with RNA later. • Place remainder of small intestine in formalin.
Colon		• Cut below cecum to isolate small intestine. • Place a small piece (a few centimeters) in an Eppendorf tube and snap freeze in dry ice/methanol until storage at -80°C. • Mince a small piece (a few centimeters) and place in Eppendorf tube with RNALater. Place on ice until storage at -80°C. • Place remainder of small intestine in formalin.
Spleen	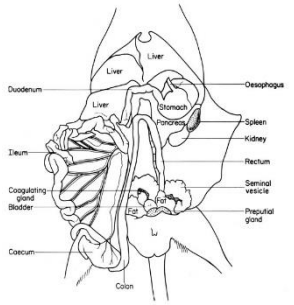	• Weigh spleen. Take photos of spleen. • Cut in half. • Place ½ in formalin. • Place ¼ in Eppendorf tube and snap freeze in dry ice/methanol until storage at -80°C. • Mince the remaining ¼ into small pieces and place in Eppendorf tube w/ RNALater. Place on ice until storage at -80°C.
Kidney		• Weigh kidney (R). • Place kidney (R) in formalin. • Place ½ kidney (L) in Eppendorf tube and snap freeze in dry ice/methanol. Place on ice until storage at -80°C. • Mince the remaining ½ into small pieces and place in Eppendorf tube w/ RNALater. Place on ice until storage at -80°C.
Liver	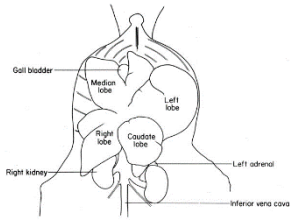	• Weigh liver. Take photos of liver. • Place left lobe in formalin. • Place median and right lobe in Eppendorf tube and snap freeze in dry ice/methanol until storage at -80°C. • Mince the caudate lobe into small pieces and place in Eppendorf tube w/ RNALater. Place on ice until storage at -80°C.

Heart	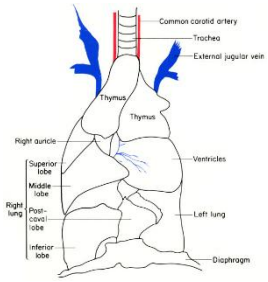	• Weigh heart. • Mince the heart into small pieces and place in Eppendorf tube w/ RNALater. Place on ice until storage at -80°C.